Università degli Studi di Padova

VENICEASIAGO2016

SUMMER SCHOOL 2016
VENICE AND ASIAGO

August 16th - September 7th

Fondazione Ricerca Biomedica Avanzata onlus
Istituto Veneto di Medicina Molecolare VIMM

Dipartimento di Fisica e Astronomia Galileo Galilei

Biochemistry and Biophysics of communication between cells

Fabio Mammano

Director

CNR Institute of Cell Biology and Neurobiology - Rome

Connexins are 4-pass transmenbrane proteins that form gap junction channels and hemichannels

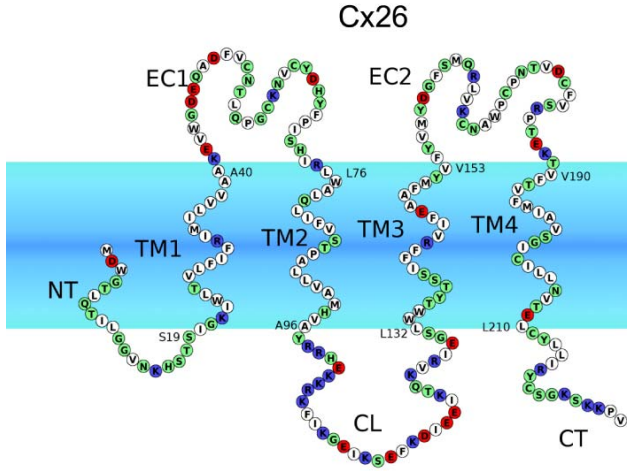

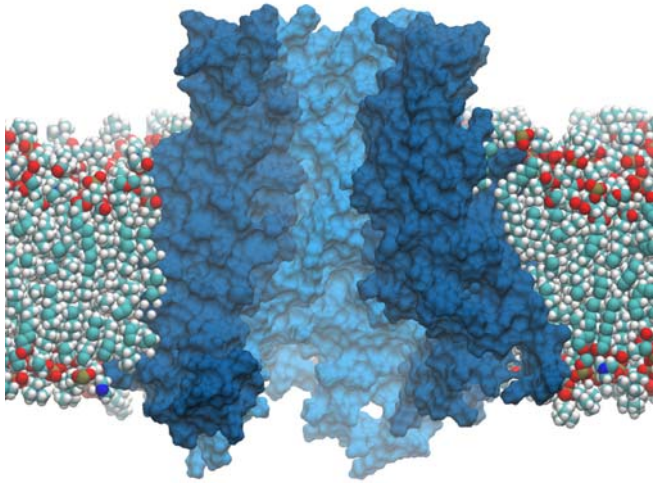

Zonta | Mammano. *J Biomolecular Structure & Dynamics* 2012

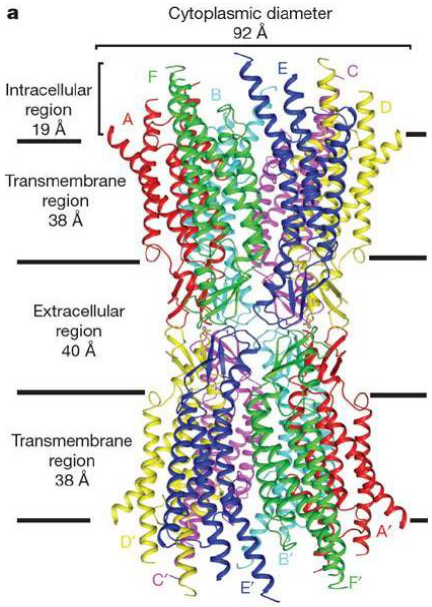

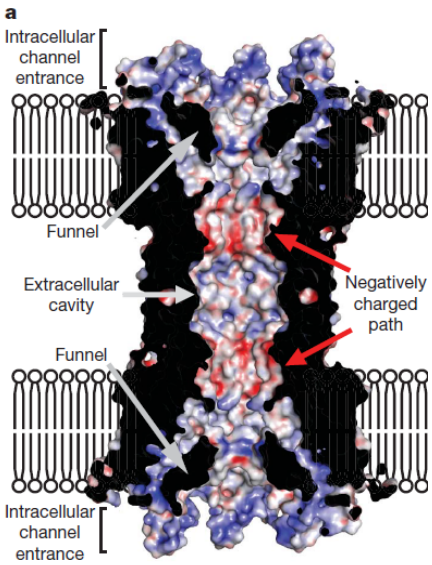

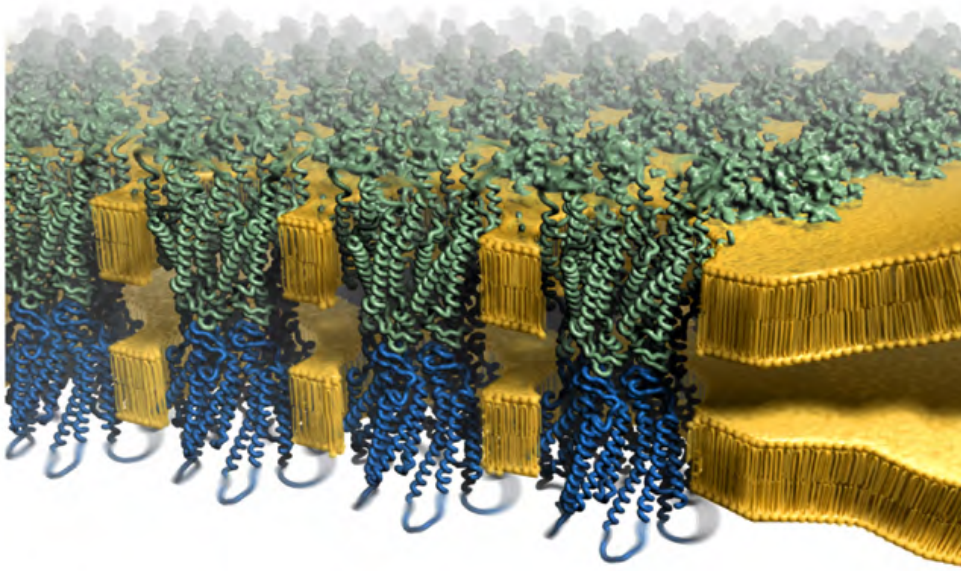

Maeda et al. *Nature 2009*

Nakagawa et al., Current Op Struc Biol 2010, 20:423–430

Connexins form gap junction channels and hemichannels

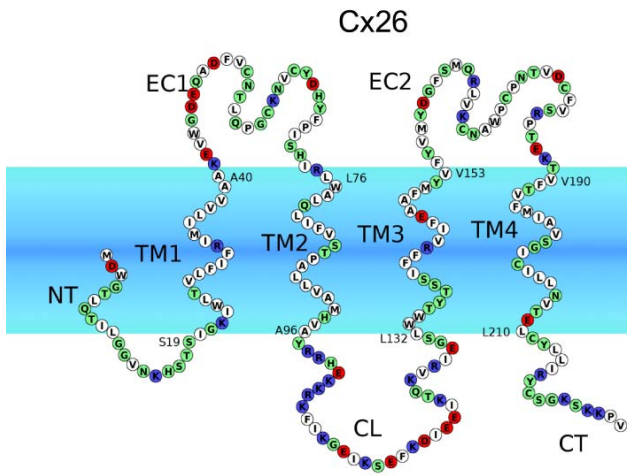

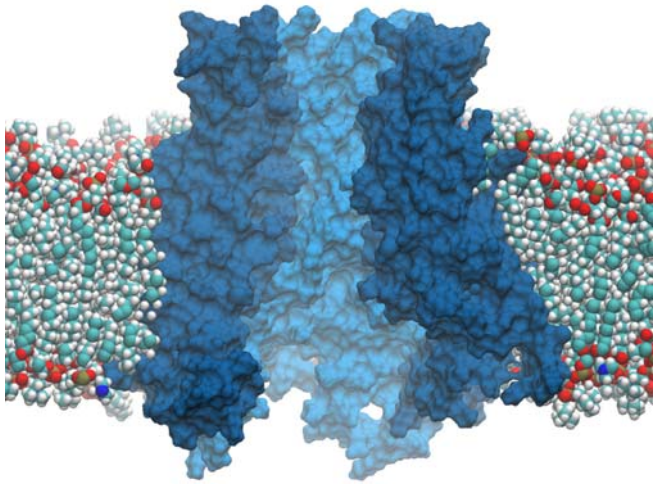

Zonta | Mammano. *J Biomolecular Structure & Dynamics* 2012

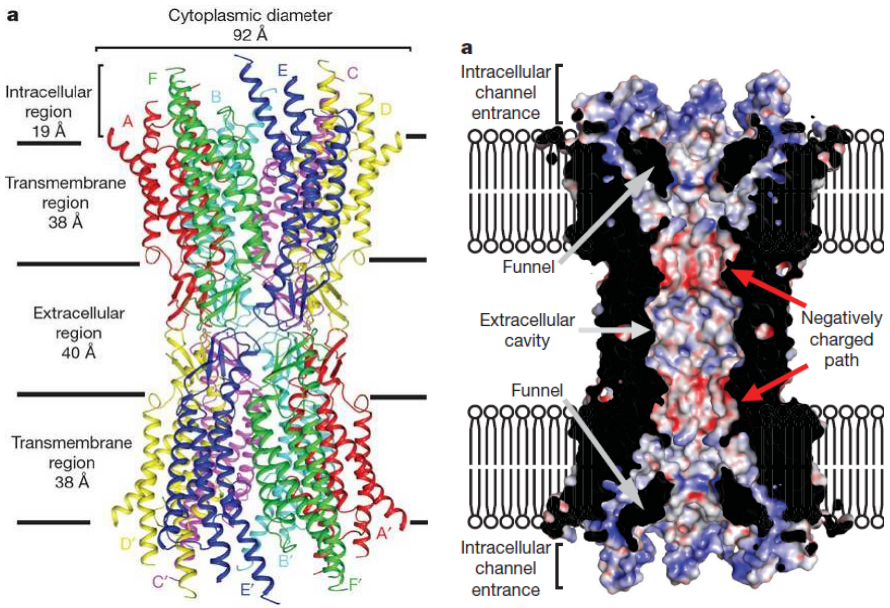

Maeda et al. *Nature 2009*

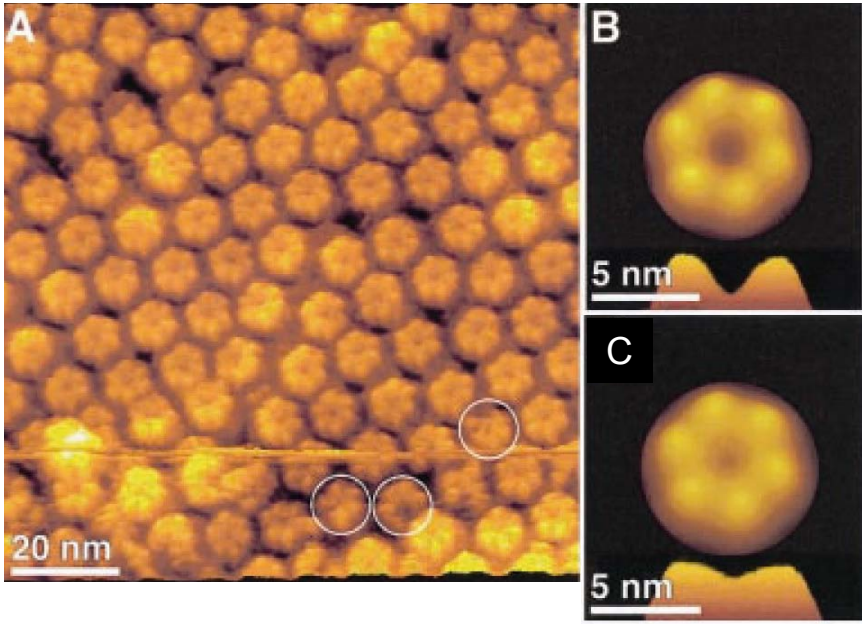

Muller | Sosinsky *The EMBO Journal* 2002

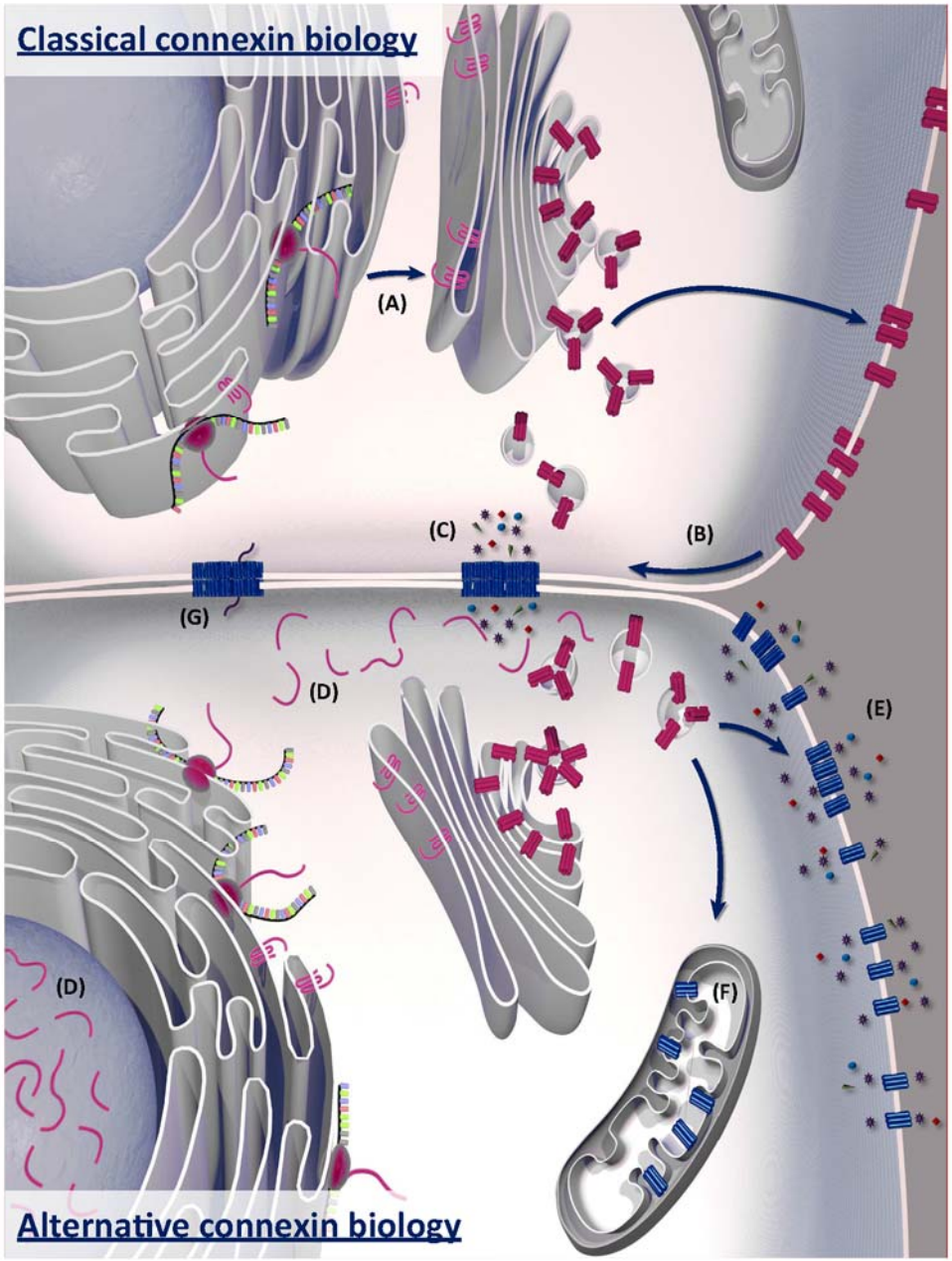

Pink depicts closed/inactive connexons while blue denotes open/active channels.

(A) Connexins are cotranslationally inserted into the endoplasmic reticulum and assemble into hexameric connexons or hemichannels in the endoplasmic reticulum or Golgi apparatus.

(B) Connexons traffic to the cell surface where they pair to form gap junctional intercellular channels, which tend to cluster into large gap junction plaques.

(C) Members of the metabolome pass through intercellular gap junction channels without exposure to the extracellular environment.

(D) In addition to full-length connexins, truncated connexin fragments may be generated through the use of internal translation initiation sites. These regulatory connexin fragments may be found within the cytoplasm, while other connexin fragments have been reported in the nucleus.

(E) Undocked hemichannels are found at the cell surface where they participate in small molecule release or uptake.

(F) Cx43 localized to the inner membrane of the mitochondria has been reported.

(G) In addition to members of the metabolome, much larger noncoding RNAs have been shown to pass through connexin channels.

The extracellular loops hold the gap junction channel together

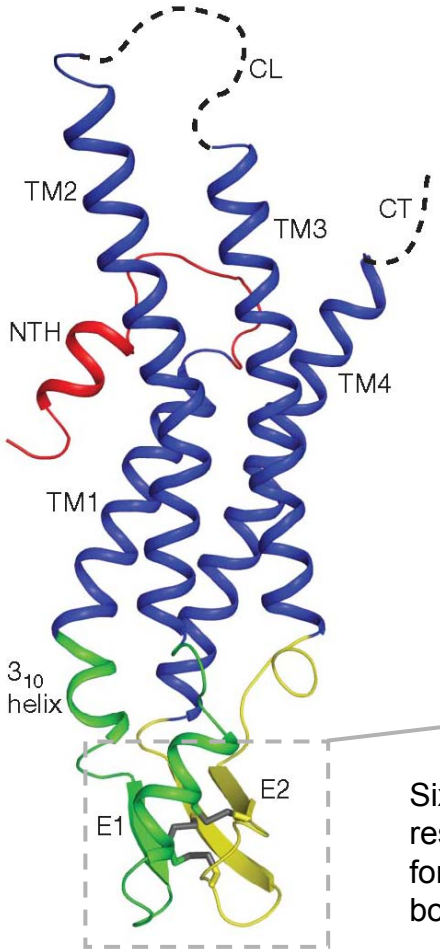

Colour code: red, NTH; blue, TM1–TM4; green, E1; yellow, E2; grey, disulphide bonds; dashed lines, cytoplasmic loop (CL) and C terminus (CT), E1 and E2 are the loops connecting TM1 and TM2, and TM3 and TM4, respectively.

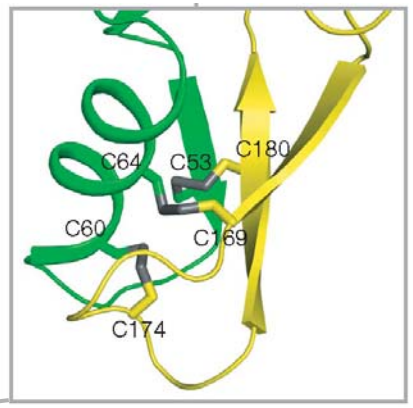

Six conserved cysteine residues, three in each loop, form intramolecular disulphide bonds between E1 and E2

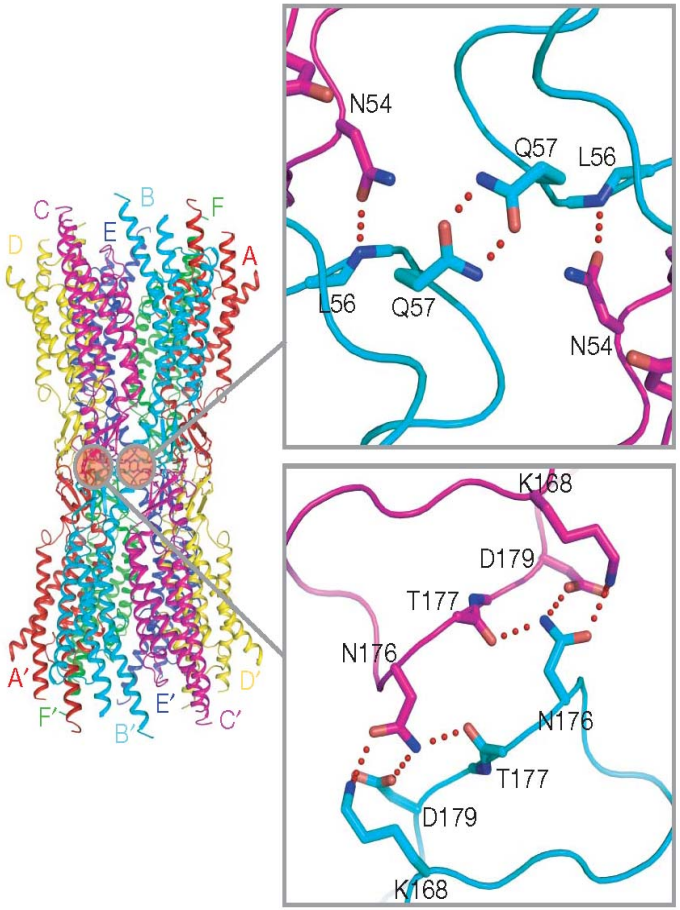

In E1, Asn 54 (N54) forms hydrogen bonds with the main-chain amide of Leu 56 (L56) in the opposite protomer, and Gln 57 (Q57) forms symmetric hydrogen bonds with the same residue of the diagonally opposite protomer.

In E2, Lys 168 (K168), Asp 179 (D179) and the main-chain carbonyl groups of Thr 177 (T177) and Asn 176 (N176) form hydrogen bonds and salt bridges with the opposite protomer.

Maeda et al. *Nature 2009*

More than 35 000 members of the metabolome are predicted to pass through gap junction channels

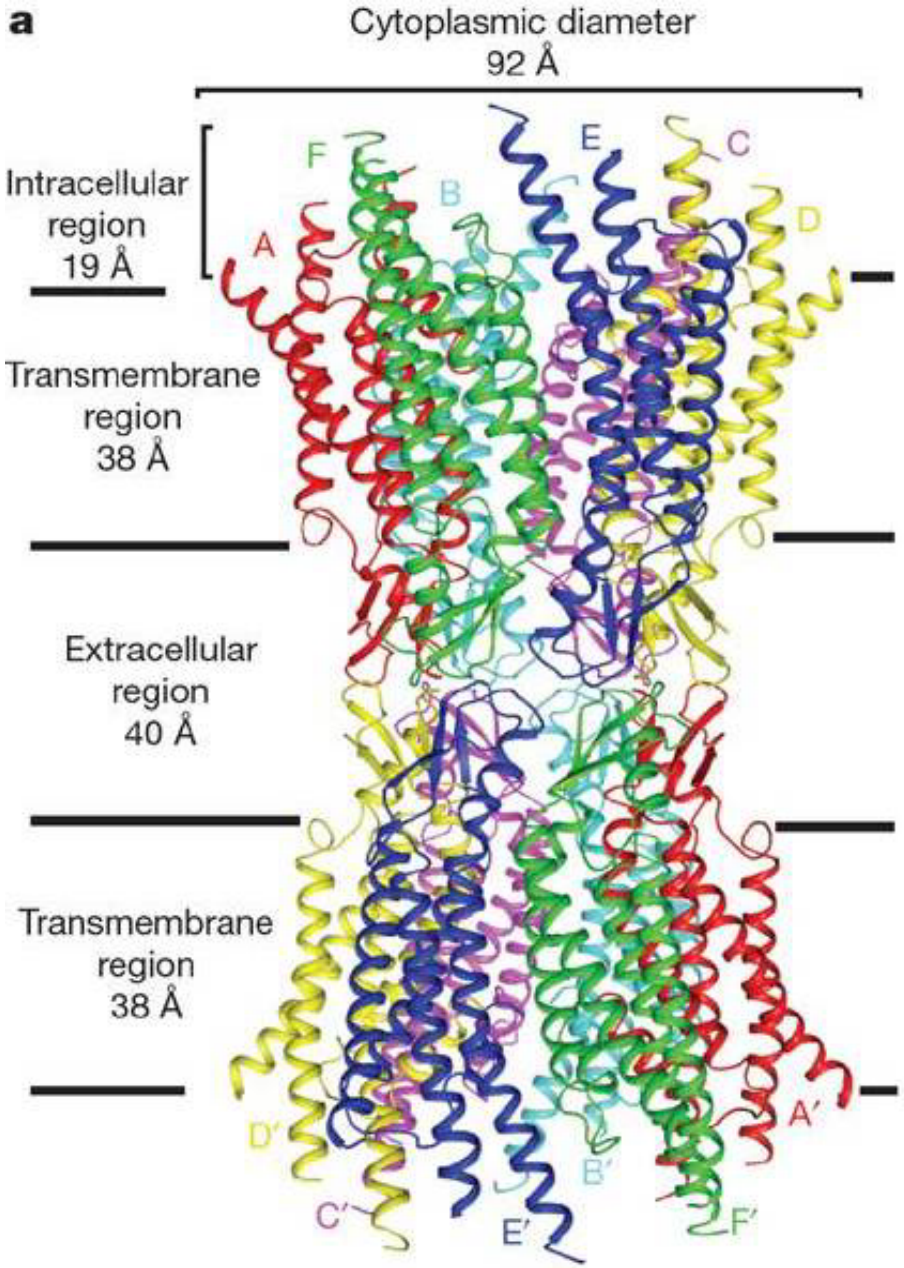

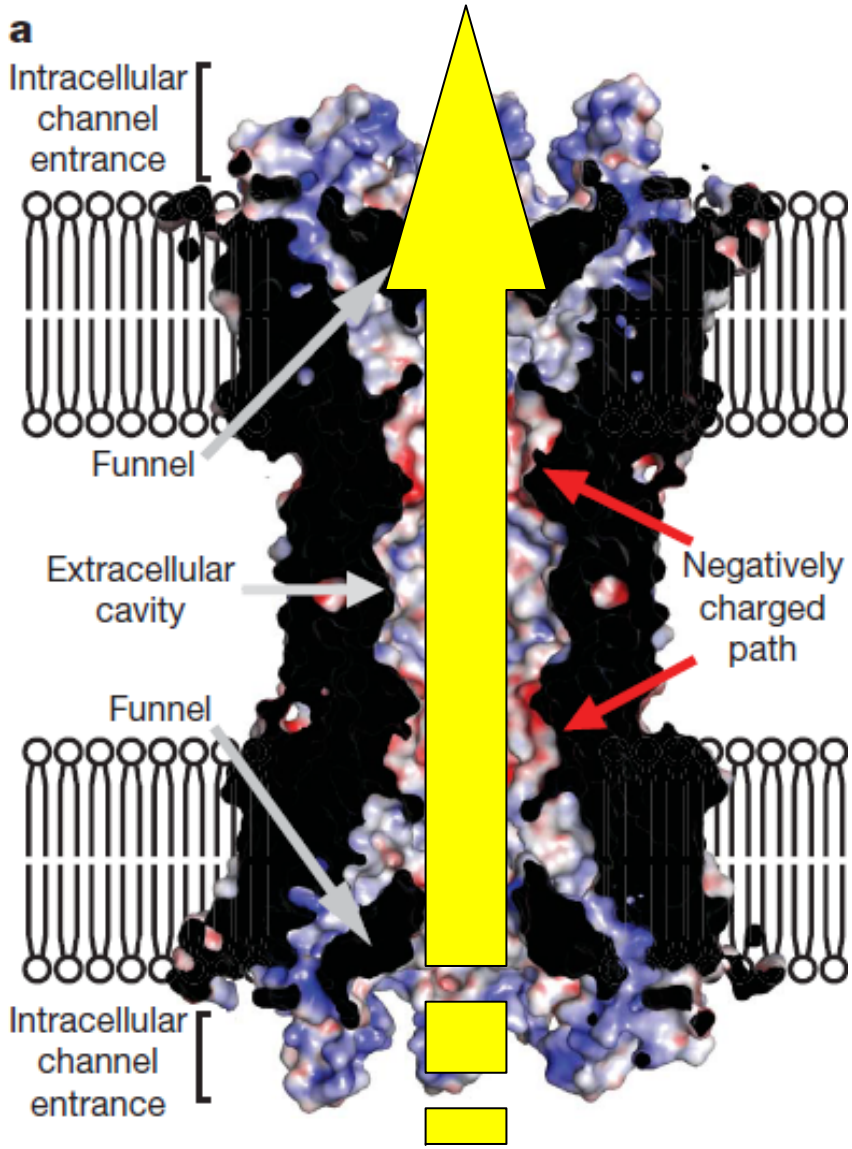

Maeda et al. *Nature 2009*

Unitary conductance of a gap junction channel measured by the dual whole cell patch clamp technique

Dual whole–cell patchclamp

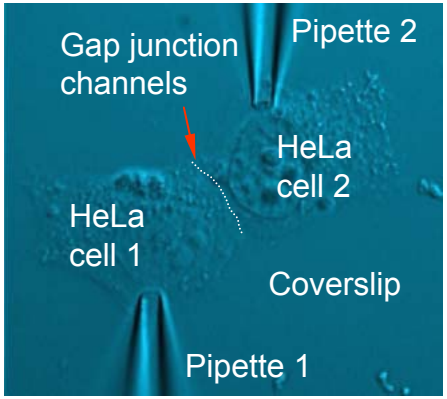

Transmitted light image

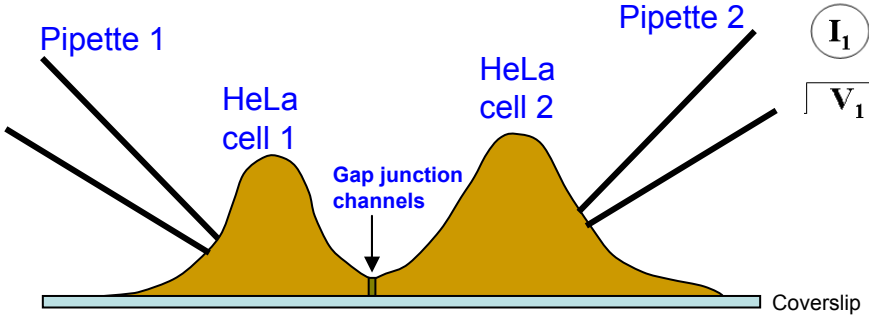

Cartoon

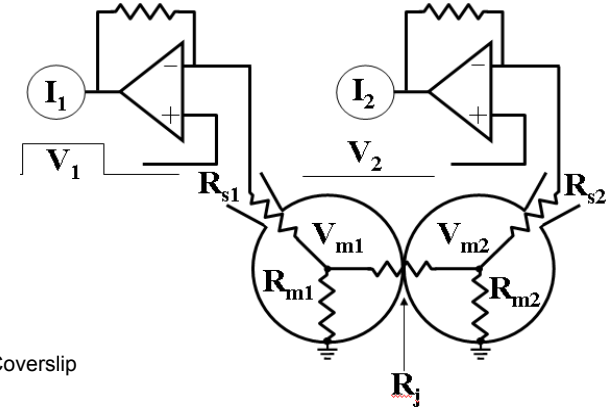

Electrical scheme

Mirror currents

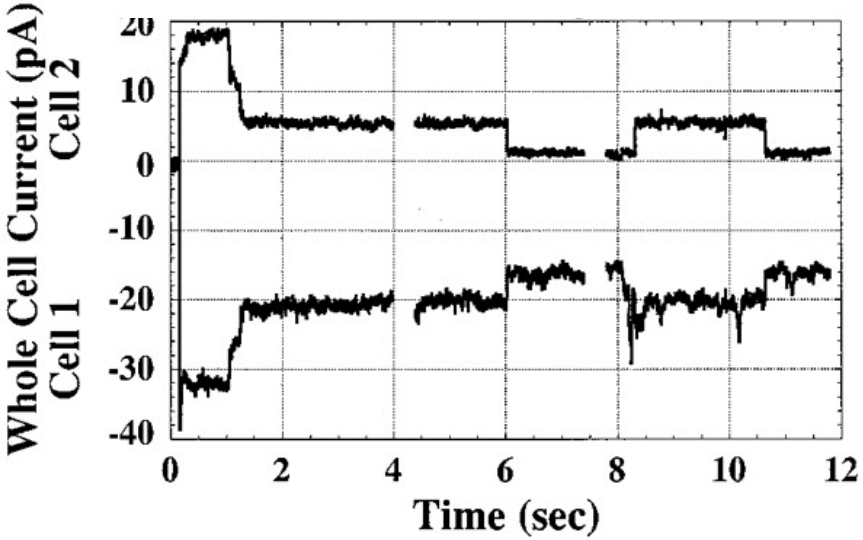

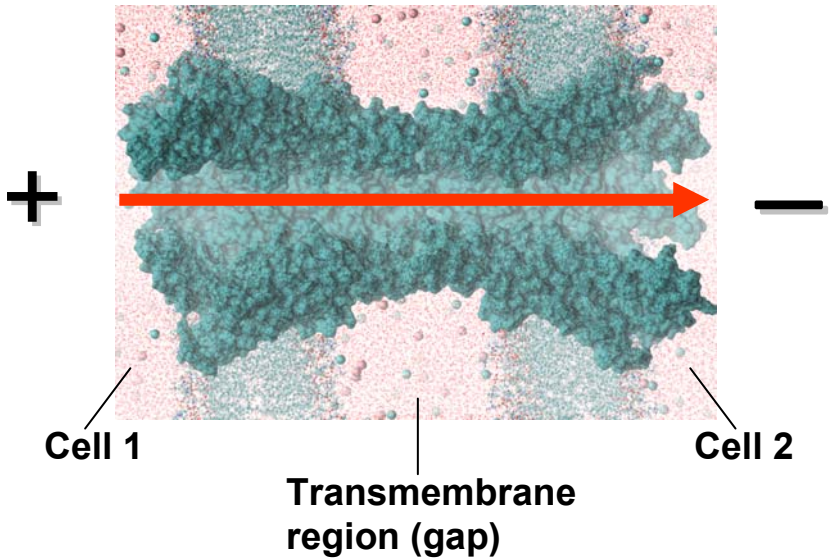

Veenstra et al. Circ Res. 1995;77:1156-1165

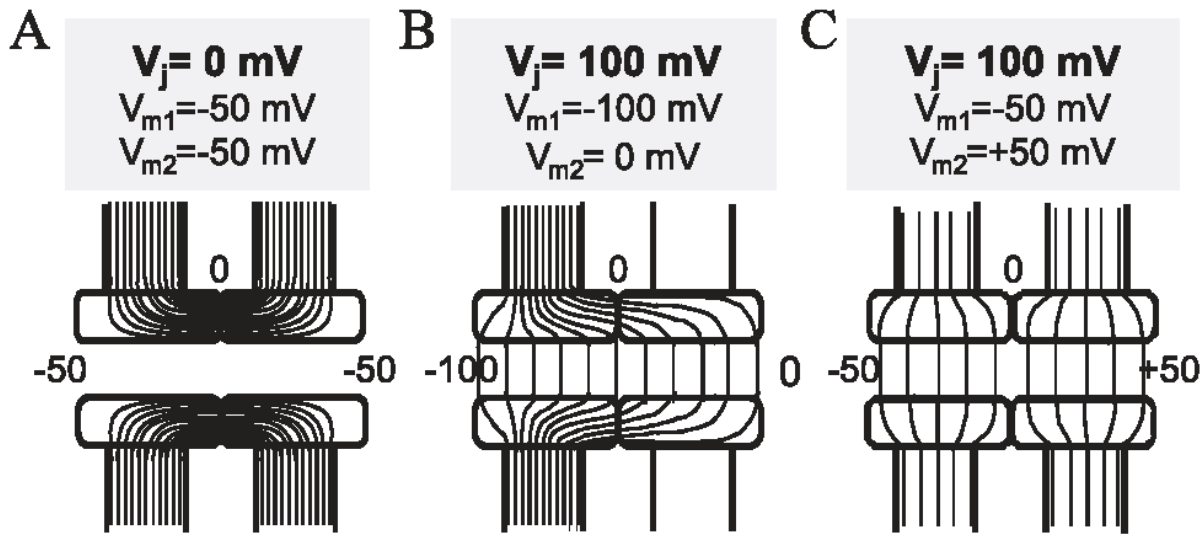

Fig. 1. Schematic representation of a GJ channel with presumed isopotential lines when both cells are held at the $V_j = 0$ mV (A), and at $V_j = 100$ mV (B & C) but at different values of V_m in each cell. In (A) the channel lumen is isopotential with cytoplasms of both cells; $V_{m1} = V_{m2} = -50$ mV. This condition establishes a strong electric field (E) or a high density of isopotential lines across the channel wall in its central region. No V_j is established and $E = 0$ along the channel pore. GJ channels that respond to this voltage profile are termed V_m-sensitive. In (B), V_{m1} differs from V_{m2} establishing a V_j and a constant E along the pore; V_m changes along the channel pore from -100 to 0 mV. In (C), the same V_j and profile of E along the channel pore are established as in (B), but with different values of V_{m1} (-50 mV) and V_{m2} (50 mV). GJ channels that respond the same way to voltage profiles in (B) and (C) are termed V_j-sensitive but not V_m-sensitive.

Voltage-dependent gating of gap junction conductance demonstrated by the dual patch clamp technique

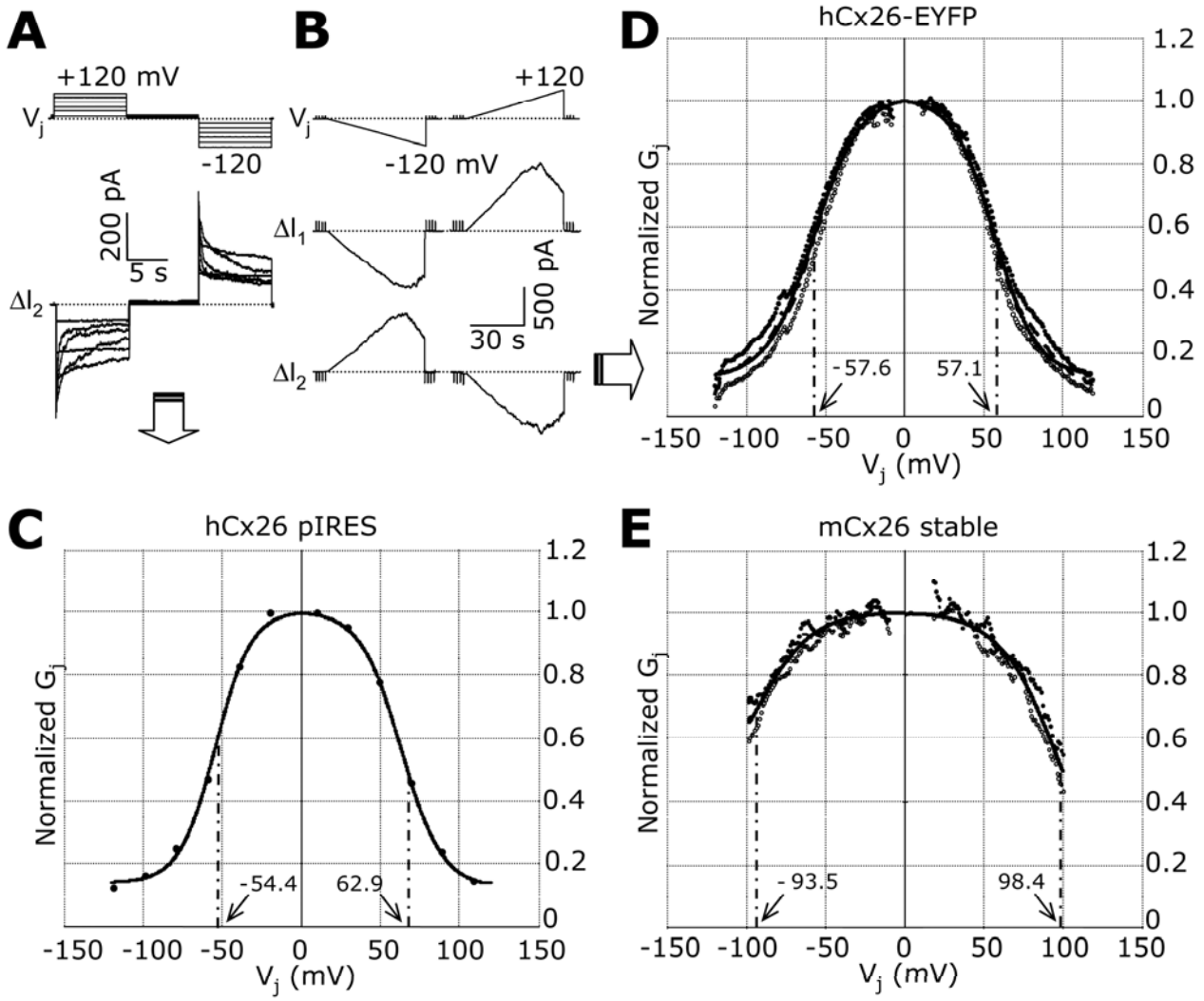

Voltage dependence of gap junction conductance in isolated HeLa cell pairs stably and transiently transfected with Cx26 and Cx30 constructs. **A**, *top*: voltage commands applied to one of two neighbouring cells (conventionally, Cell 1), each one separately patch-clamped with a different amplifier; *bottom*: junctional currents recorded from the adjacent cell (Cell 2), which was kept at the common pre-stimulus holding potential (-20 mV). Cells in A were transiently transfected with hCx26 cDNA hosted in a bicistronic vector that carried also the cDNA of EGFP. Dotted lines indicate pre-stimulus values of voltage and current, from which differences (V_j, $\Delta I2$) were measured to compute junctional conductance. **B**, *top*: voltage ramps applied to Cell 1 in a culture stably transfected with mCx26; *bottom*: whole cell currents recorded simultaneously from Cell 1 and the adjacent Cell 2, which was kept at the common pre-stimulus holding potential (-20 mV). Dotted lines indicate pre-stimulus values of voltage and current, from which differences (V_j, $\Delta I1$, $\Delta I2$) were measured to compute junctional conductance. **C**, normalised conductance Gj (*circles*) vs. transjunctional potential Vj (*abscissa*) from steady-state data in A (currents measured 10 ms before the end of each voltage step). **D**, normalised conductance (*ordinates*) vs. transjunctional voltage (*abscissa*) measured from ramp responses in cell pairs transiently transfected with the fusion product hCx26-EYFP: mean (*squares*), minima (*open circles*) and maxima (*closed circles*) of n=25 pairs. **E**, same as D for pairs stably transfected with mCx26 (n=2). Arrows in C-E point to the values of the half-inactivation voltages Vo derived by fitting the data with offset and scaled Boltzmann functions (*solid lines*). Fit parameters are provided in Tab.II. The same ramp protocol shown in B was applied to all recordings used to construct plots in D,E.

Beltramello | Mammano, *BBRC* 2003

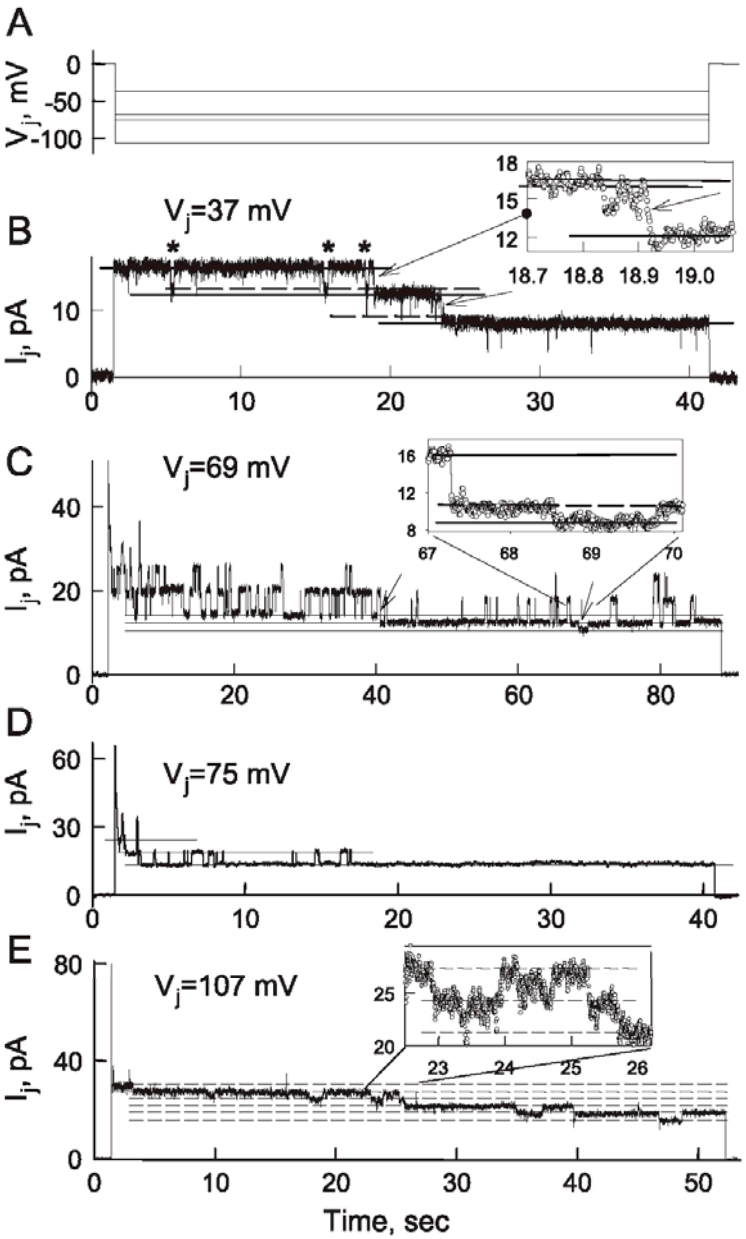

$g_j - V_j$ dependence of Cx43 at the single channel level. (A) V_j steps applied to individual cell pairs. (B – E) I_j responses to V_j steps of 37 mV (B), 69 mV (C), 75 mV (D) and 105 mV (E). With a V_j step of 37 mV (B), four channels open at the beginning of the step and two closing transitions occur between open and closed states of ~ 110 pS (arrows) during the duration of the step. Also evident are several brief transitions, ~ 85 pS in magnitude (asterisks) representing transitions to the residual conductance state (γ_{res}). An expanded time scale (inset; sampling interval 1 ms) shows that the ~ 110-pS transitions are slow, taking several milliseconds to fully close the channel. At V_j = 69 mV (C), I_j declines rapidly through stepwise transitions of 85 pS indicating that the decline in g_j is via gating to γ_{res}. One channel undergoes a full 110-pS closing transition (first arrow). Also evident is a small 30-pS slow transition ascribable to a full closure of a channel from γ_{res} (second arrow; also see inset, sampling interval, 5 ms). At V_j = 75 mV (D), all the channels rapidly close to the residual state with transitions of 85 pS. At V_j = 107 mV (E), I_j declines very rapidly to a level that corresponds to all channels residing in γ_{res} and is followed by a slow decline in I_j through stepwise 30-pS transitions corresponding to full channel closures from γ_{res}. The expanded time scale (inset; sampling interval, 2 ms) shows the 30-pS transitions to be slow, taking several milliseconds to complete. Adapted from Ref. [51].

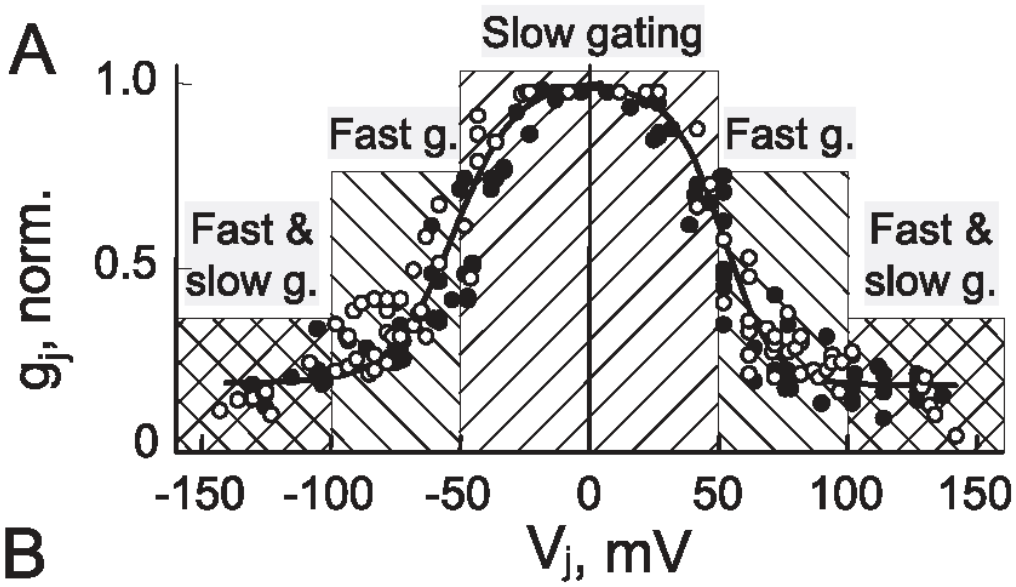

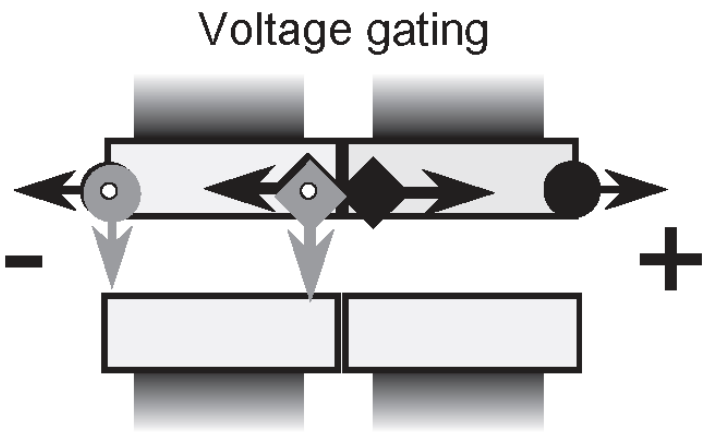

Schematics of a gap junction channel containing fast (arrow with circle) and slow (arrow with square) gates.

Potential differences between the two cell initiates gating mediated by both fast and slow gating mechanisms.

The fast gate (arrows with circle) exhibits fast gating transitions (1 ms) to the residual state, and the slow Vj gate (arrows with square) exhibits slow gating transitions (10 ms) to the fully closed state.

Cochlear supporting and epithelial cells express two major connexin isoforms

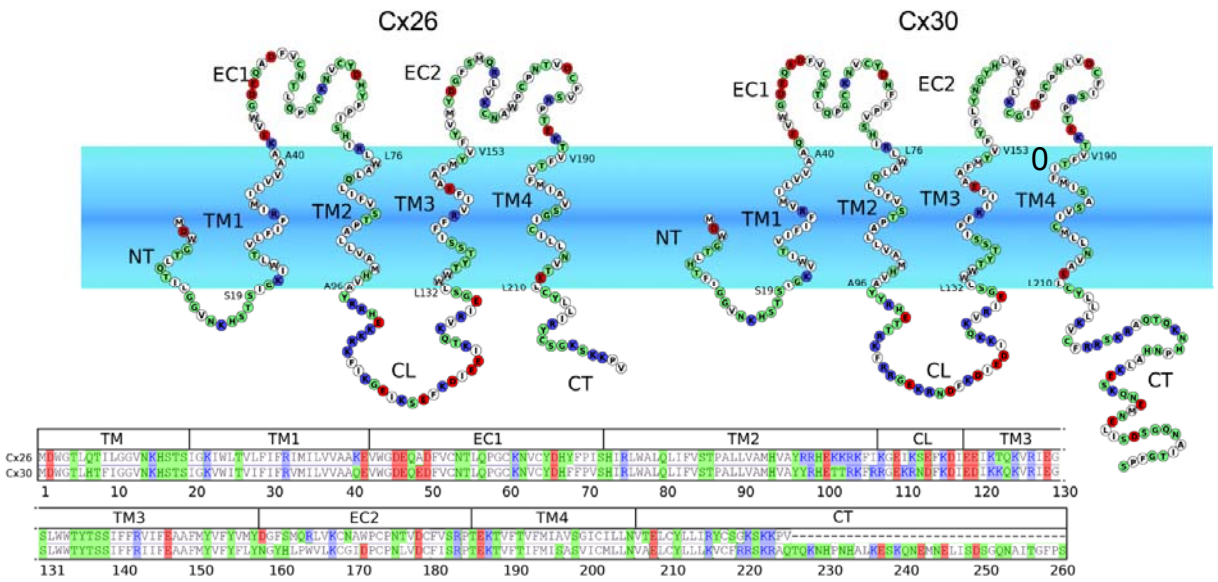

Zonta | Mammano. *J Biomolecular Structure & Dynamics* 2012

FORGE et al. THE JOURNAL OF COMPARATIVE NEUROLOGY 467:207–231 (2003)

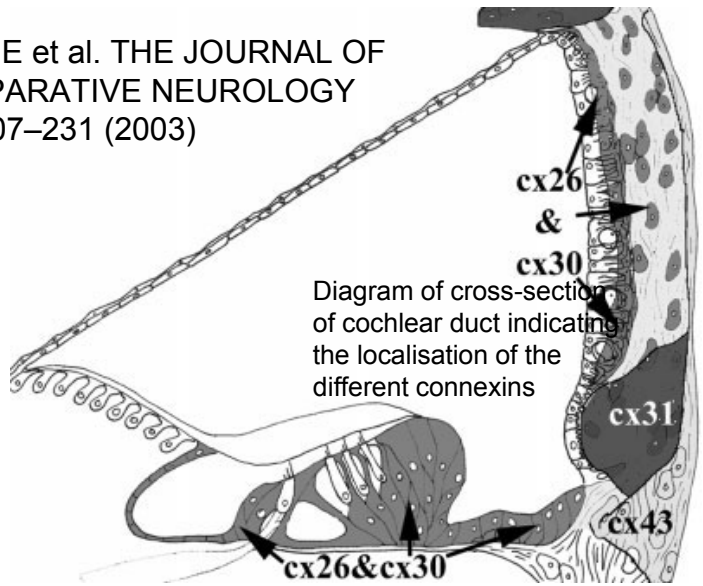

Diagram of cross-section of cochlear duct indicating the localisation of the different connexins

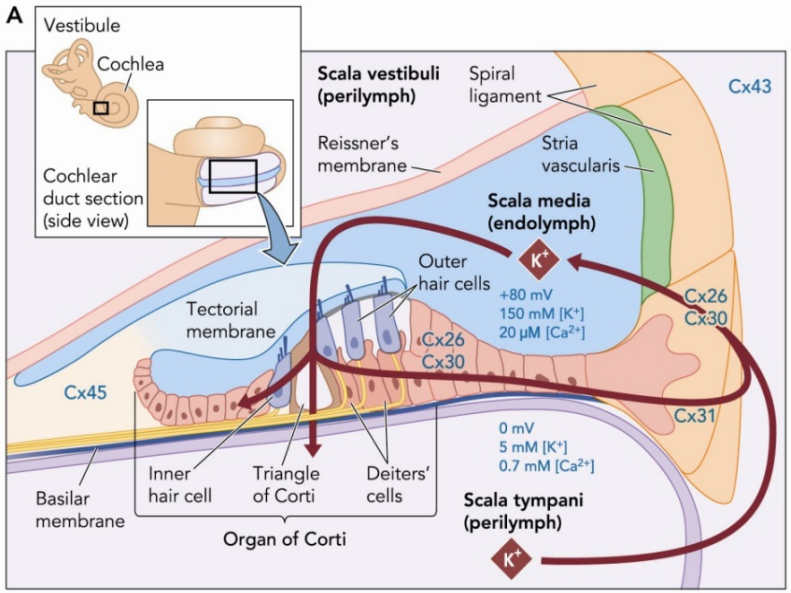

Mammano et al. *Physiology* 2007

Connexin expression in the sensory epithelium of the mouse cochlea (P6)

Midmodiolar sections

Cx26

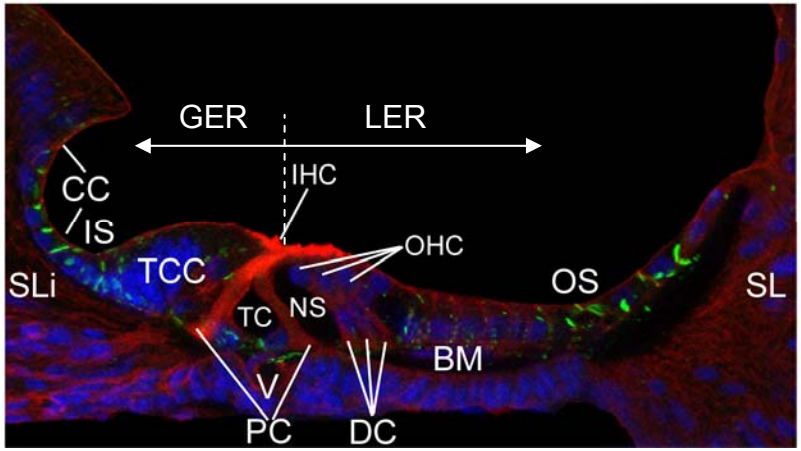

Cx30

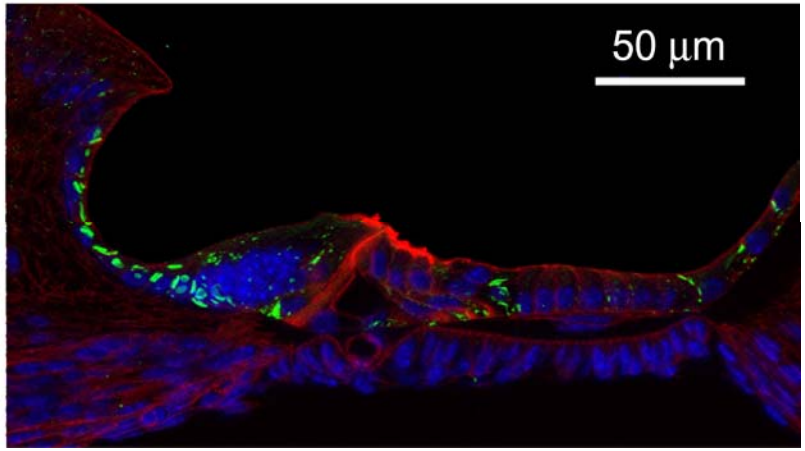

Cx/actin/nuclei

Whole mounts

GER

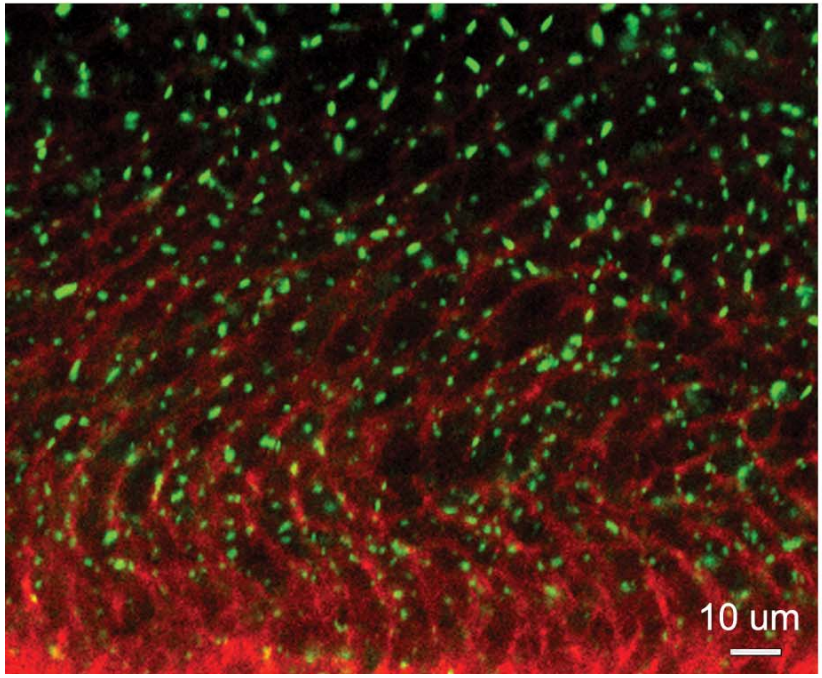

LER

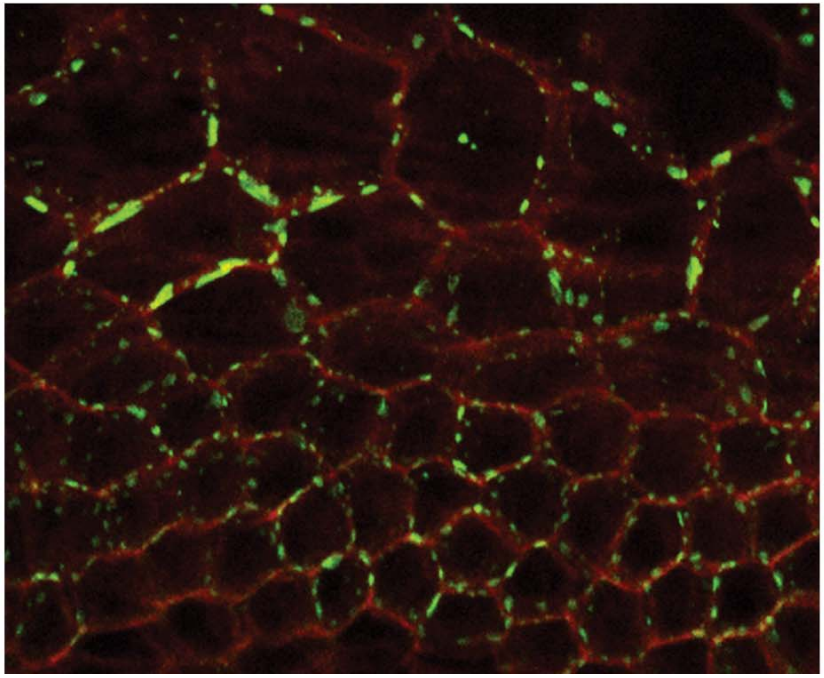

Cx26/actin

Crispino | Mammano. *PlosOne* 2011

Mutations in Cx26 are the primary cause of prelingual inherited deafness

letters to nature

NATURE | VOL 387 | 1 MAY 1997

Connexin 26 mutations in hereditary non-syndromic sensorineural deafness

D. P. Kelsell*†, J. Dunlop*, H. P. Stevens*, N. J. Lench‡, J. N. Liang§, G. Parry‖, R. F. Mueller‡ & I. M. Leigh*

* Academic Department of Dermatology, St Bartholomew's and the Royal London School of Medicine and Dentistry, Queen Mary and Westfield College, 2 Newark Street, London E1 2AT, UK
‡ Molecular Medicine Unit, St James's University Hospital, Leeds LS9 7TF, UK
§ The Temporal Bone Laboratory, The Institute of Laryngology and Otology, University College London, 330/332 Gray's Inn Road, London, WC1X 8EE, UK
‖ Department of Paediatrics, St Luke's Hospital, Bradford, BD5 0NA, UK

Severe deafness or hearing impairment is the most prevalent inherited sensory disorder, affecting about 1 in 1,000 children[1]. Most deafness results from peripheral auditory defects that occur as a consequence of either conductive (outer or middle ear) or sensorineuronal (cochlea) abnormalities. Although a number of mutant genes have been identified that are responsible for syndromic (multiple phenotypic disease) deafness such as Waardenburg syndrome and Usher 1B syndrome[2–4], little is known about the genetic basis of non-syndromic (single phenotypic disease) deafness. Here we study a pedigree containing cases of autosomal dominant deafness and have identified a mutation in the gene encoding the gap-junction protein connexin 26 (Cx26) that segregates with the profound deafness in the family. Cx26 mutations resulting in premature stop codons were also found in three autosomal recessive non-syndromic sensorineuronal deafness pedigrees, genetically linked to chromosome 13q11–12 (DFNB1), where the Cx26 gene is localized. Immunohistochemical staining of human cochlear cells for Cx26 demonstrated high levels of expression. To our knowledge, this is the first non-syndromic sensorineural autosomal deafness susceptibility gene to be identified, which implicates Cx26 as an important component of the human cochlea.

Human Molecular Genetics, 1997, Vol. 6, No. 9 1605–1609

Connexin26 mutations associated with the most common form of non-syndromic neurosensory autosomal recessive deafness (DFNB1) in Mediterraneans

Leopoldo Zelante, Paolo Gasparini, Xavier Estivill[1], Salvatore Melchionda, Leonardo D'Agruma, Nancy Govea[2], Monserrat Milá[2], Matteo Della Monica[3], Jaber Lutfi[4], Mordechai Shohat[4], Elaine Mansfield[5], Kathleen Delgrosso[6], Eric Rappaport[7], Saul Surrey[6] and Paolo Fortina[7,8,*]

nature International weekly journal of science

Search This journal

Journal home > Archive > Scientific Correspondence > Full Text

- Journal home
- Advance online publication
- Current issue
- Nature News
- Archive

Scientific Correspondence

Nature 393, 319-320 (28 May 1998) | doi:10.1038/30639

Connexin 26 gene linked to a dominant deafness

Françoise Denoyelle[1], Genevieve Lina-Granade[2], Henri Plauchu[2], Roberto Bruzzone[3], Hassan Chaïb[4], Fabienne Lévi-Acobas[4], Dominique Weil[4] and Christine Petit[4]

Cx26$^{Otog\text{-}Cre}$ and Cx30 KO mice are deaf

Current Biology, Vol. 12, 1106–1111, July 9, 2002, ©2002 Elsevier Science Ltd. All rights reserved. PII S0960-9822(02)00904-1

Targeted Ablation of Connexin26 in the Inner Ear Epithelial Gap Junction Network Causes Hearing Impairment and Cell Death

Martine Cohen-Salmon,[1,6] Thomas Ott,[2,6] Vincent Michel,[1] Jean-Pierre Hardelin,[1] Isabelle Perfettini,[1] Michel Eybalin,[3] Tao Wu,[4] Daniel C. Marcus,[4] Philine Wangemann,[4] Klaus Willecke,[2] and Christine Petit[1,5]
[1]Unité de Génétique des Déficits Sensoriels
CNRS URA 1968
Institut Pasteur
25 rue du Dr. Roux
75724 Paris cedex 15
France
[2]Institut für Genetik
Abt. Molekulargenetik
Universität Bonn
53117 Bonn
Germany
[3]Neurobiologie de l'Audition
INSERM U254
Université Montpellier I
71 rue de Navacelles
34090 Montpellier cedex
France
[4]Department of Anatomy and Physiology
College of Veterinary Medicine
Kansas State University
1600 Denison Avenue
Manhattan, Kansas 66506

Results and Discussion

Generation of Cx26-Deficient Mice in the Epithelial Gap Junction Network of the Inner Ear

In the inner ear, gap junctions assemble into two independent cellular networks, i.e., the epithelial and connective tissue gap junction networks [7, 8] (see Figure 1). Cx26 seems to be present in all gap junctions of both networks [7, 8]. To specifically inactivate *Cx26* in the epithelial gap junction network of the inner ear, which is composed of supporting cells of the sensory hair cells and flanking epithelial cells, we generated two recombinant mouse lines (Figure 2). *Cx26$^{loxP/loxP}$* mice were obtained by homologous recombination in embryonic stem (ES) cells. In these mice, the *Cx26* coding exon (exon II) and the neo selection marker are flanked by *loxP* sites (Figures 2A–2C). The *Otog-Cre* mouse line was obtained by transgenesis using a recombinant bacterial artificial chromosome (BAC) containing the *Cre* gene under the control of the murine *Otog* promoter. *Otog* is exclusively transcribed in the inner ear [9]. *Otog* expression is detected as early as embryonic day 10 (E10) in the otic vesicle and at E18 in all cells of the gap junction epithelial network [10].

Cx26$^{loxP/loxP}$ and *Otog-Cre* mice were both viable and had no hearing loss, and the distribution of Cx26 in the inner ear was identical to that of wild-type mice (see Figure 2F). *Otog-Cre* mice were crossed with *Cx26$^{loxP/loxP}$* mice. In *Cx26$^{loxP/loxP}$OtogCre* (abbreviated *Cx26^{OtogCre}*) double transgenic mice, from birth onward, Cx26 was

Human Molecular Genetics, 2003, Vol. 12, No. 1 13–21
DOI: 10.1093/hmg/ddg001

Connexin30 (Gjb6)-deficiency causes severe hearing impairment and lack of endocochlear potential

Barbara Teubner[1,†], Vincent Michel[2], Jörg Pesch[3], Jürgen Lautermann[4], Martine Cohen-Salmon[2], Goran Söhl[1], Klaus Jahnke[4], Elke Winterhager[5], Claus Herberhold[3], Jean-Pierre Hardelin[2], Christine Petit[2] and Klaus Willecke[1,*]

PNAS

Connexin30 deficiency causes instrastrial fluid–blood barrier disruption within the cochlear stria vascularis

Martine Cohen-Salmon*†‡§, Béatrice Regnault¶, Nadège Cayet‖, Dorothée Caille**, Karine Demuth††, Jean-Pierre Hardelin*†, Nathalie Janel‡‡, Paolo Meda**, and Christine Petit*†

*Unité de Génétique des Déficits Sensoriels, Unité Mixte de Recherche S 587, Institut National de la Santé et de la Recherche Médicale, ¶Plate-Forme Puces à ADN, and ‖Plate-Forme Microscopie Électronique, Institut Pasteur, 25 Rue du Docteur Roux, 75724 Paris Cedex 15, France; †Chaire de Génétique et Physiologie Cellulaire, Collège de France, 75005 Paris, France; **Département de Physiologie Cellulaire et Métabolisme, Ecole de Médecine, Université de Genève, 1 Rue Michel Servet, CH-1211 Geneva 4, Switzerland; ††Laboratoire de Biochimie Cardiovasculaire, Hôpital Européen Georges Pompidou, AP-HP, 75015 Paris, France; and ‡‡EA 3508, Université Paris 7-Denis Diderot, Case 7104, 2 Place Jussieu, 75251 Paris Cedex 5, France

Edited by Michael V. L. Bennett, Albert Einstein College of Medicine, Bronx, NY, and approved February 16, 2007 (received for review June 19, 2006)

More than 250 missense, nonsense, frame-shift, insertion and deletion mutations in Cx26 linked to deafness, of which 26 recessive mutations linked to both deafness and skin disorders

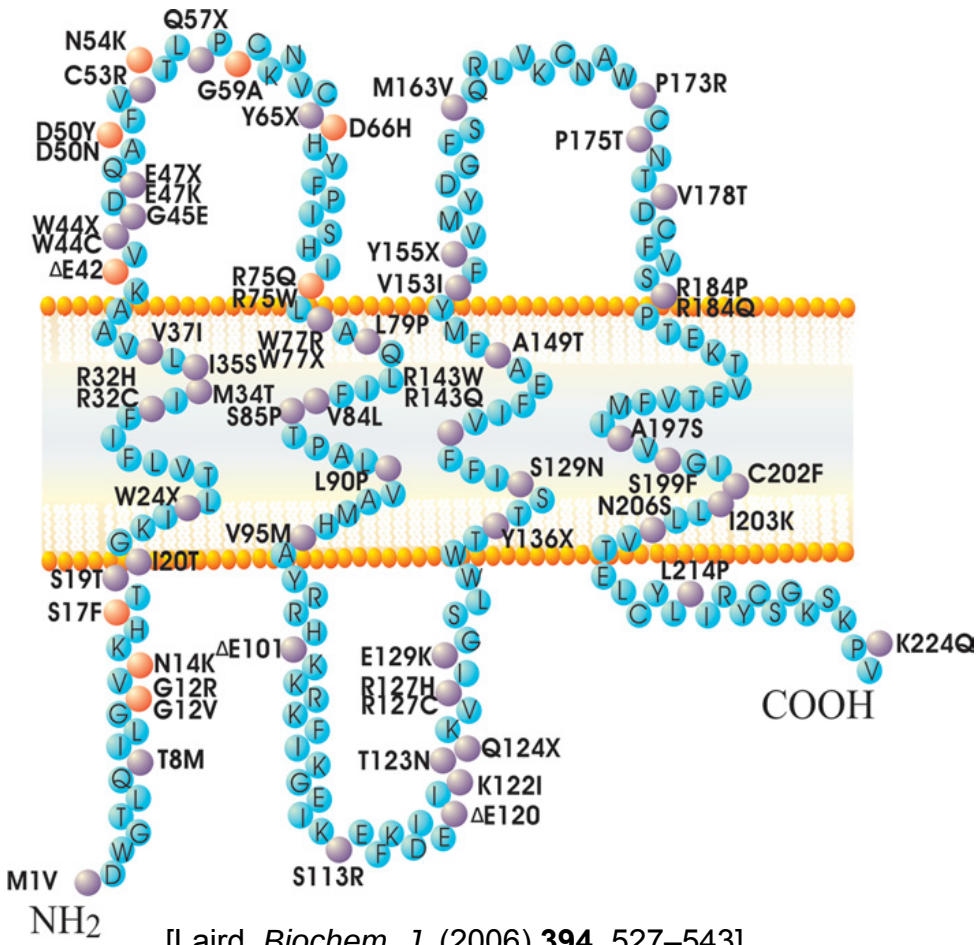

[Laird, *Biochem. J.* (2006) **394**, 527–543]

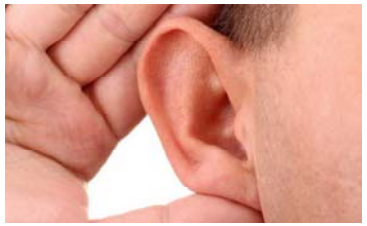

http://cdn.ent-surgery.com.au/

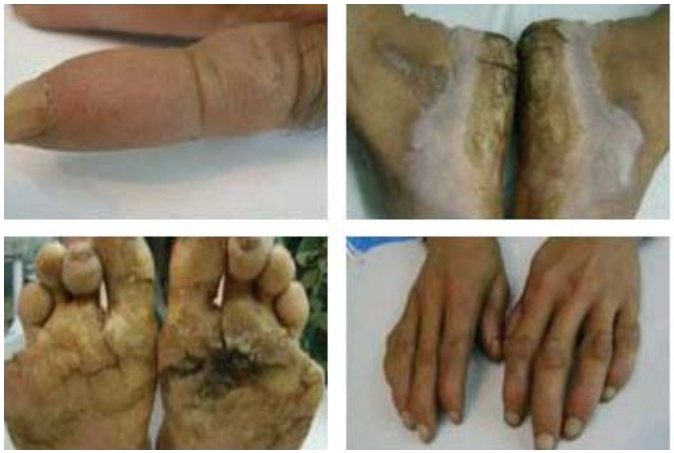

Patients with Vohwinkel syndrome

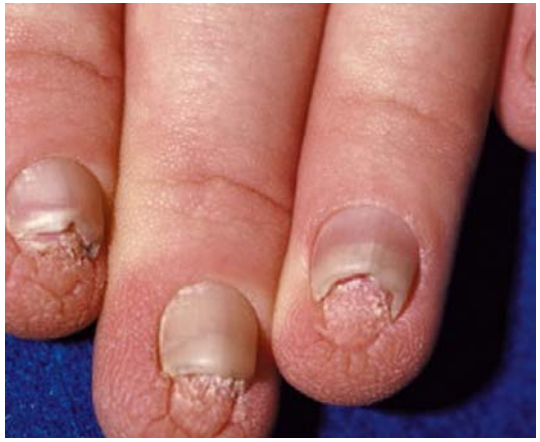

Clouston syndrome

[Ashamulova, *International J Dermatol* 2014, 53, 192–205]

Deafness–related M34T mutation of connexin 26

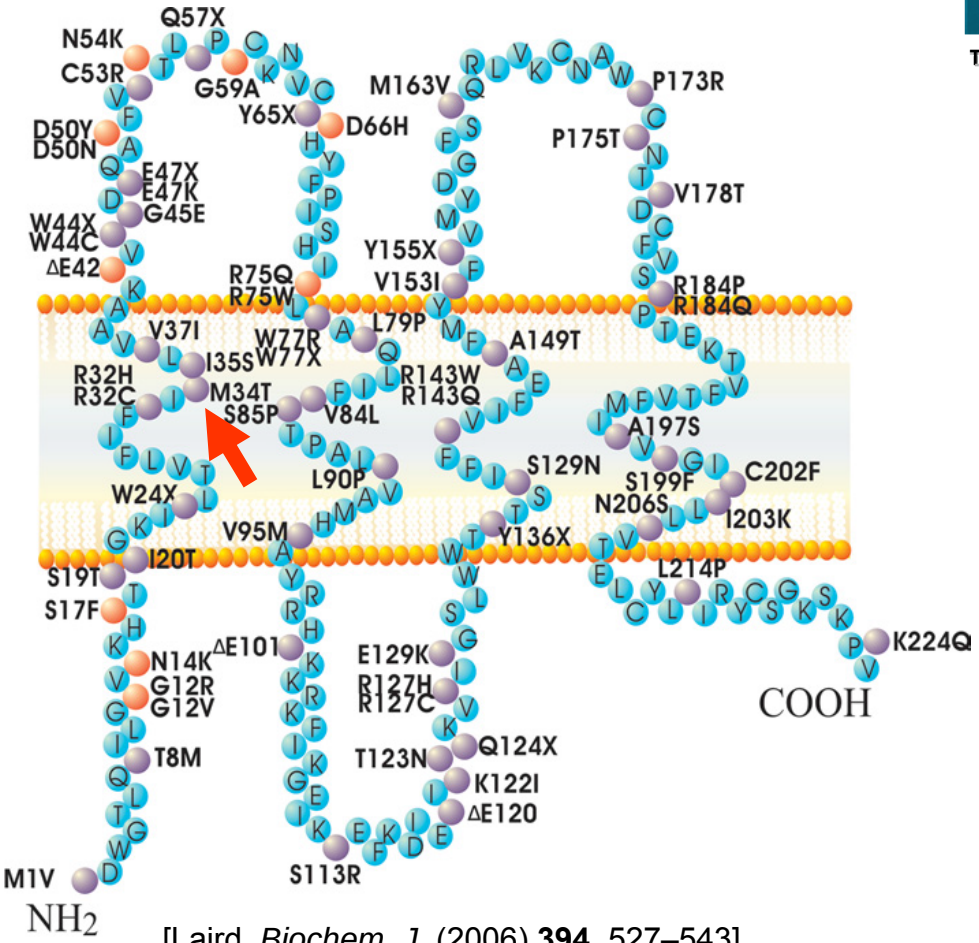

[Laird, *Biochem. J.* (2006) **394**, 527–543]

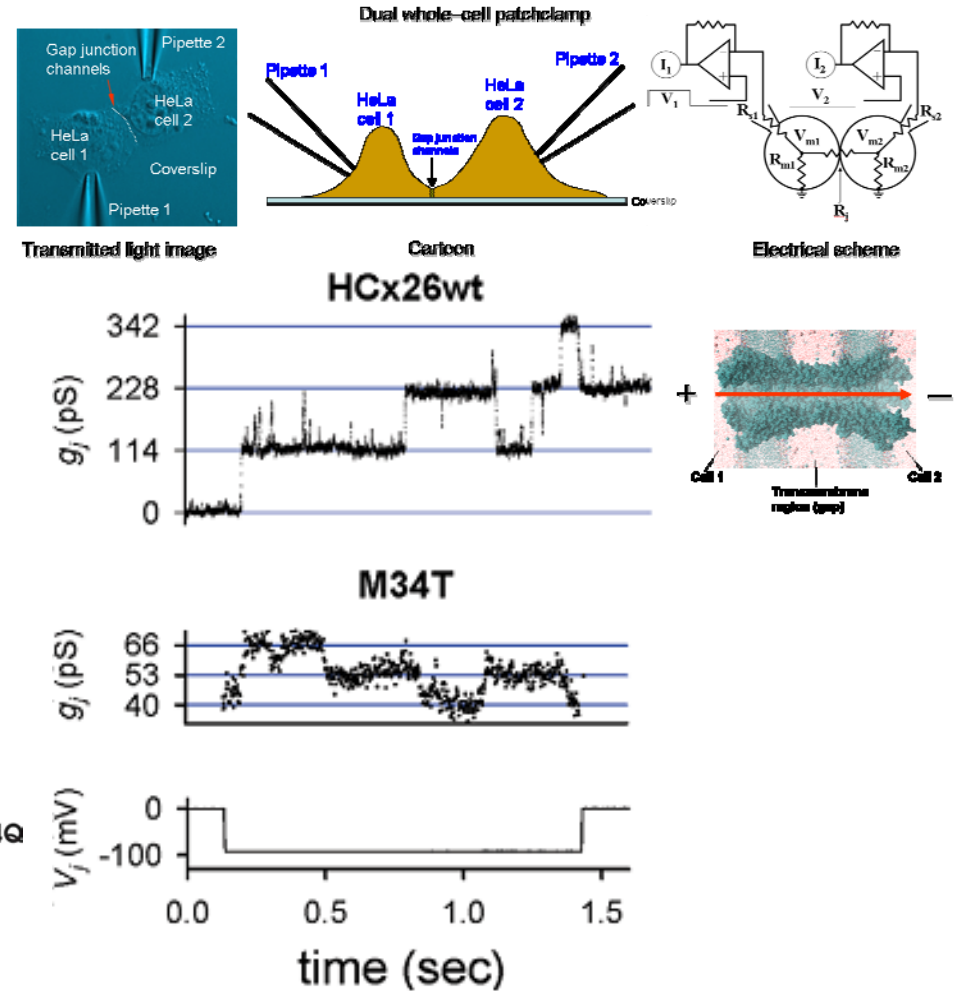

	Unitary conductance
Wild type channel (WT)	114 pS
M34T mutant channel	13 pS
Ratio M34T/WT	11.4%

Bicego | Mammano, *Human Mol Genetics* 2006

Molecular Dynamics Model of a Cx26 Hemichannel

206.188 atoms

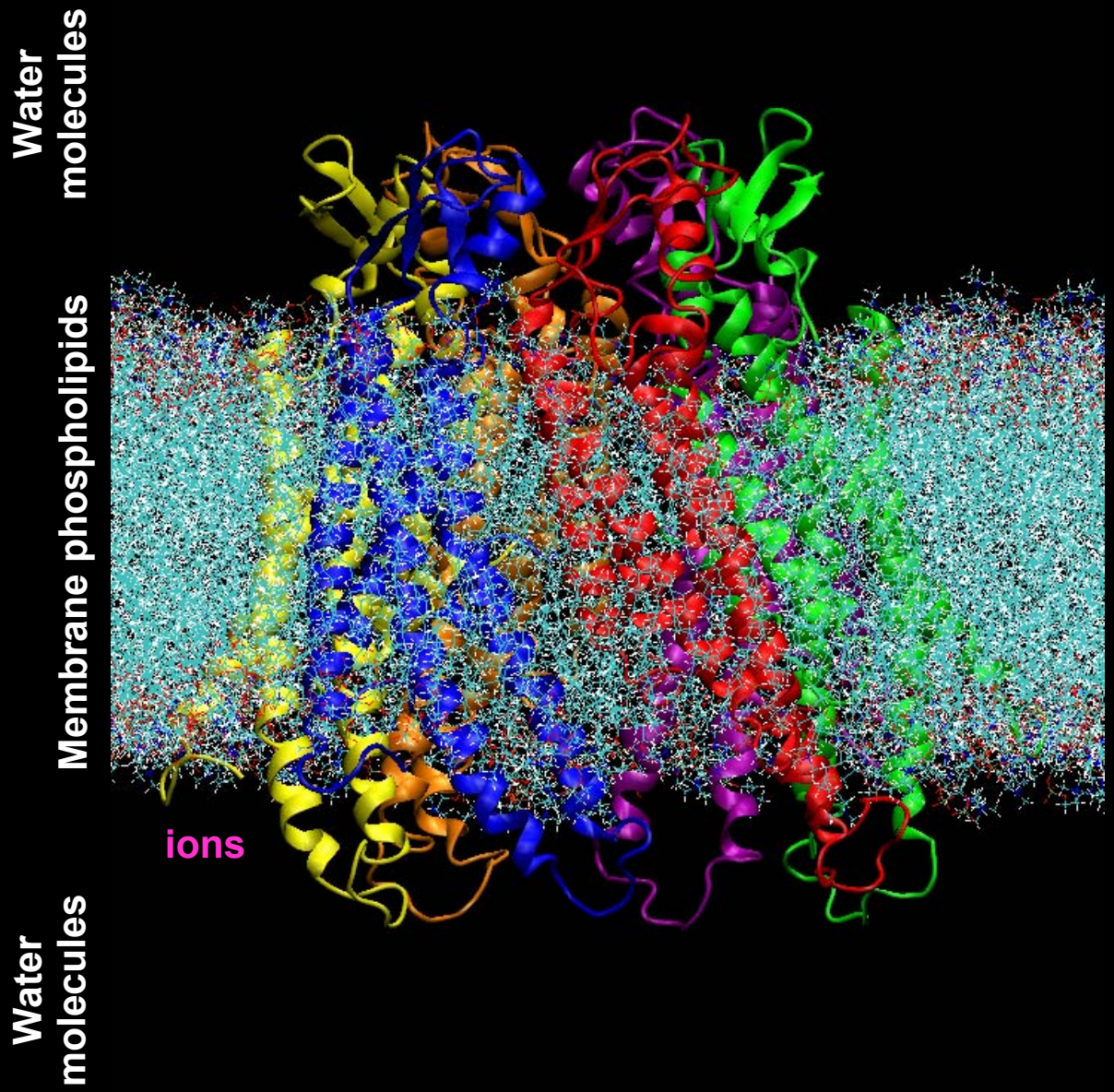

Zonta | Mammano, *J Biomolecular Structure and Dynamics* 2012

MD model of a Cx26 WT connexon

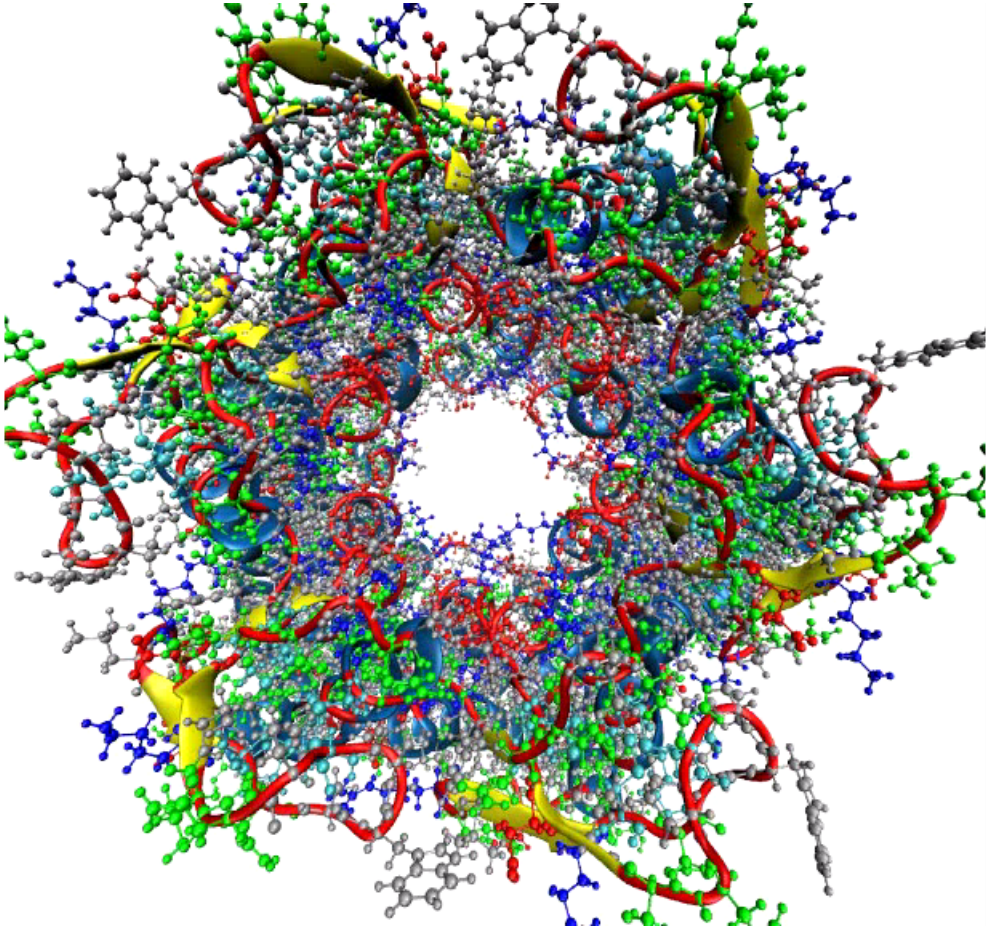

MAIN CHAIN

- Alpha Helix
- Beta strands
- Turn/Coil

SIDE CHAINS

- Acidic
- Basic
- Hydrophobic
- Polar

Zonta | Mammano, *J Biomolecular Structure and Dynamics* 2012

In the wild type channel, Met 34 (purple) in the first transmebrane helix (TM1) interacts hydrophobically with Trp 3 (blue) in the N-terminal helix of the adjacent connexin

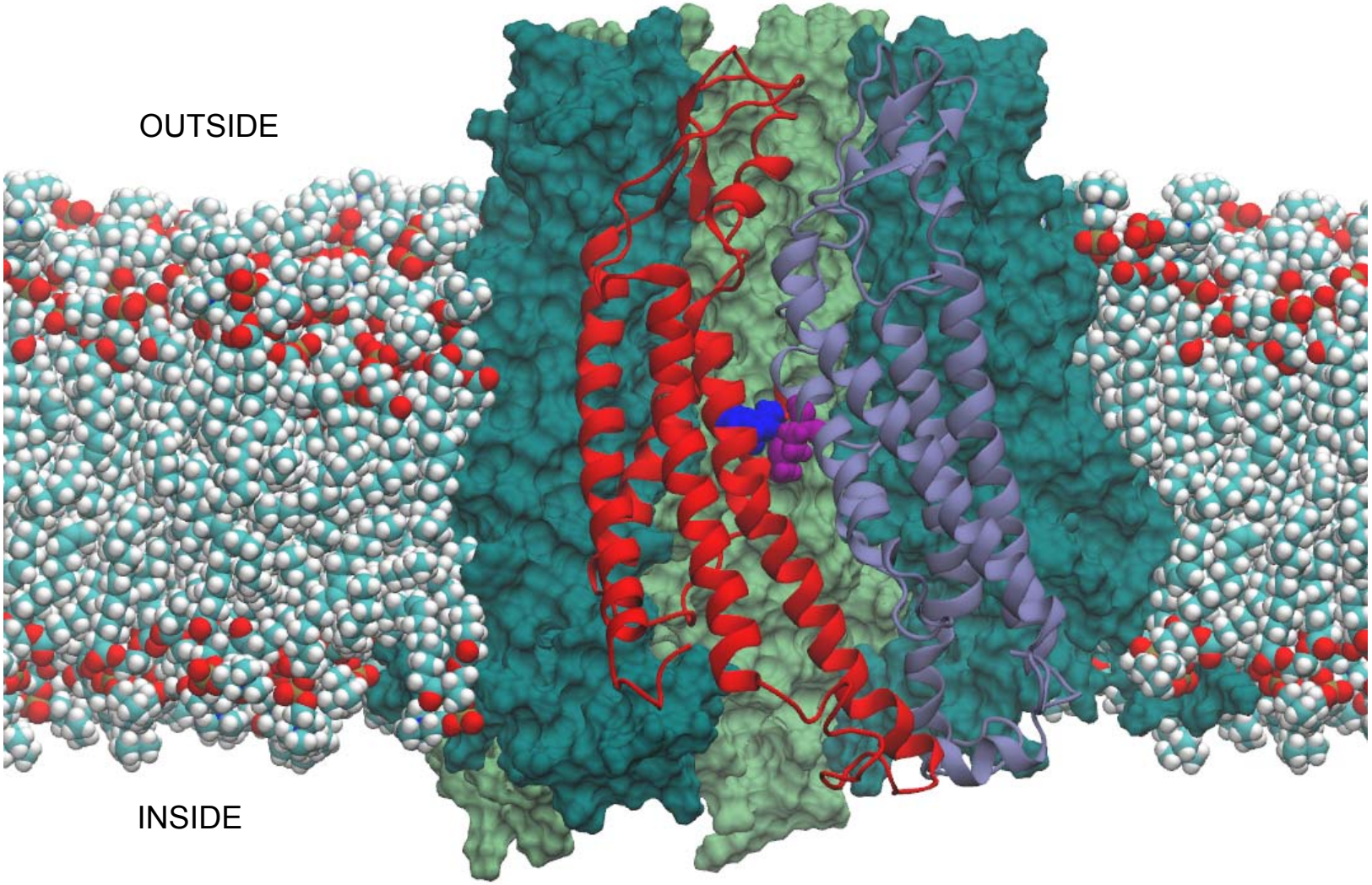

Zonta | Mammano, *Frontiers in Physiology* 2014

Molecular dynamics simulations highlight structural and functional alterations in deafness–related M34T mutation of connexin 26

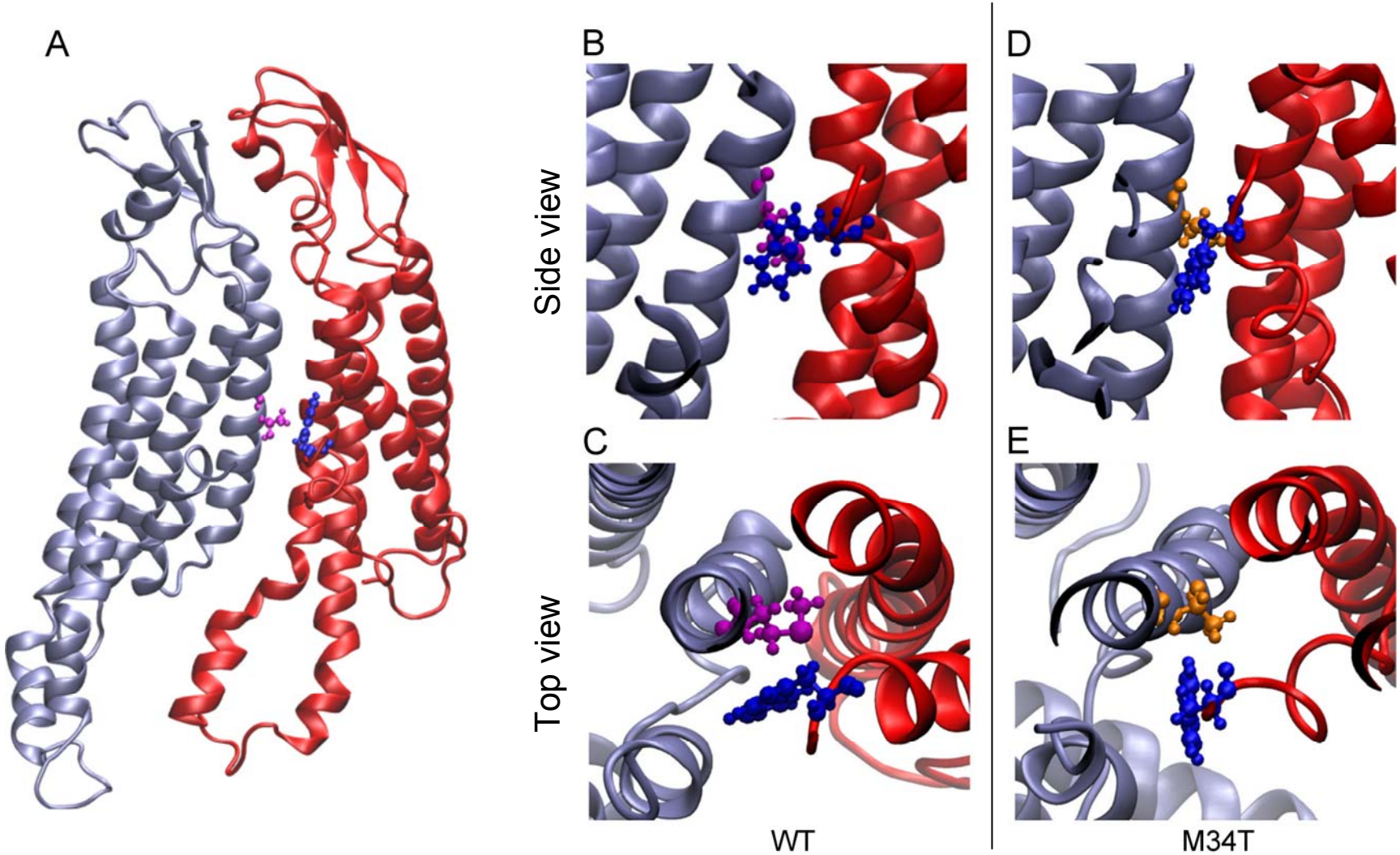

In the wild type channel Met34 (purple) in the first transmebrane helix (TM1) interacts hydrophobically with Trp3 (blue) in the N-terminal helix of the adjacent connexin.

The hydrophobic interaction between Met34 (purple) and Trp3 (blue) disappears when the hydrophobic Met is replaced by a polar Thr (gold) in position 34 (M34T mutation).

Zonta | Mammano, *Frontiers in Physiology* 2014

The M34T mutation destabilizes the NTH binding to the cytoplasmic mouth of the channel altering its shape, which is significantly more asymmetric in the mutant hemichannel model compared to the wild type model.

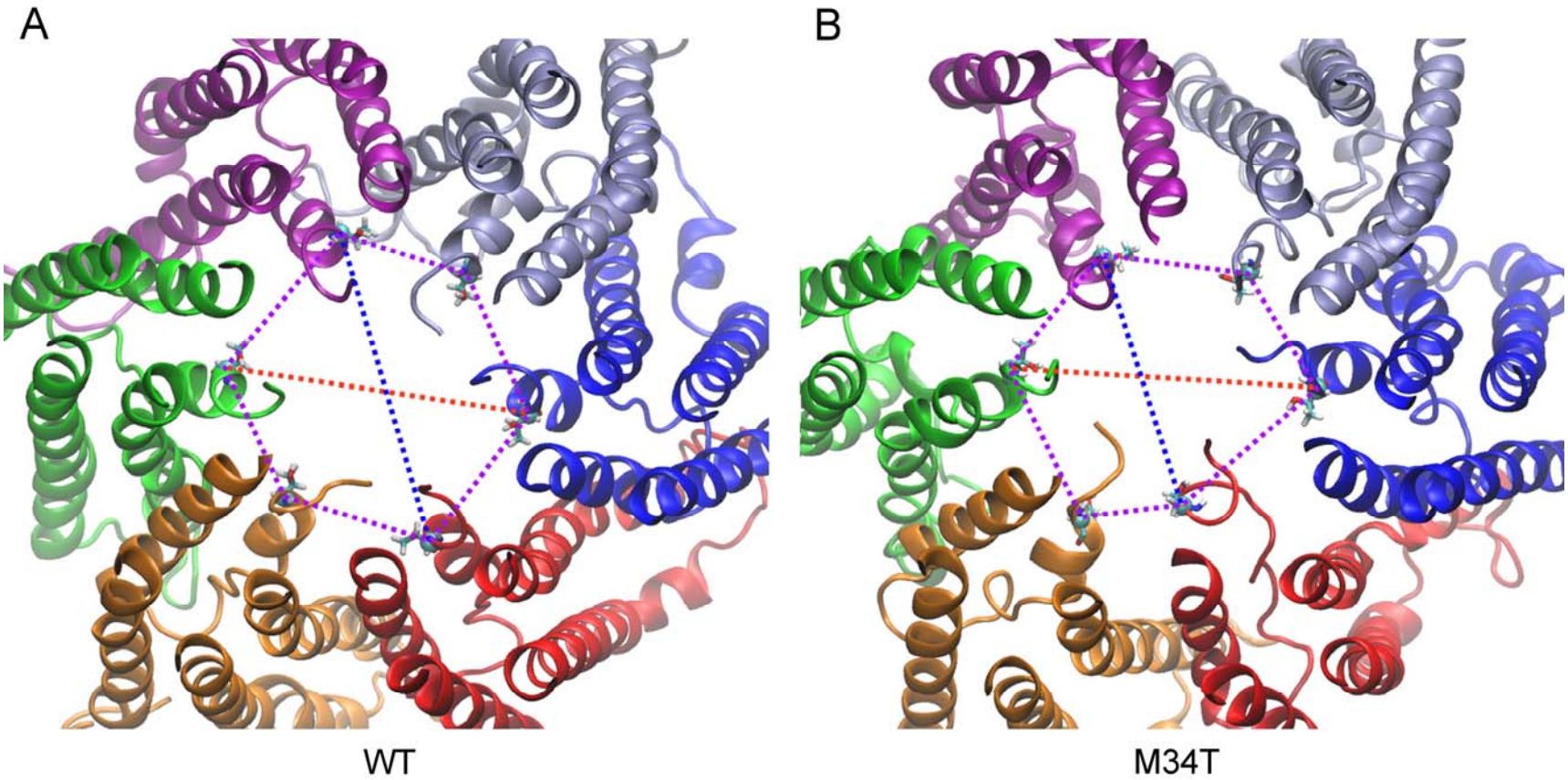

Analysis of symmetry index. Shown are the major (red) and minor (blue) diameter and the angles (purple) of the hexagon built on T5 alpha carbons for snapshot of the equilibrium dynamics. The six connexins are colored with different colors and represented in ribbons. T5 alpha carbon is represented with its Van der Waals radius, while the rest of the amino acid is represented in licorice.

Effect of a pull force applied to the N-terminal helix of wt and M34T connexon

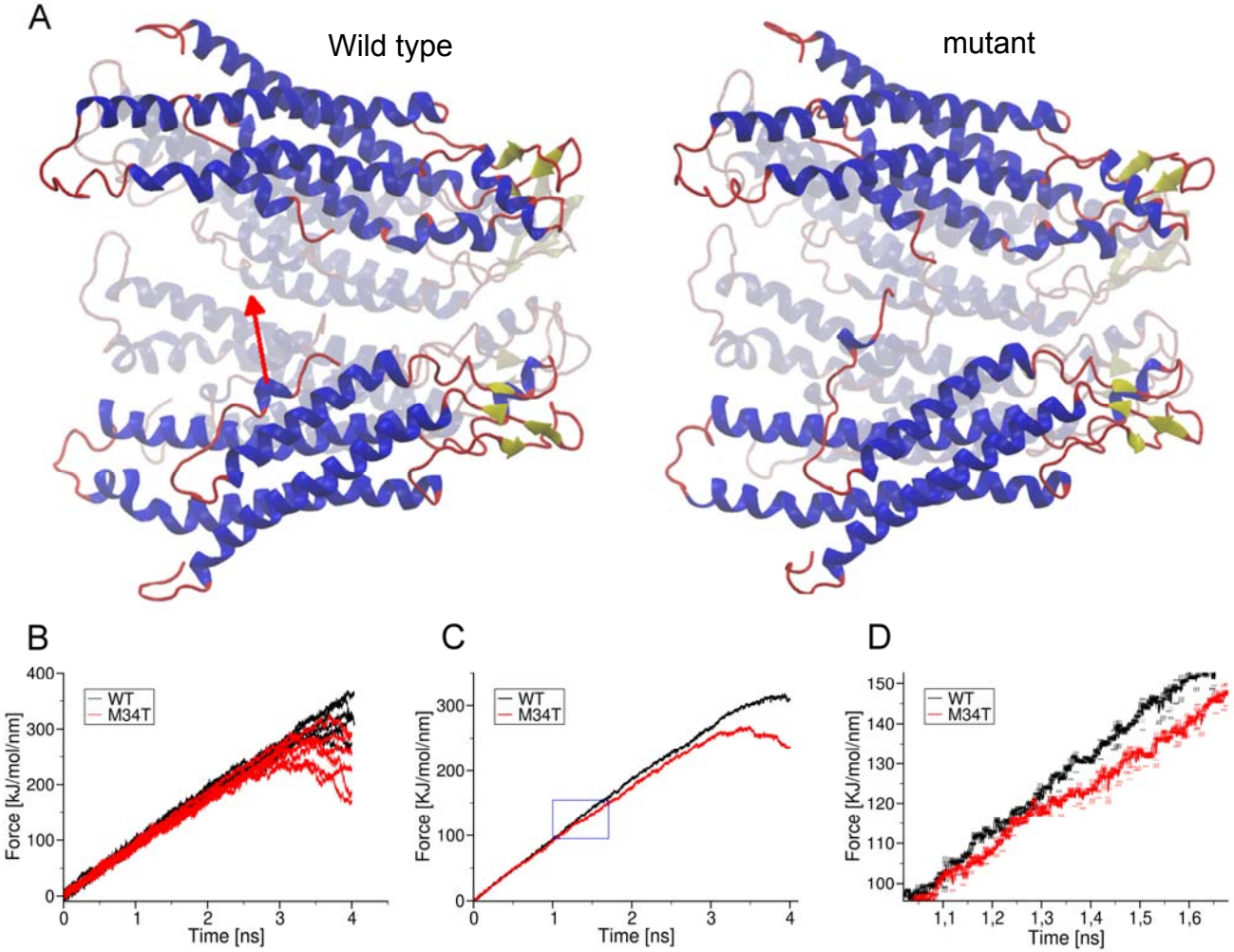

Panel A shows schematically the effect of pulling one NTH: shown are the initial and final frames of a pulling simulation. In panel B, we plot raw pull force data for of each trajectory corresponding to the six different helices for Cx26WT (black traces) and Cx26M34T (red traces). Panel C shows the mean obtained from the six raw traces, after application of a further running average over 200 fs in order to reduce thermal noise. The blue box is zoomed in panel D, showing more clearly the point where the two traces separate. Error bars shown are standard deviation obtained from the running average. Visual inspection of trajectories revealed that, in the mutant, the detached helix interacts with a neighboring NTH, due to the more asymmetric shape of the pore mouth. This interaction obstacles the motion of the helix towards the center, until the pulling force is large enough to break it. This effect was not observed in wild the type.

Zonta | Mammano, *Frontiers in Physiology* 2014

Study of M34T single channel conductance by steered molecular dynamics

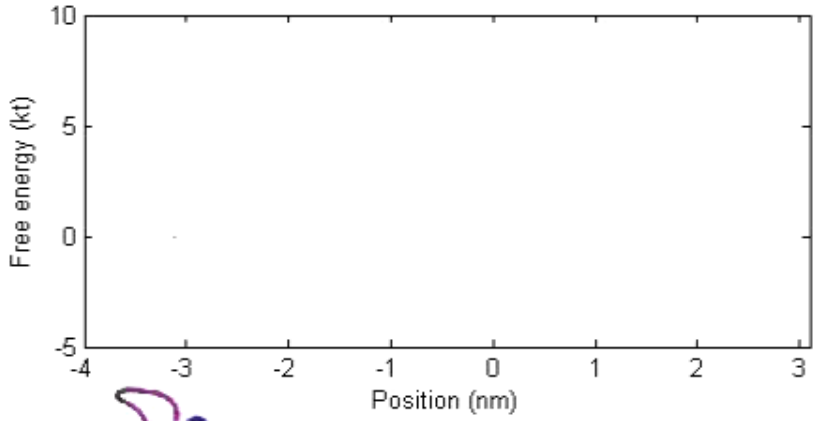

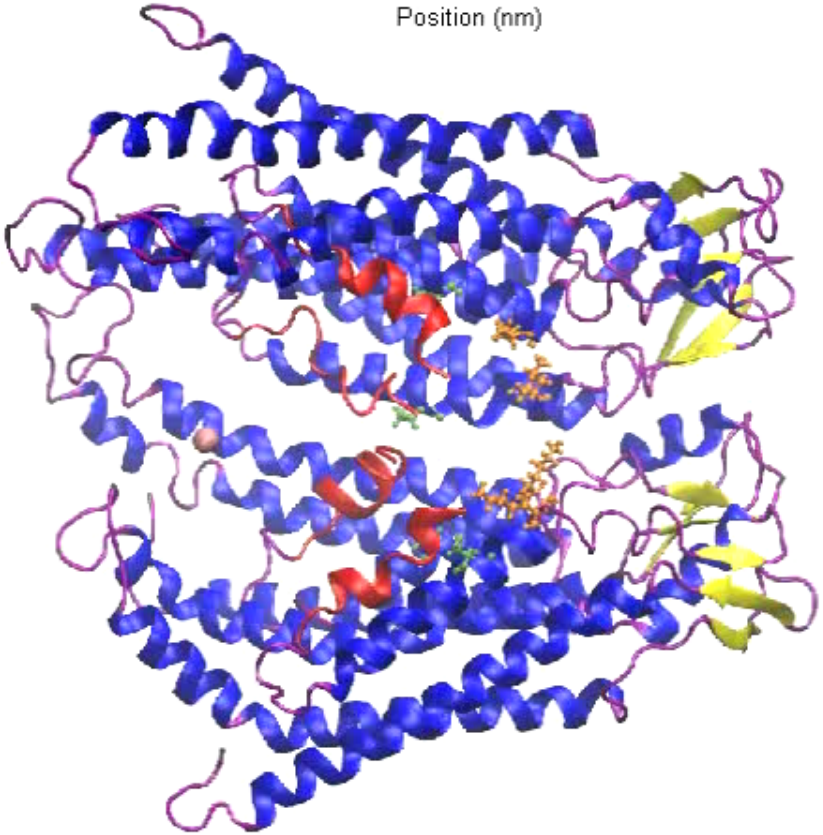

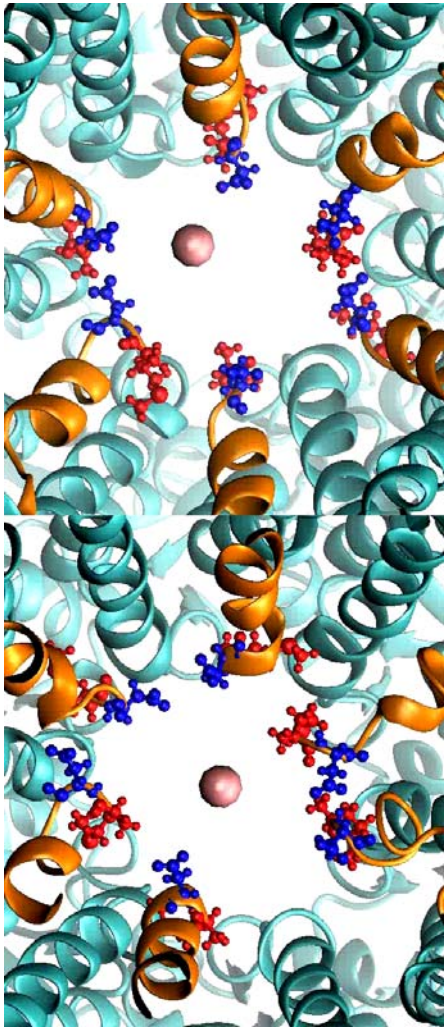

Wild type

M34T

M1 (blue) and D2 (red) residues are drawn in ball and stick representation. In the mutant, these residues protrude more towards the center of the channel and consequently the energy of interaction is higher and results in an increased total PMF.

Zonta | Mammano, *Frontiers in Physiology* 2014

Deafness–related M34T mutation of connexin 26 explained at atomic level

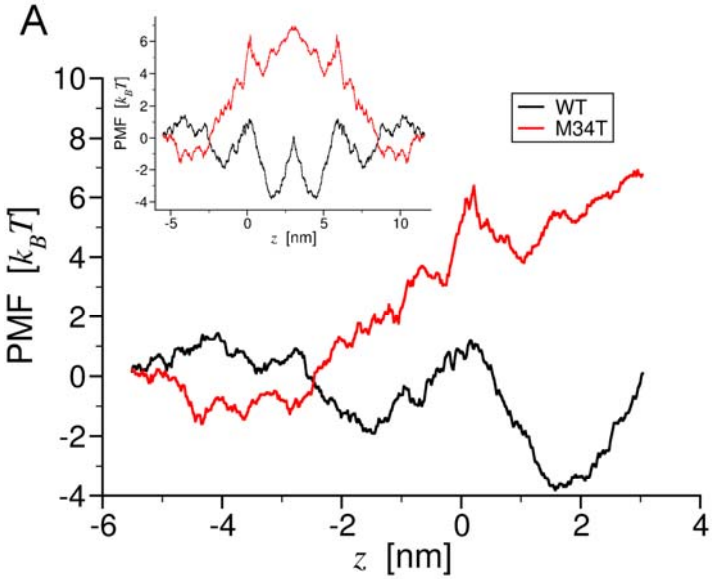

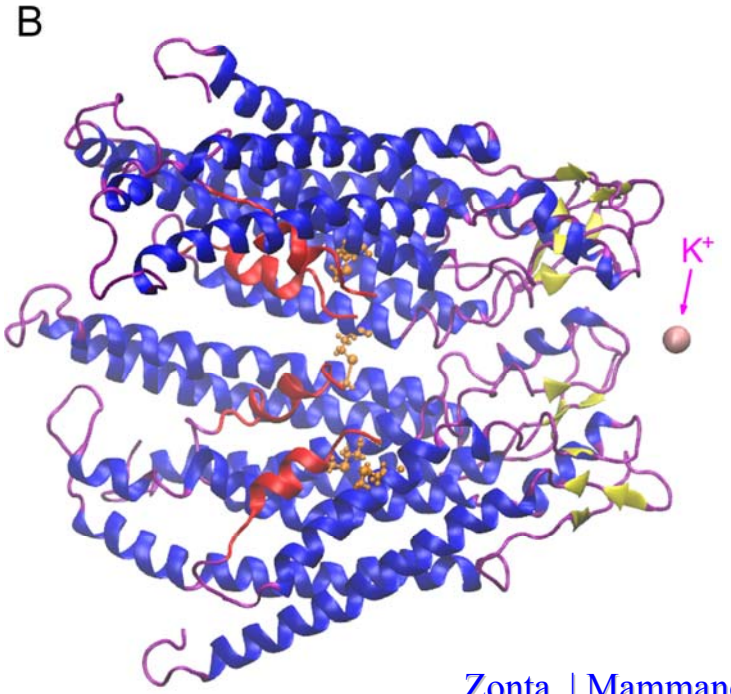

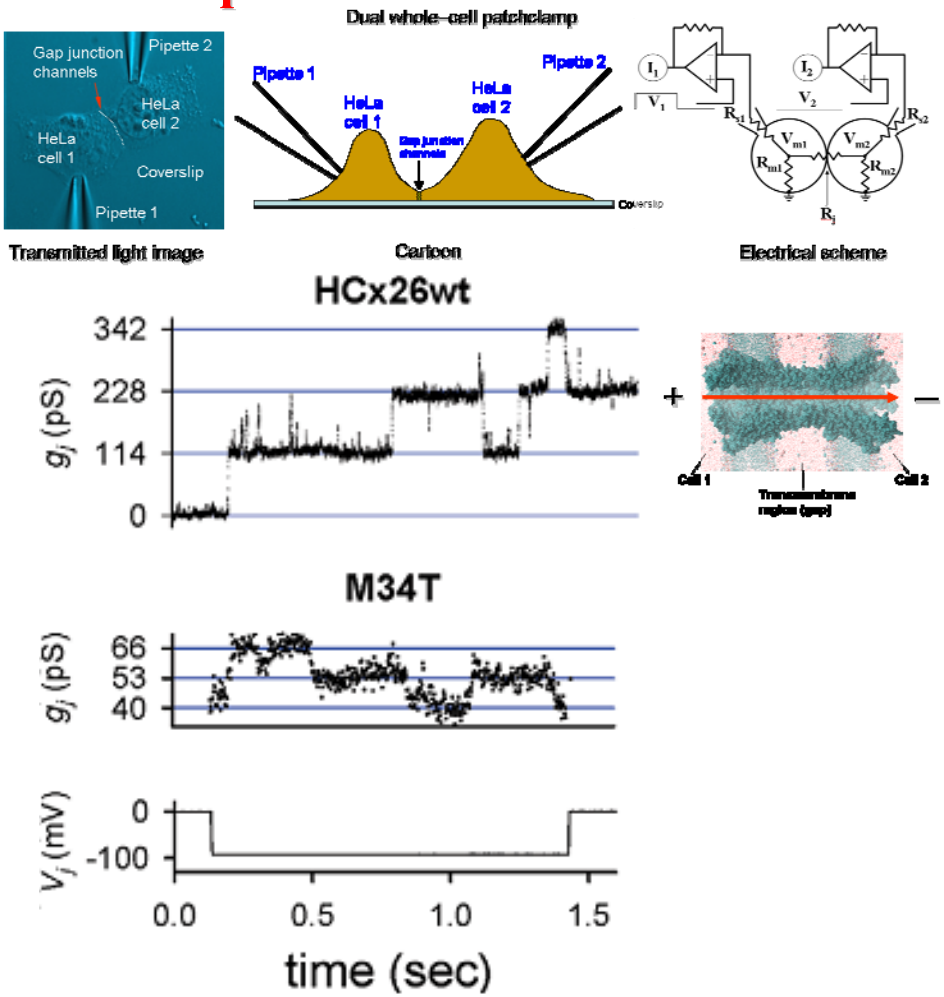

	Experimental value	Molecular Dynamics
Wild type channel (WT)	114 pS	105 pS
M34T mutant channel	13 pS	10 pS
Ratio M34T/WT	11.4%	9.6 %

Zonta | Mammano, *Frontiers in Physiology* 2014

Deafness–related V84L mutation of connexin 26

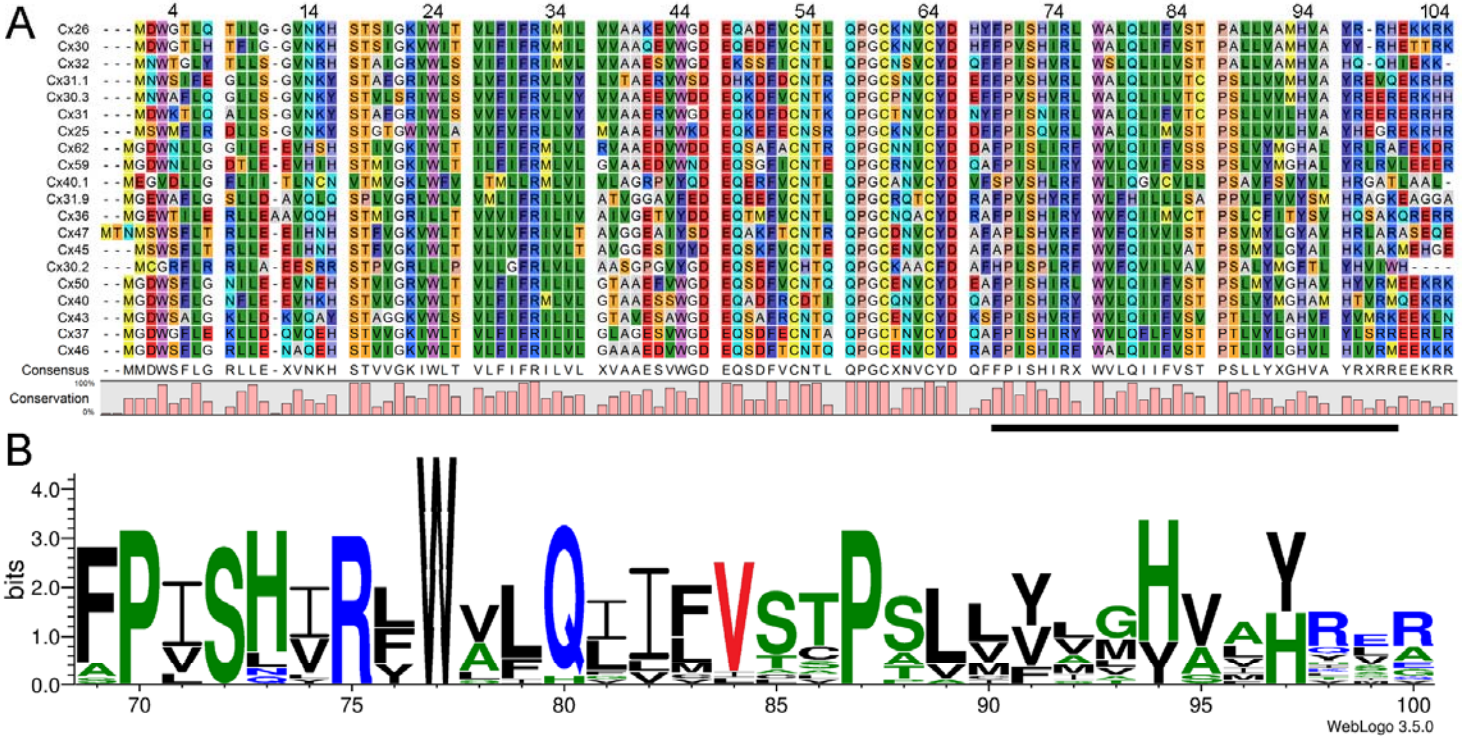

Inositol triphosphate (IP_3) opens channels that release calcium from intracellular stores

Inositol triphosphate (IP_3) opens channels that release intracellular calciuim stores

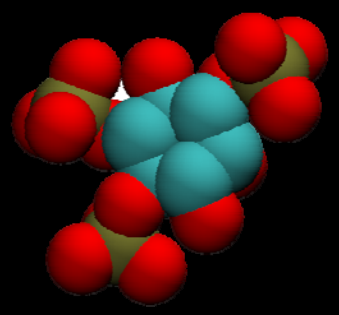

IP_3 molecule

Study of IP_3 permeability in wild type and V84L mutant connexins

HeLa cells loaded with Fura-2

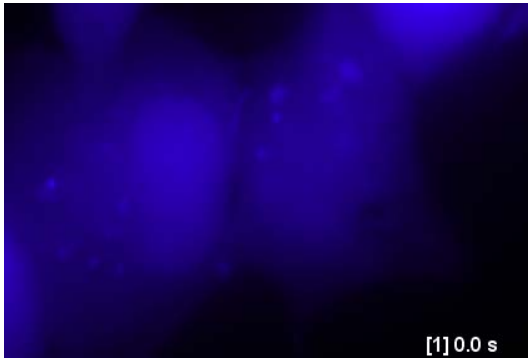

Wild type Cx26

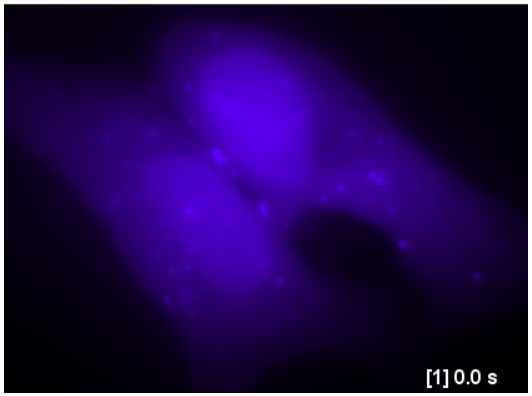

Mutant V84L

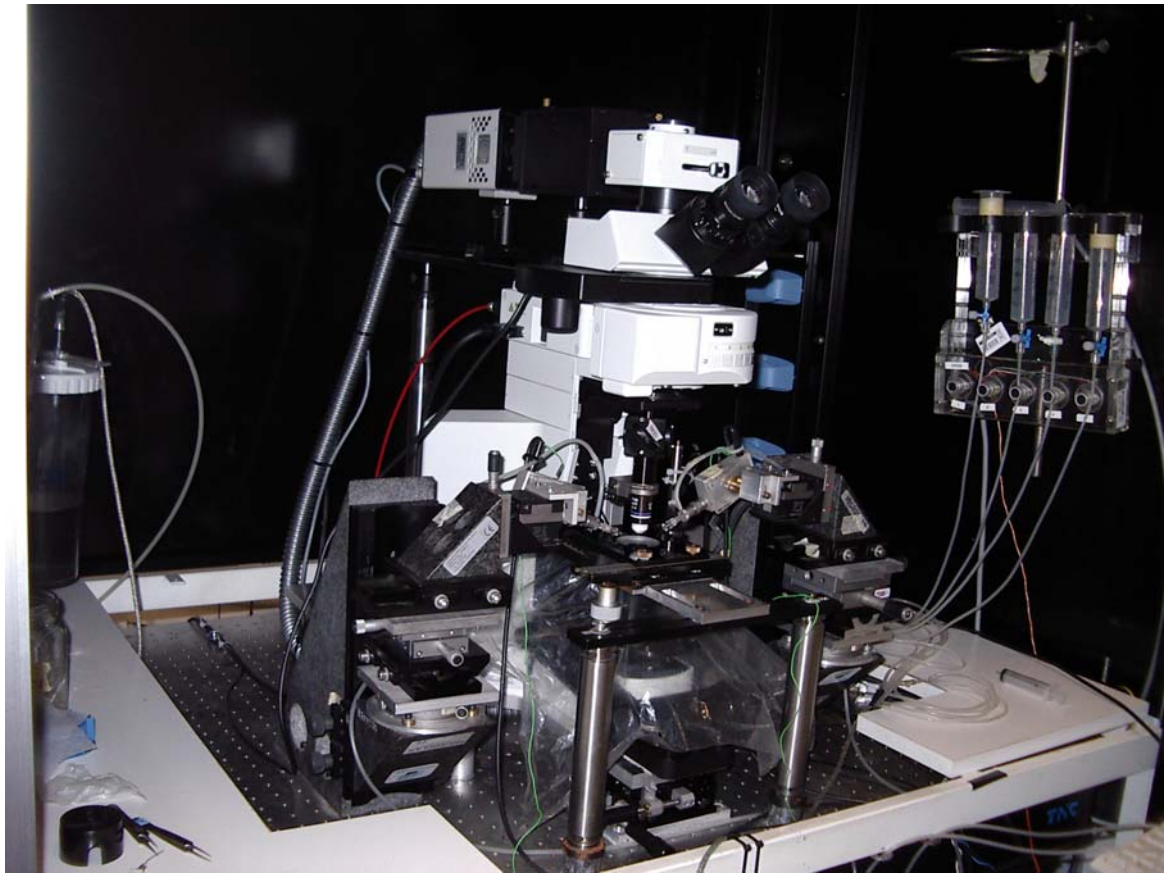

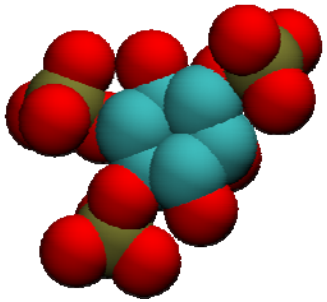

IP_3 molecule

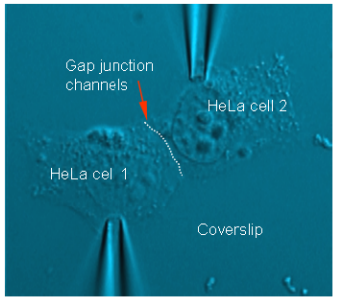

Transmitted light image

Dual whole–cell patchclamp

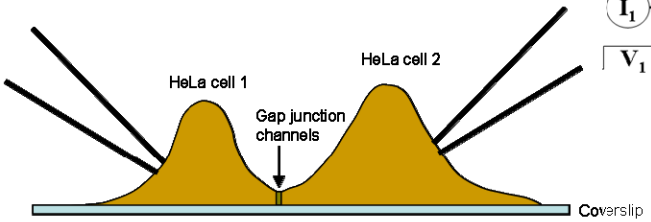

Cartoon

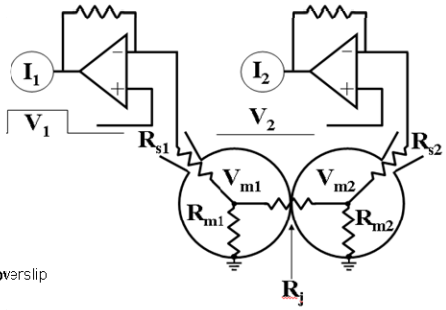

Electrical scheme

Impaired permeability to IP_3 in a mutant connexin underlies recessive hereditary deafness

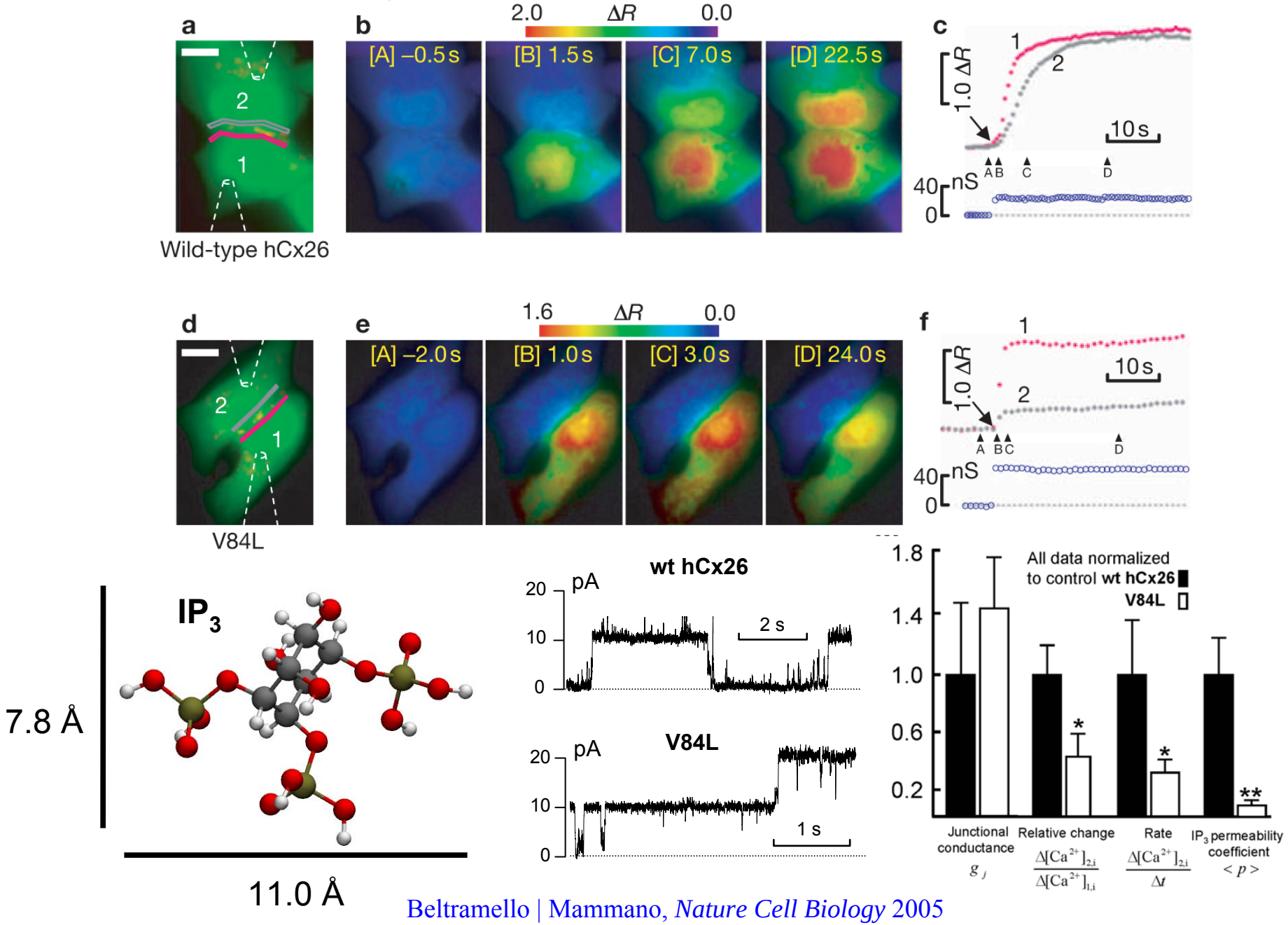

Beltramello | Mammano, *Nature Cell Biology* 2005

Cell Death and Differentiation (2012) 19, 947–957

www.nature.com/cdd

Transfer of IP_3 through gap junctions is critical, but not sufficient, for the spread of apoptosis

E Decrock[1,11], DV Krysko[2,3,12], M Vinken[4,12], A Kaczmarek[2,3,11], G Crispino[5], M Bol[1], N Wang[1], M De Bock[1], E De Vuyst[1], CC Naus[6], V Rogiers[4], P Vandenabeele[2,3], C Erneux[7], F Mammano[5,8,9], G Bultynck[10] and L Leybaert*[,1]

Decades of research have indicated that gap junction channels contribute to the propagation of apoptosis between neighboring cells. Inositol 1,4,5-trisphosphate (IP_3) has been proposed as the responsible molecule conveying the apoptotic message, although conclusive results are still missing. We investigated the role of IP_3 in a model of gap junction-mediated spreading of cytochrome *C*-induced apoptosis. We used targeted loading of high-molecular-weight agents interfering with the IP_3 signaling cascade in the apoptosis trigger zone and cell death communication zone of C6-glioma cells heterologously expressing connexin (Cx)43 or Cx26. Blocking IP_3 receptors or stimulating IP_3 degradation both diminished the propagation of apoptosis. Apoptosis spread was also reduced in cells expressing mutant Cx26, which forms gap junctions with an impaired IP_3 permeability. However, IP_3 by itself was not able to induce cell death, but only potentiated cell death propagation when the apoptosis trigger was applied. We conclude that IP_3 is a key necessary messenger for communicating apoptotic cell death *via* gap junctions, but needs to team up with other factors to become a fully pro-apoptotic messenger.
Cell Death and Differentiation (2012) **19,** 947–957; doi:10.1038/cdd.2011.176; published online 25 November 2011

Unitary permeability of gap junction channels to second messengers measured by FRET microscopy and dual whole cell patch clamp

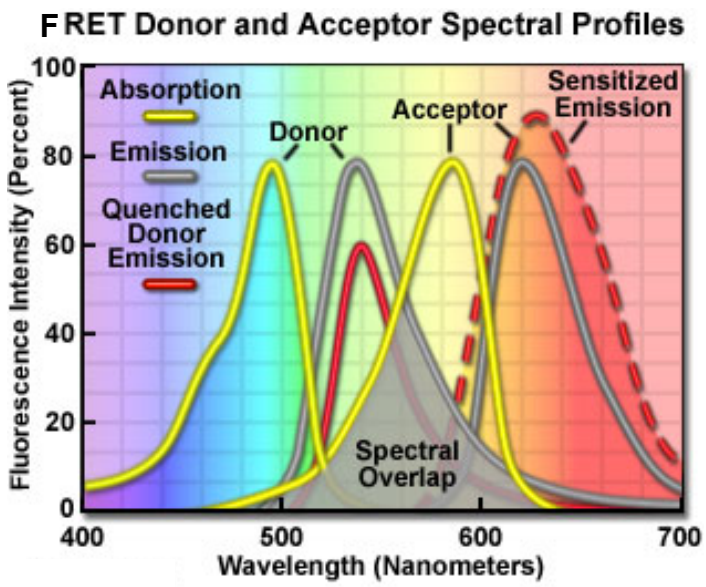

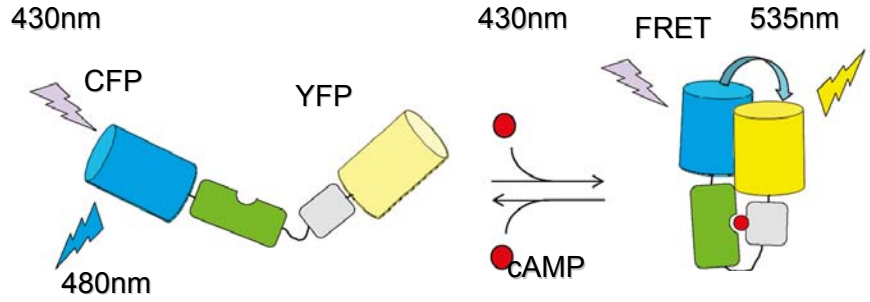

[Newman et al. *Chem. Rev.* 2011]

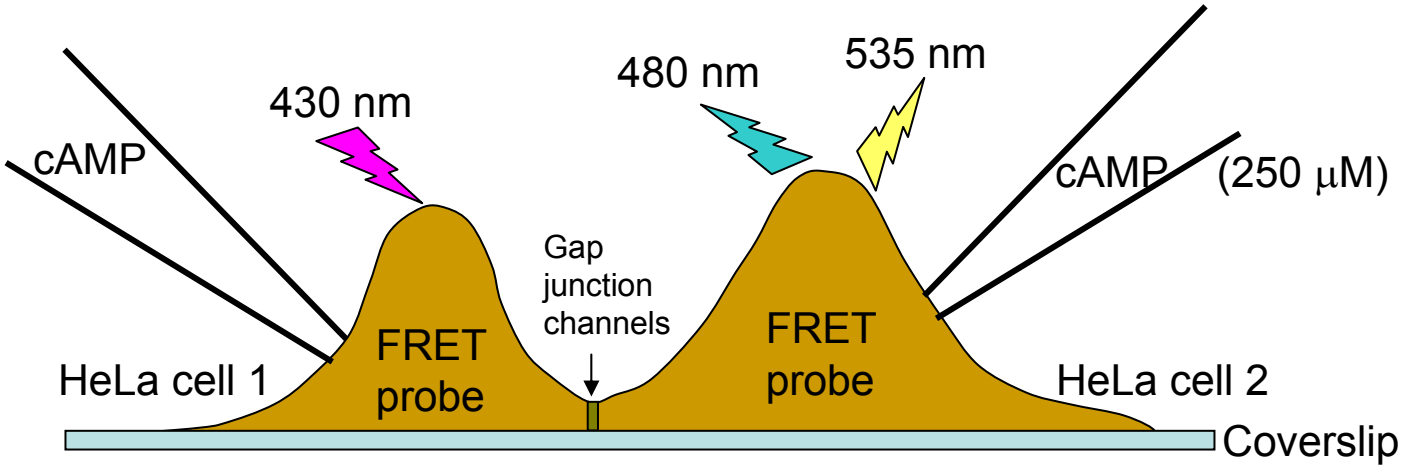

FRET scheme

Unitary permeability of gap junction channels to second messengers measured by FRET microscopy and dual whole cell patch clamp

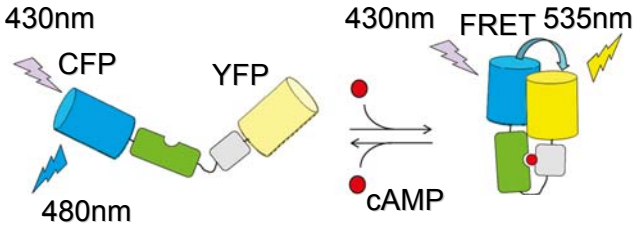

[Newman et al. *Chem. Rev.* 2011]

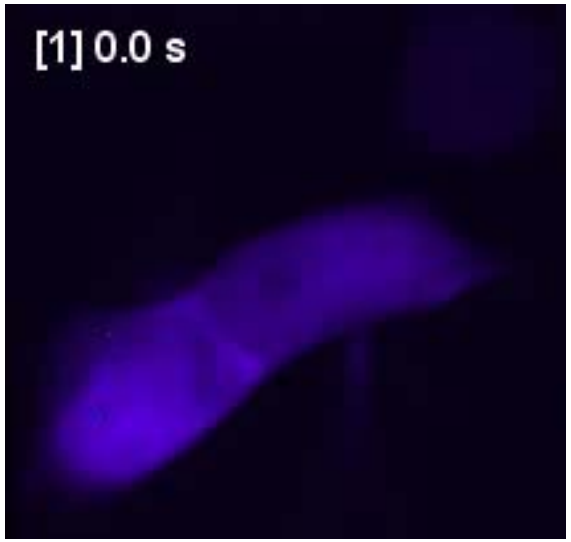

HeLa cell pair expressing the Epac-camps probe developed in the lab of Martin Lohse, Wurzburg, Germany

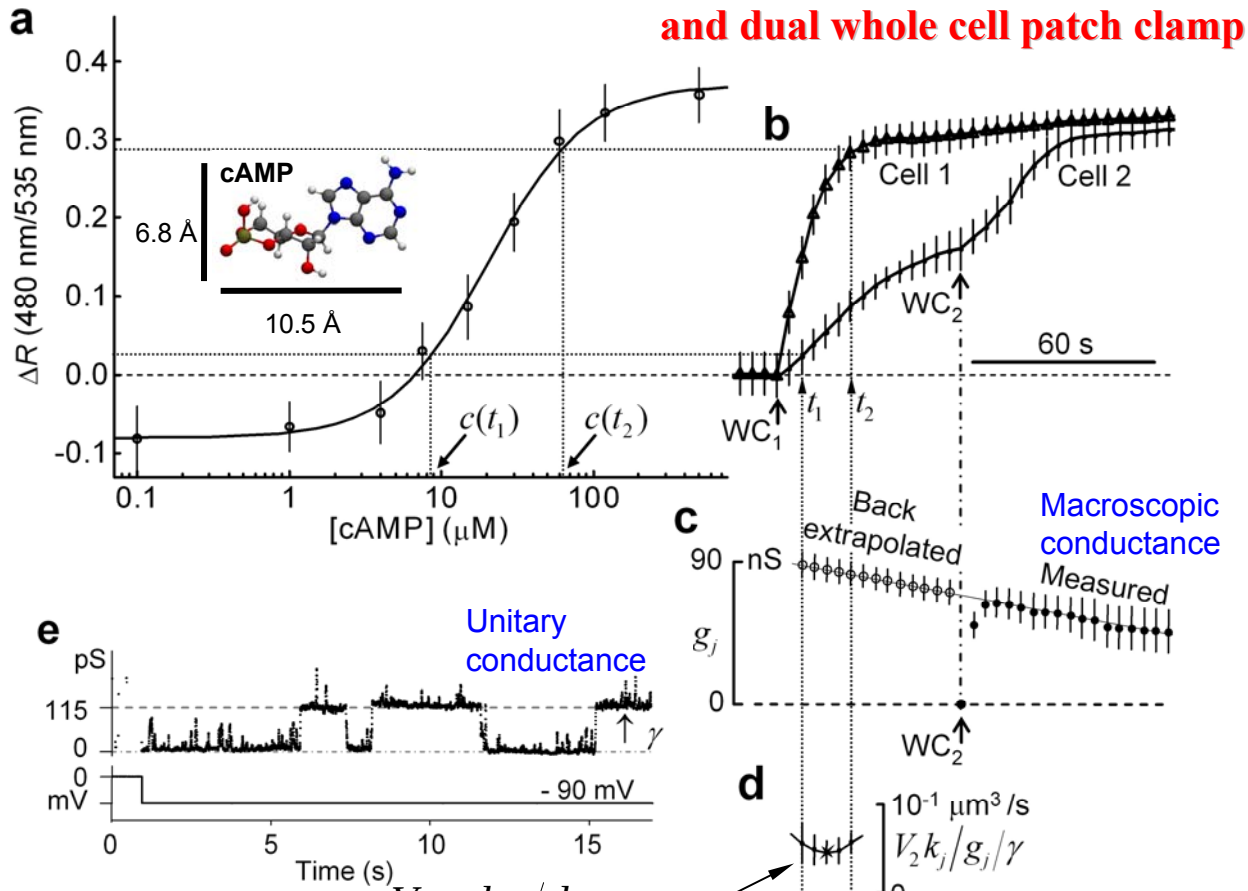

$$\frac{V_2}{N_{\text{pore}}}\frac{dc_2/dt}{c_1-c_2}=p_u$$

Unitary permeability p_u [10^{-3} μm³/s]	IP_3	cAMP	Lucifer yellow	Calcein
	60 ± 12	47 ± 15	7.0 ± 3.0	3.0 ± 1.0
Flux [molec./s] $J_u=p_u(c_1-c_2)$ (c_1-c_2) = 1 μM = 602 molec./ μm³	36 ± 7	28 ± 9	4.2 ± 1.8	1.8 ± 0.6

Hernandez | Mammano *Nature Methods* 2007

Zonta | Mammano, *Cell Communication & Signaling* 2013

Study of deafness in mouse models of human hereditary hearing loss

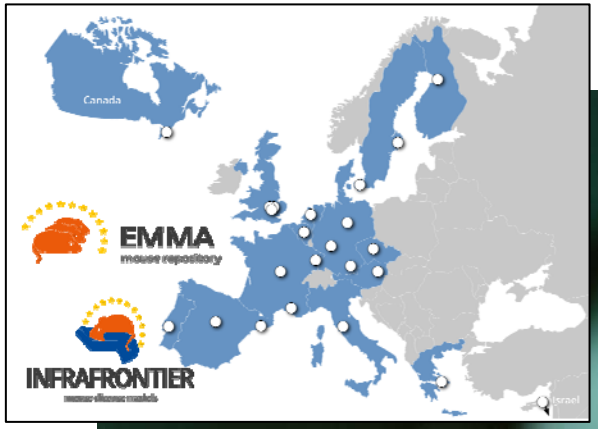

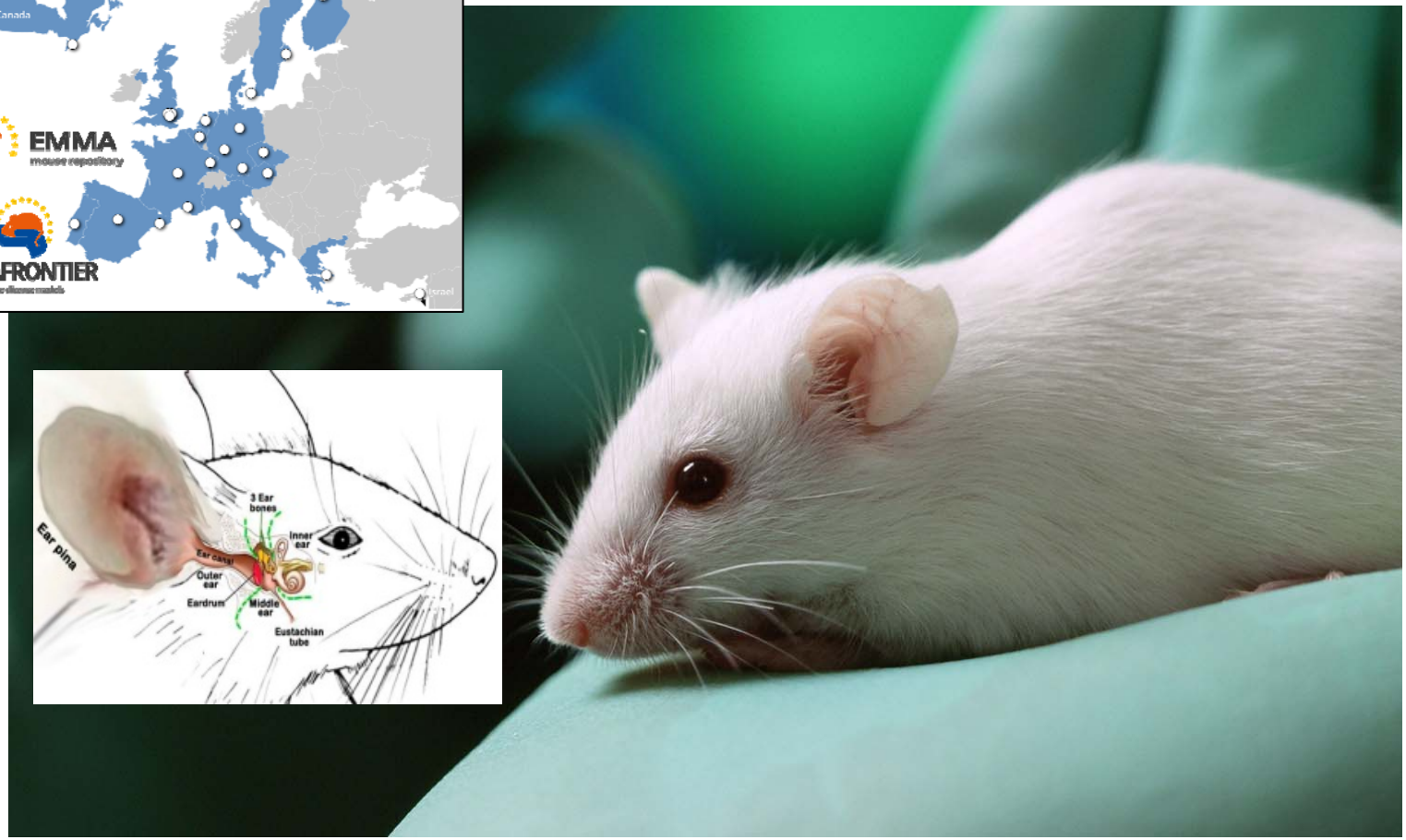

Assay of hearing performance by the auditory brainstem recording technique

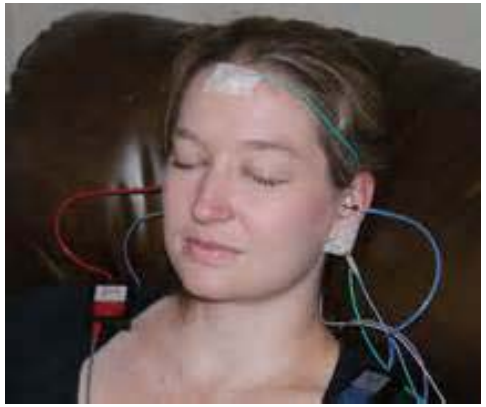

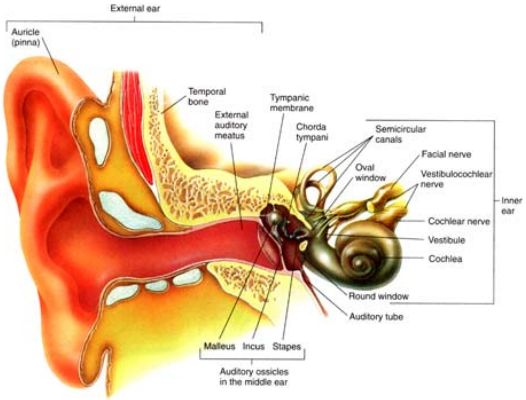

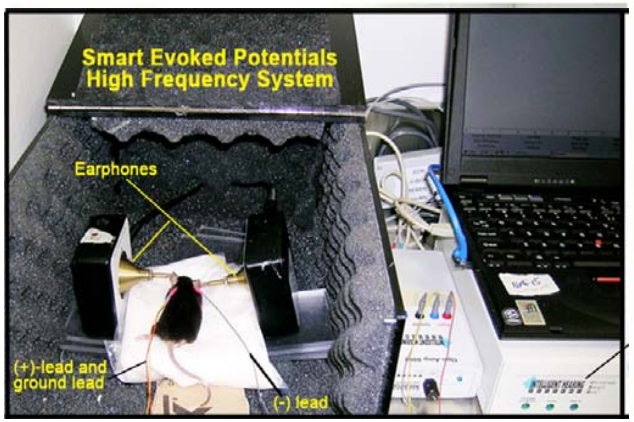

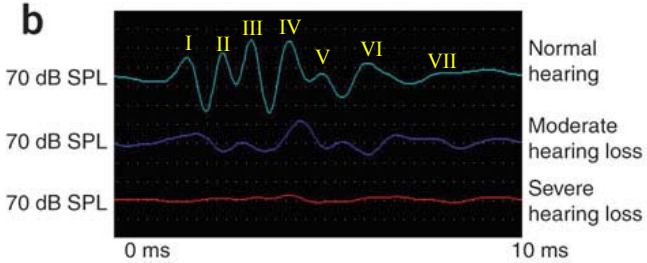

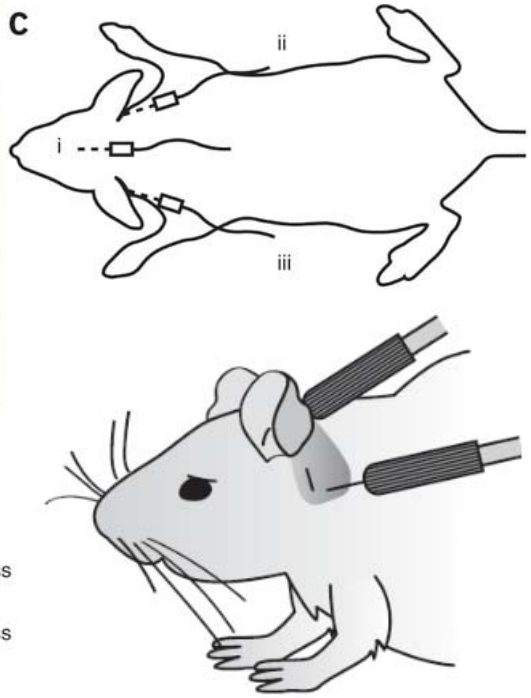

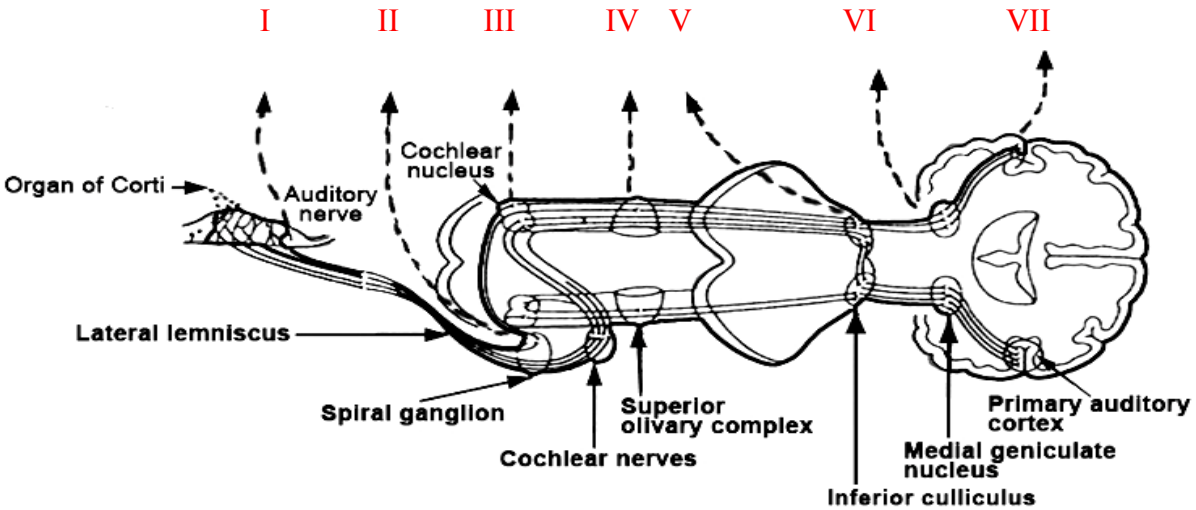

Hearing loss in mice with defective or mutant connexin expression

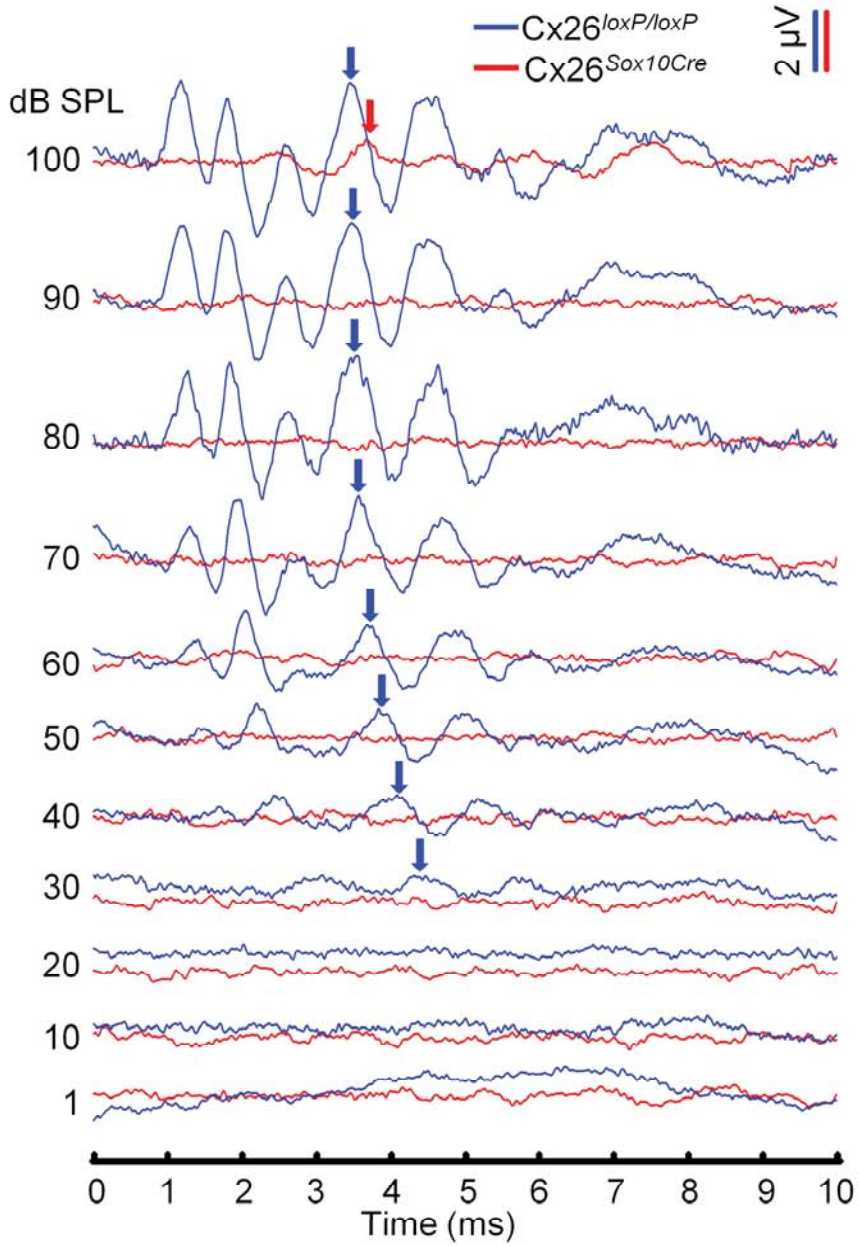

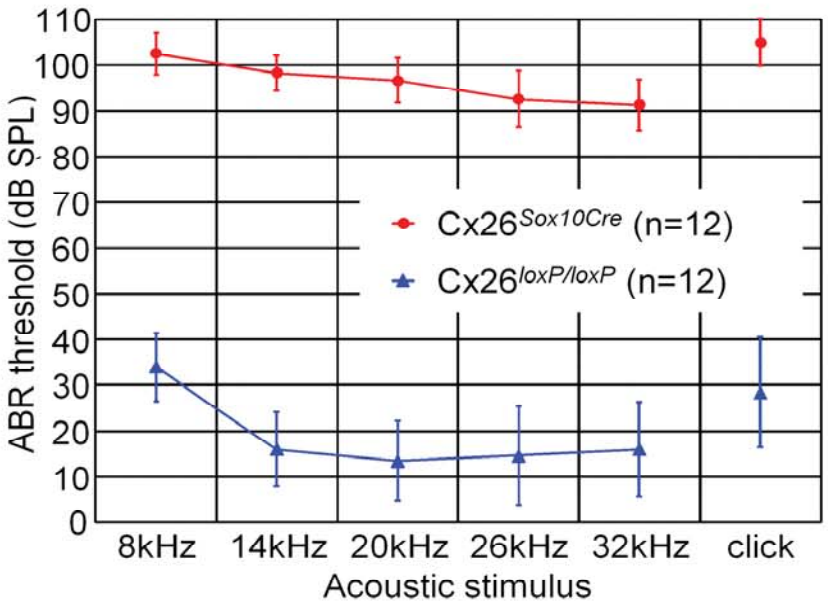

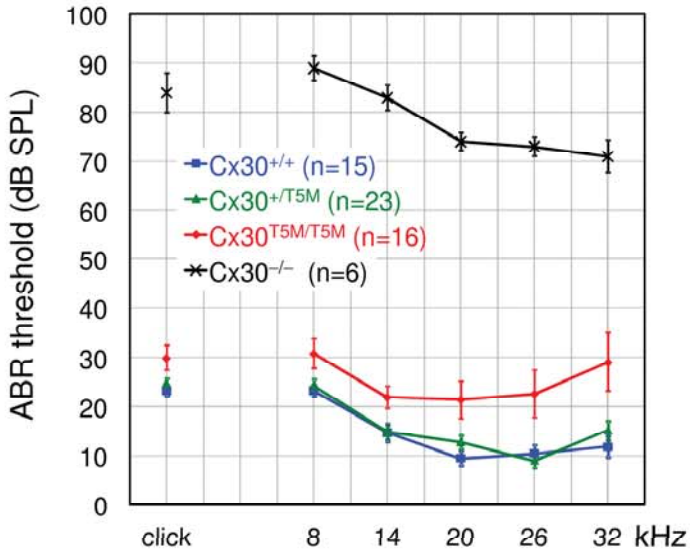

Crispino | Mammano *PlosOne* 2011

Schütz | Mammano *Human Molecular Genetics* 2010

Organotypic cultures of the mouse postnatal cochlea

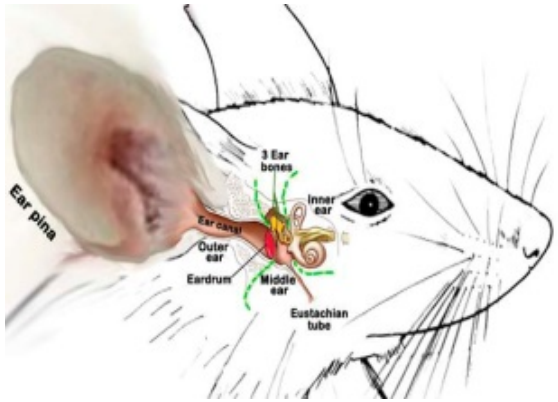

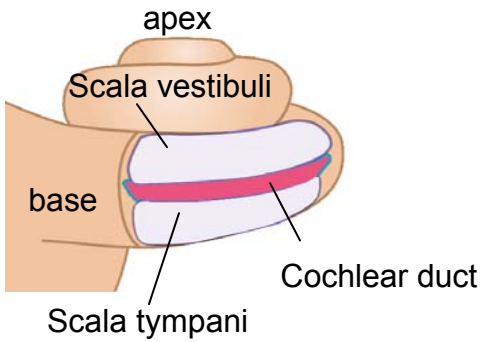

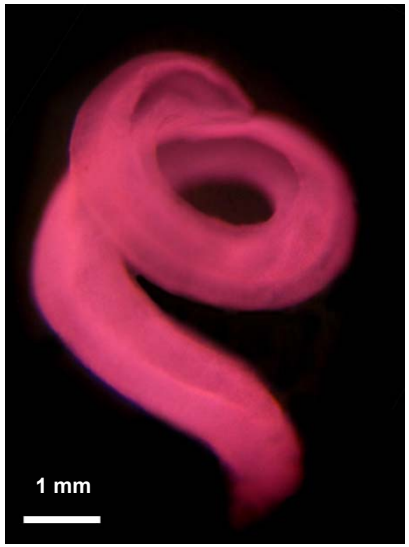

Cochlear duct (mouse, P6)

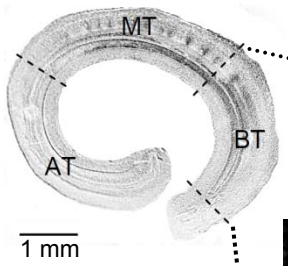

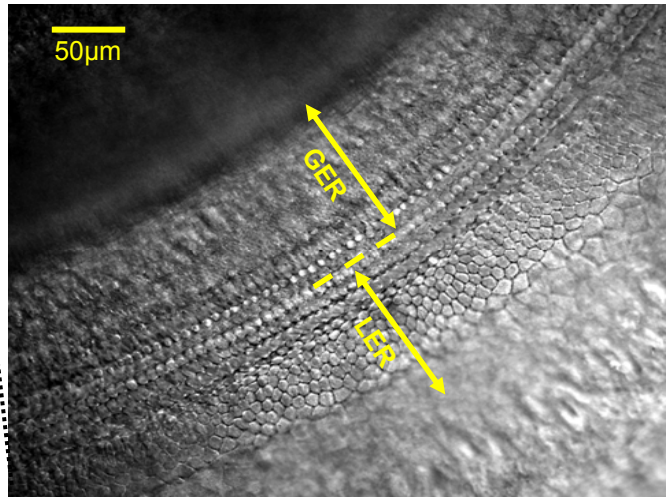

Sensory epithelium viewed from scala vestibuli (mouse, P6)

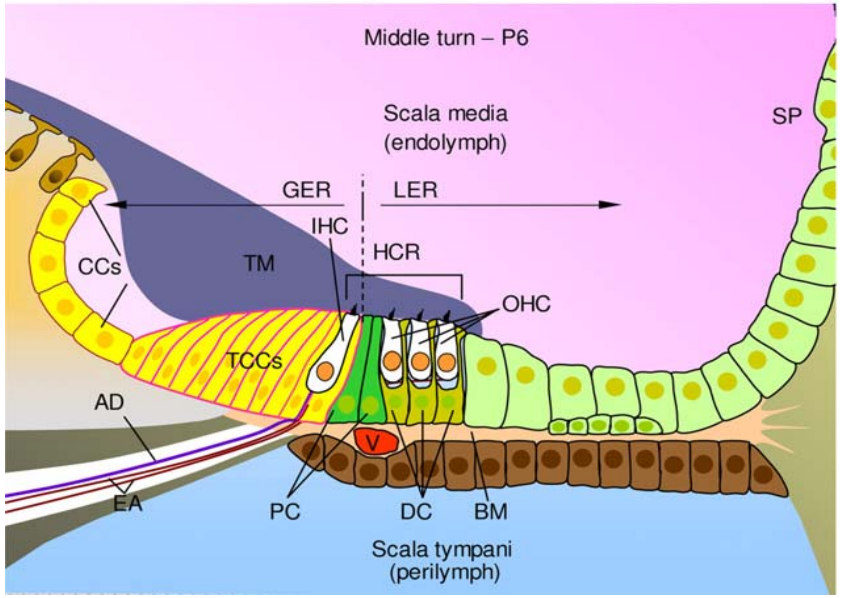

Mammano F. *Seminars in Cell & Dev Biol* 2013

FRAP

Fluorescence Recovery After Photobleaching (FRAP) with Green Fluorescent Protein

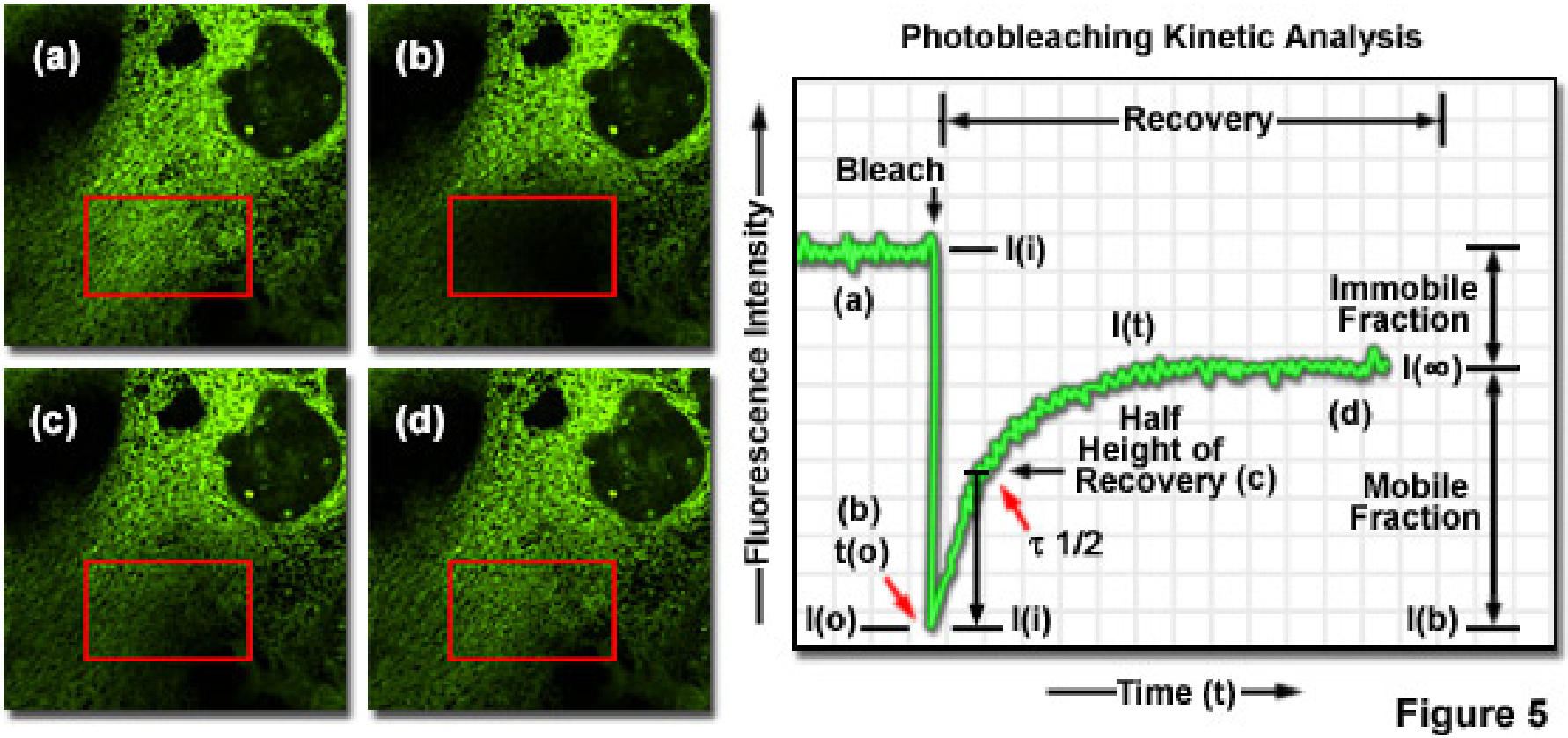

In *fluorescence recovery after photobleaching* (FRAP) experiments, fluorophores within a target region are intentionally bleached with excessive levels of irradiation. As new fluorophore molecules diffuse into the bleached region of the specimen (recovery), the fluorescence emission intensity is monitored to determine the lateral diffusion rates of the target fluorophore. In this manner, the translational mobility of fluorescently labeled molecules can be ascertained within a very small (2 to 5 micrometer) region of a single cell or section of living tissue.

Gap-FRAP assays show impaired calcein transfer in the cochlea of Cx30$^{T5M/T5M}$ mice (P6)

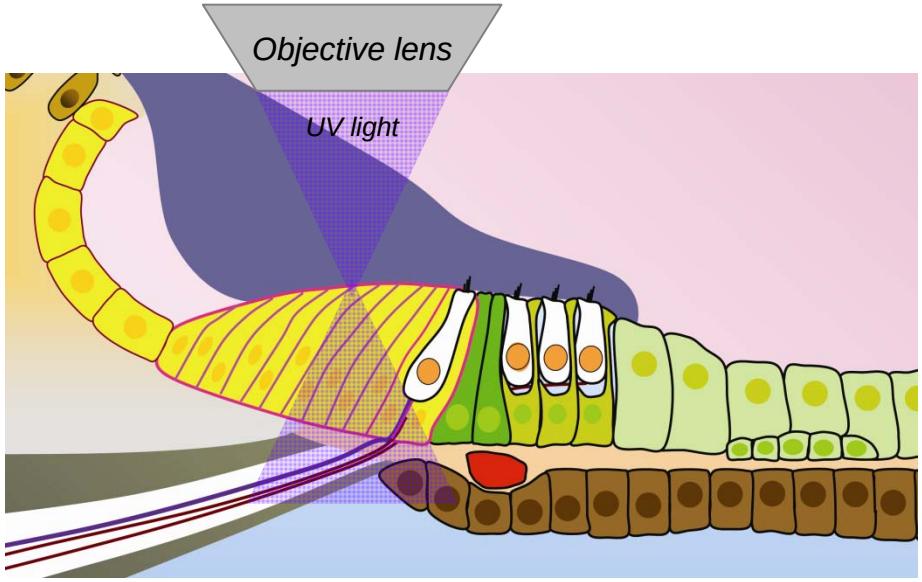

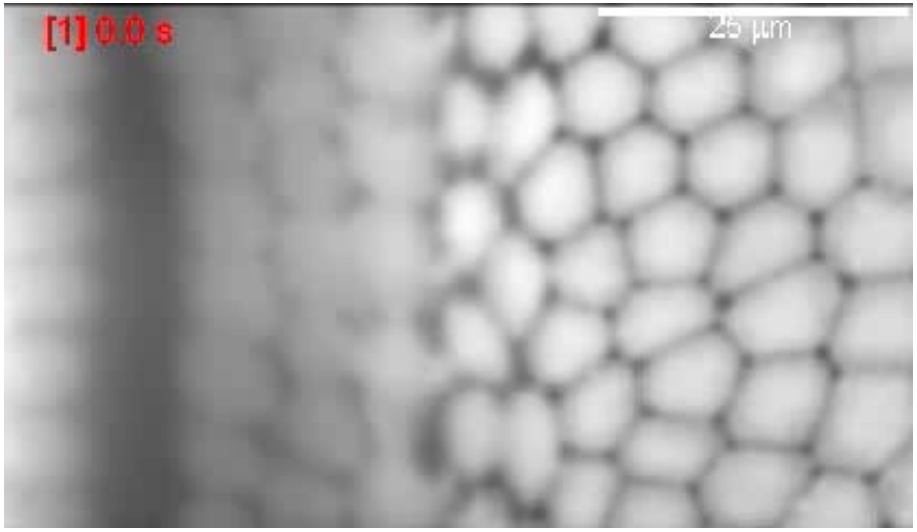

Cochlear organotypic culture loaded with calcein-AM

Gap-FRAP assays show impaired calcein transfer in the cochlea of Cx30$^{T5M/T5M}$ mice (P6)

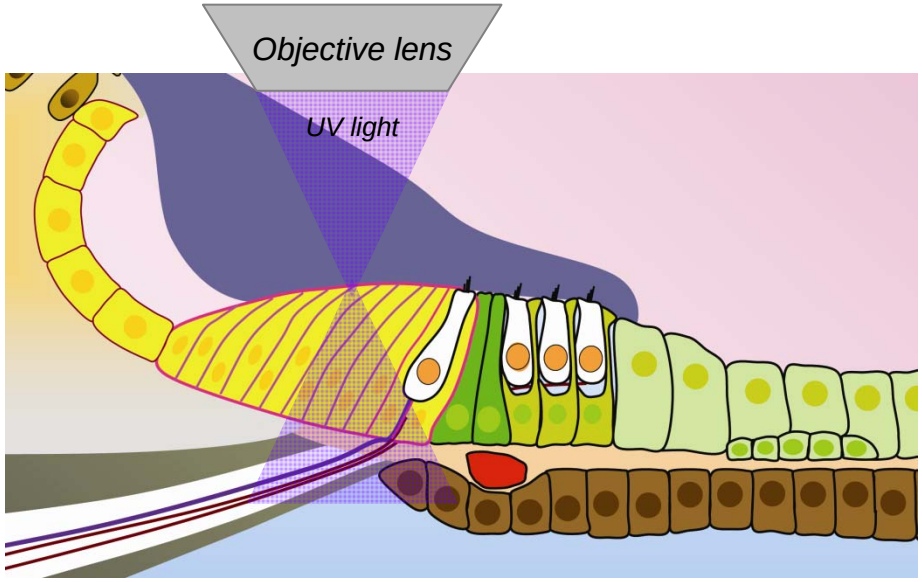

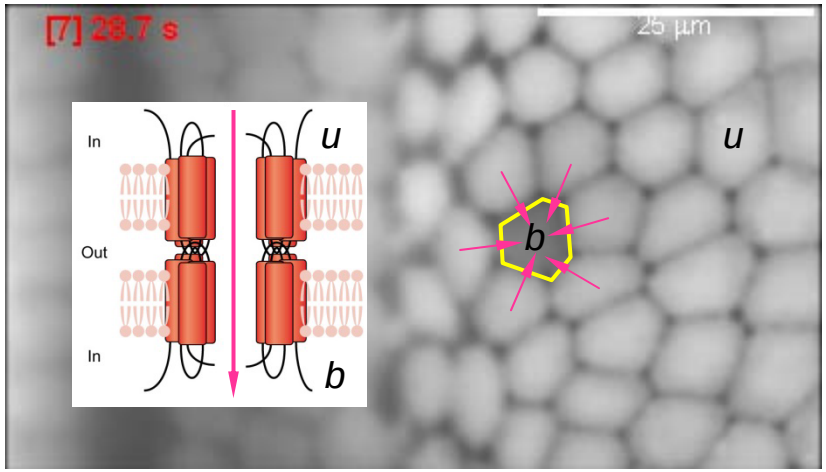

Cochlear organotypic culture loaded with calcein-AM

Recovery of fluorescence after photobleaching is due to calcein diffusion through connexin channels, from unbleached (*u*) to bleached (*b*) cells

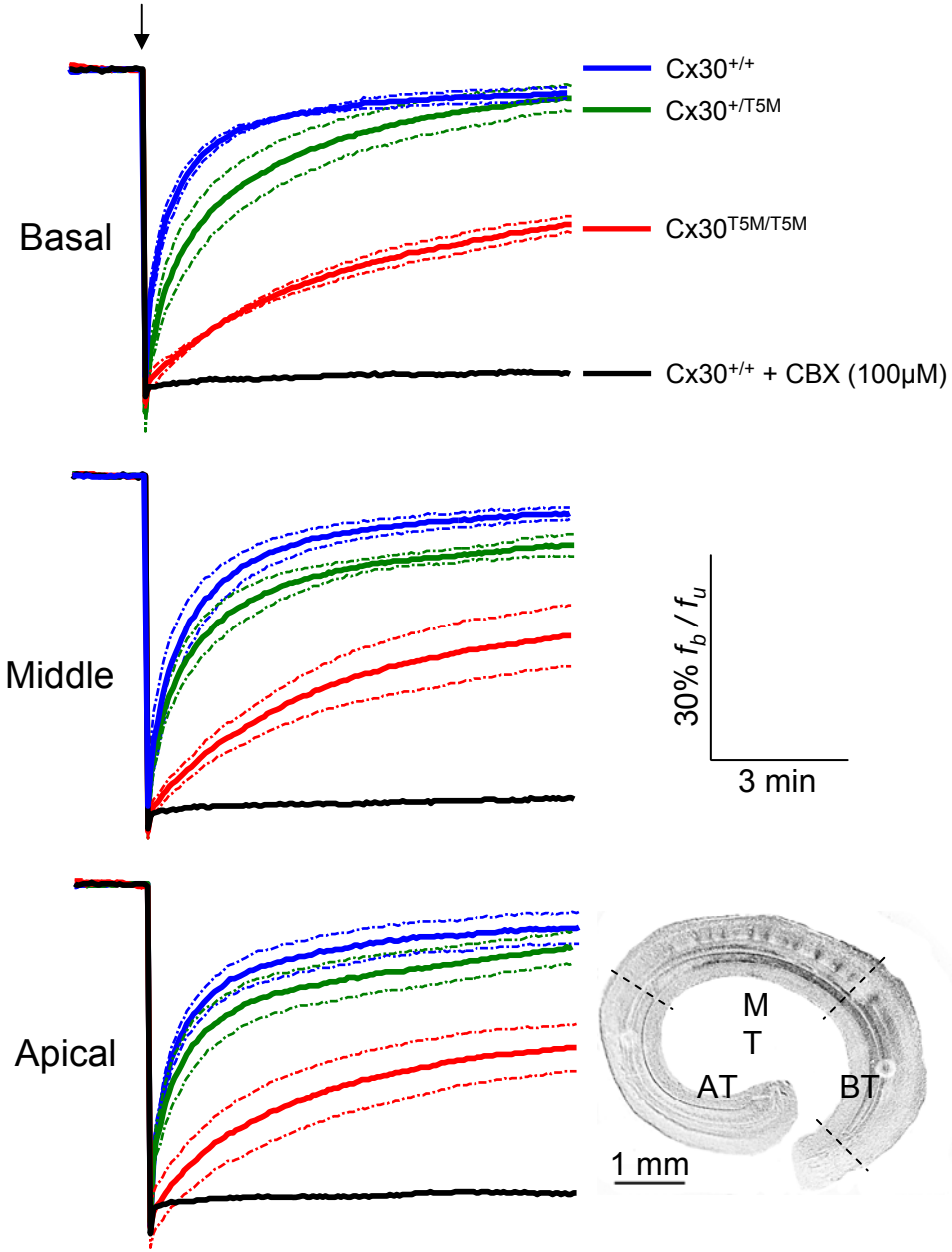

Optically monitoring intercellular communication mediated by gap junction channels

Classical methods

- Long loading times (minutes)
- Sensitivity varies significantly with the size of the molecule and the type of gap junction under study
- Limited spatial information regarding network connectivity

Aim

- To develop of a method to assess gap junction communication which permits to visualize instantly intercellular connectivity among hundreds of cells.

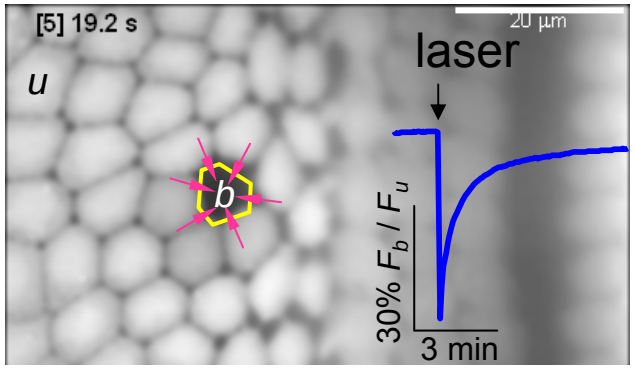

Recovery of fluorescence after photobleaching (FRAP)

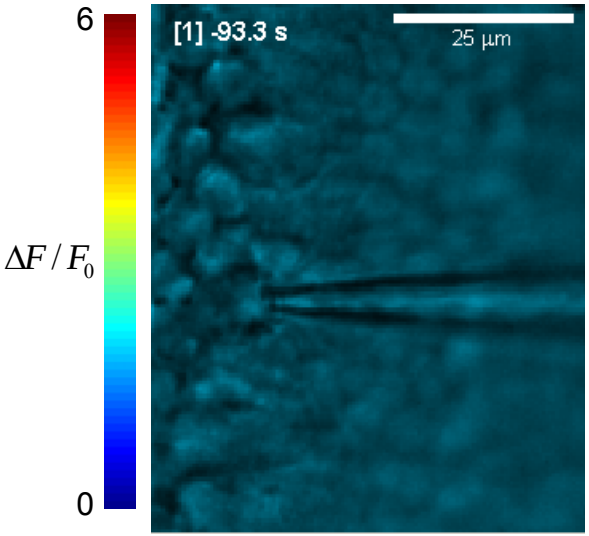

Lucifer Yellow microinjection and intercellular diffusion

Optically monitoring voltage in neurons by photo-induced electron transfer through molecular wires

Evan W. Miller[a], John Y. Lin[a], E. Paxon Frady[b], Paul A. Steinbach[a,c], William B. Kristan, Jr.[d], and Roger Y. Tsien[a,c,e,1]

[a]Department of Pharmacology, [b]Neurosciences Graduate Group, [d]Division of Biological Sciences, [e]Department of Chemistry and Biochemistry, and [c]Howard Hughes Medical Institute, University of California at San Diego, La Jolla, CA 92093

Contributed by Roger Y. Tsien, December 21, 2011 (sent for review November 26, 2011)

vol. 109, no. 06, February 7, 2012

Vf.2.1.Cl

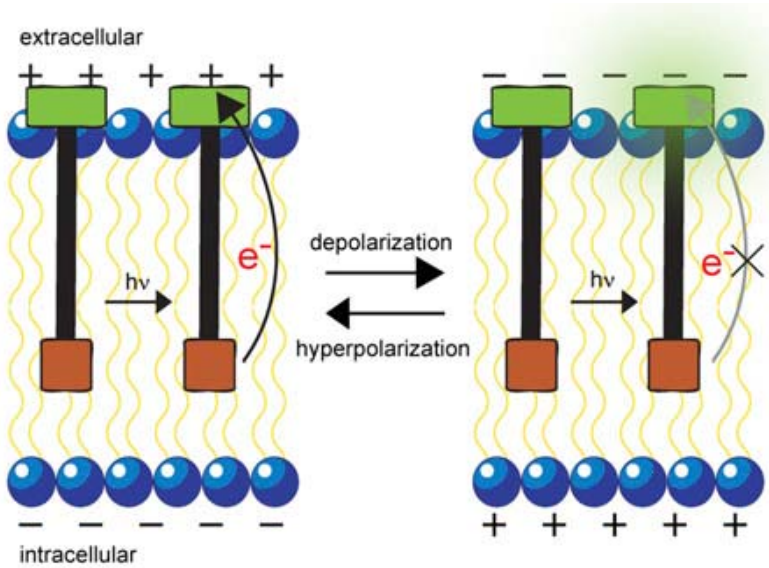

Photo-induced Electron Transfer

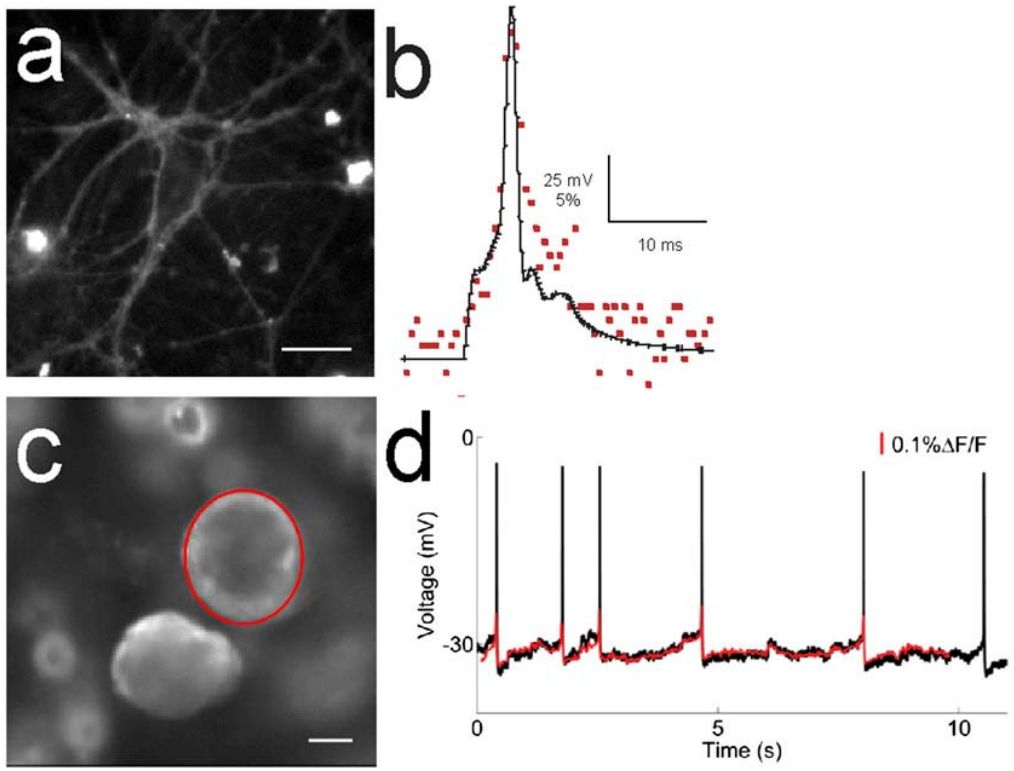

Vf.2.1.Cl fluorescence responses elicited by a sinusoidal voltage command

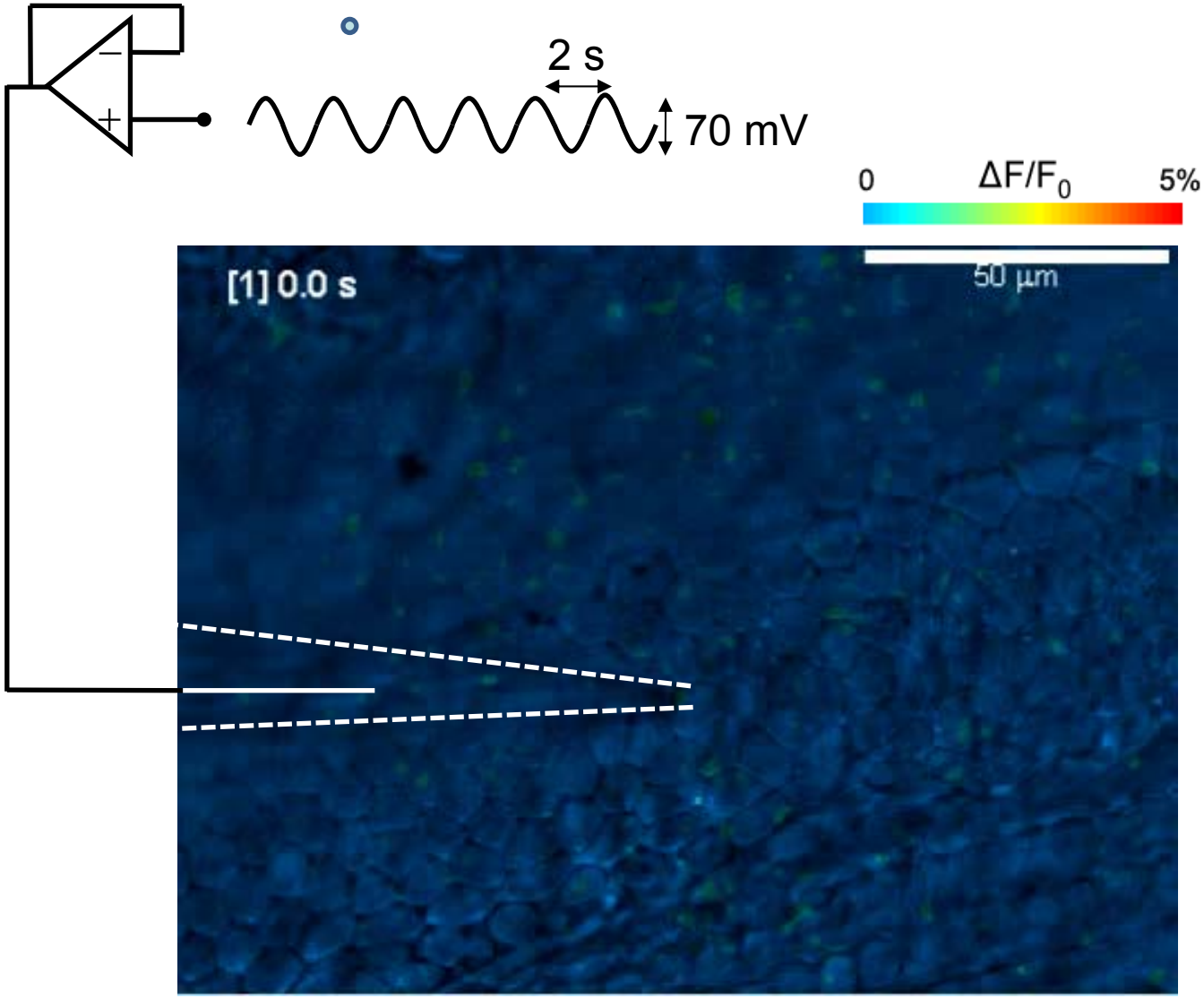

Ceriani and Mammano *Cell Communication and Signaling* 2013, **11**:78

Calibration of voltage responses in cochlear organotypic cultures loaded with Vf2.1.Cl.

A

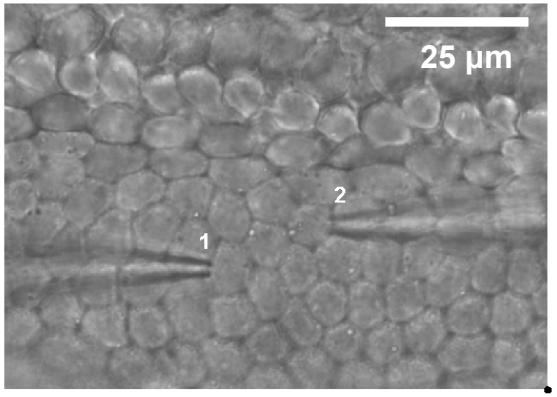

B

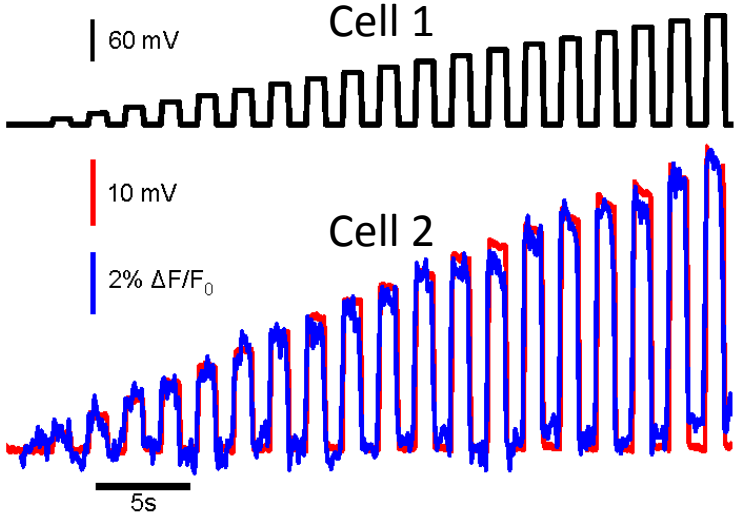

C

Responsivity: 23% $\Delta F/F_0$ per 100 mV

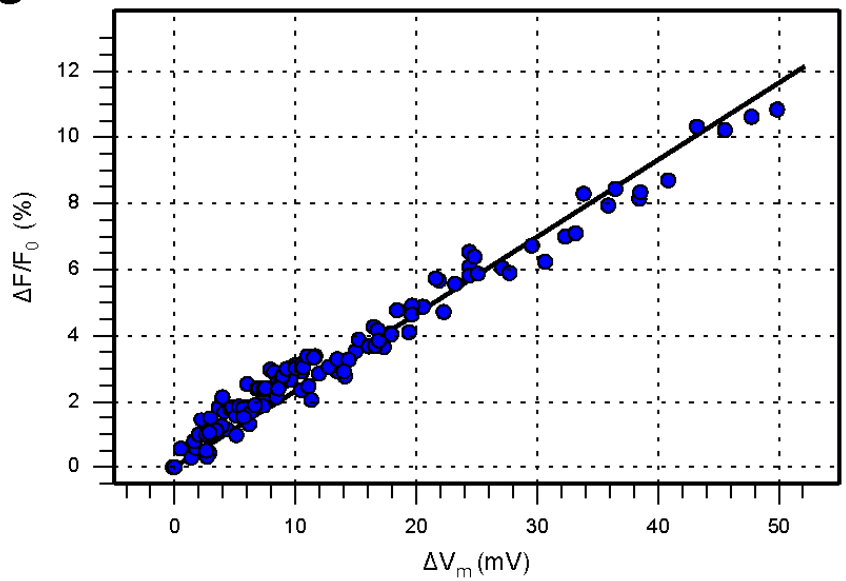

D

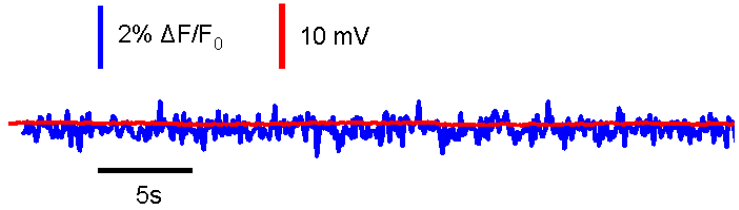

Effect of carbenoxolone (CBX, 100 µM)

Ceriani and Mammano *Cell Communication and Signaling* 2013, **11**:78

Phase-sensitive detection of Vf.2.1.Cl fluorescence responses

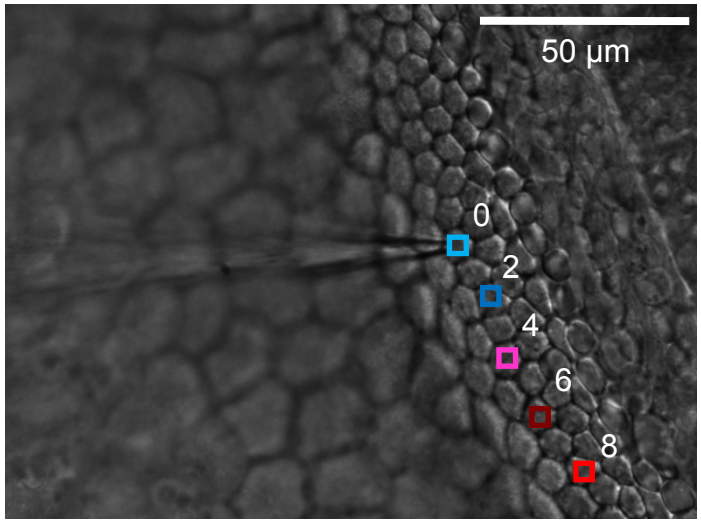

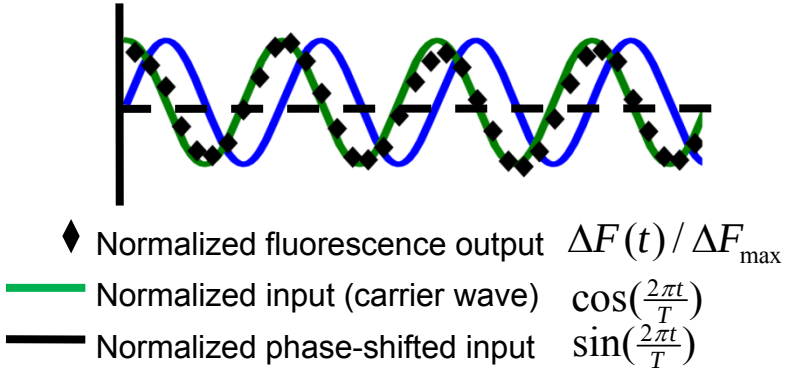

$$a_1 = \frac{1}{nT \cdot F_0} \int_0^{nT} \Delta F(t) \cos\left(\frac{2\pi t}{T}\right) dt$$

$$a_2 = \frac{1}{nT \cdot F_0} \int_0^{nT} \Delta F(t) \sin\left(\frac{2\pi t}{T}\right) dt$$

$$\text{Amplitude} = \sqrt{a_1^2 + a_2^2}$$

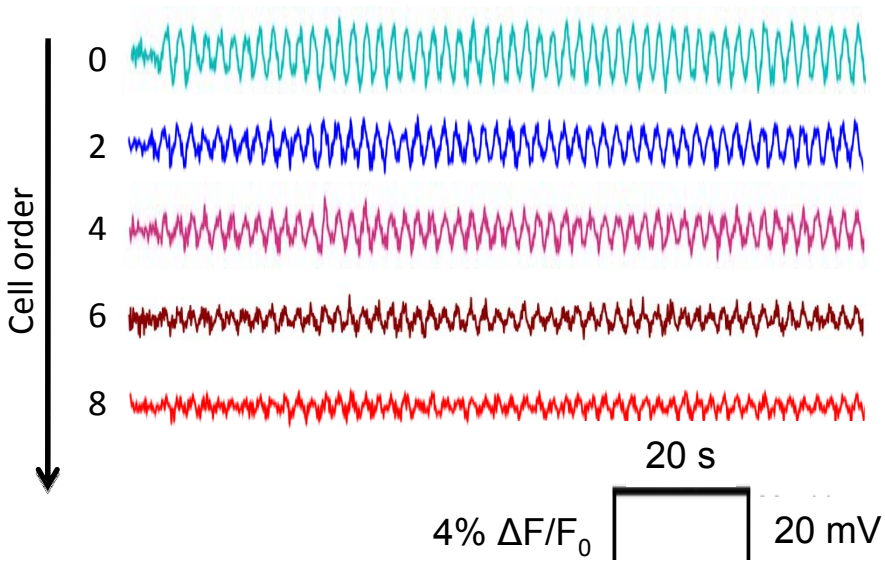

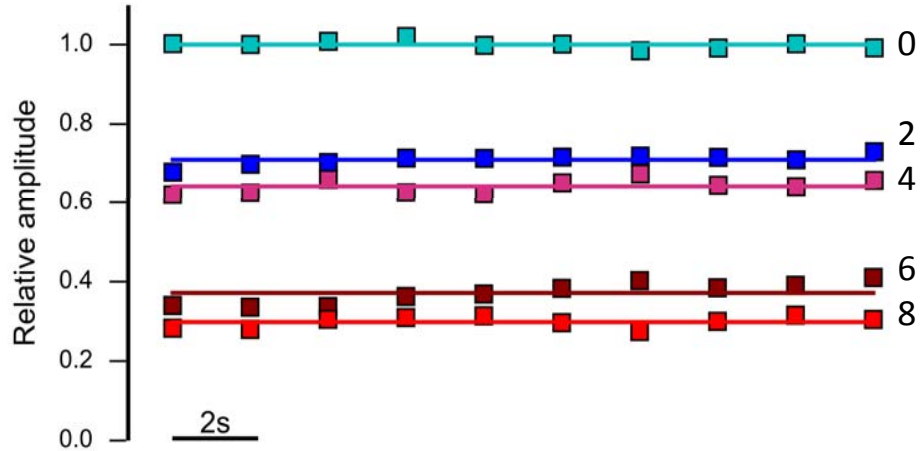

Ceriani and Mammano *Cell Communication and Signaling* 2013, **11**:78

Phase-sensitive detection of Vf.2.1.Cl fluorescence responses

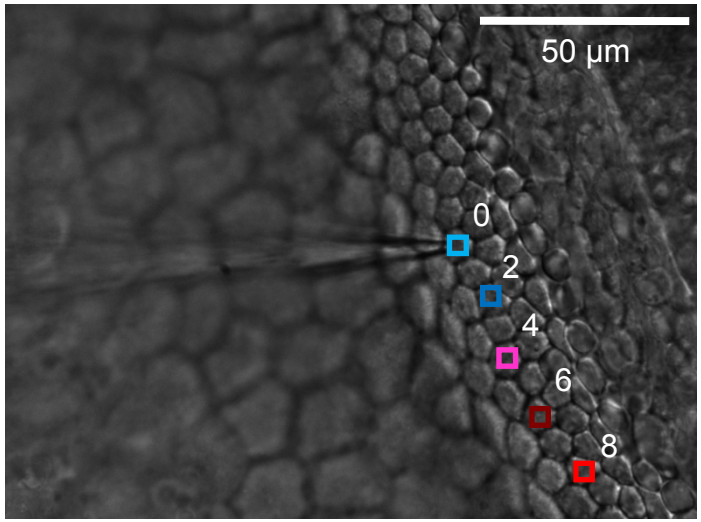

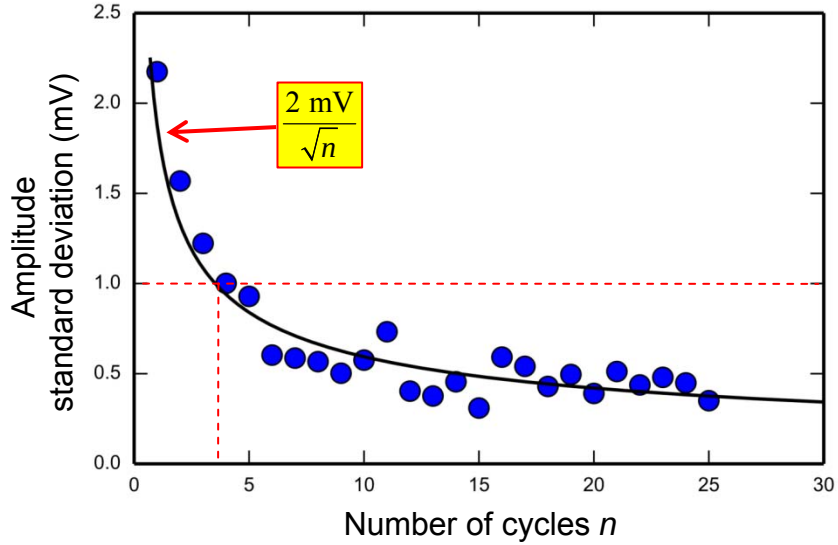

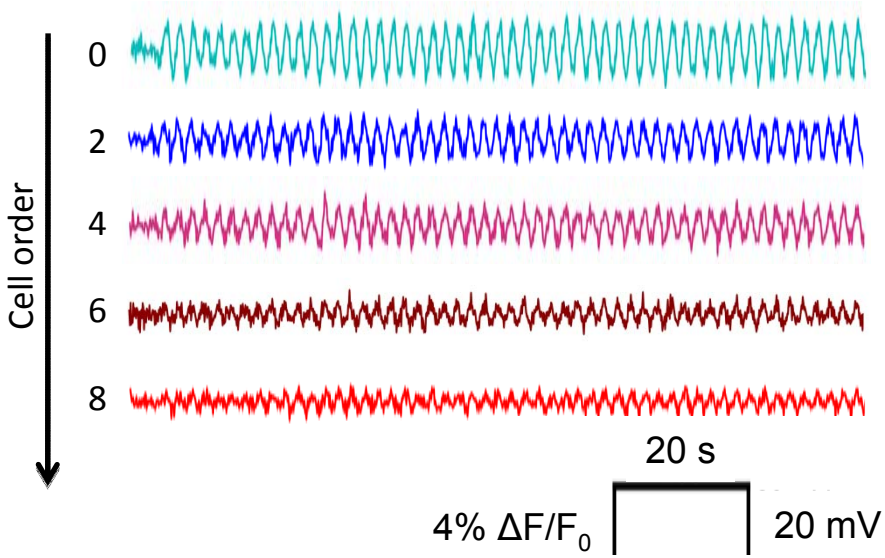

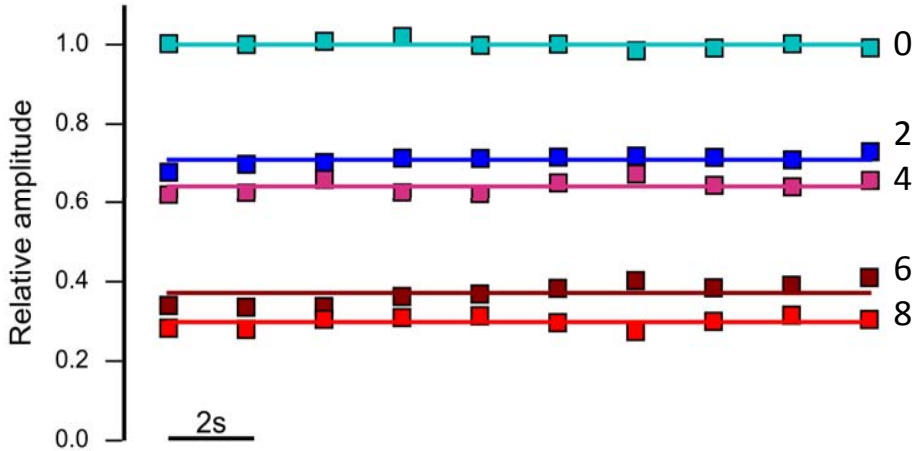

Ceriani and Mammano *Cell Communication and Signaling* 2013, **11**:78

Direct readout of network connectivity in wild type and DFNB1 mouse model cultures

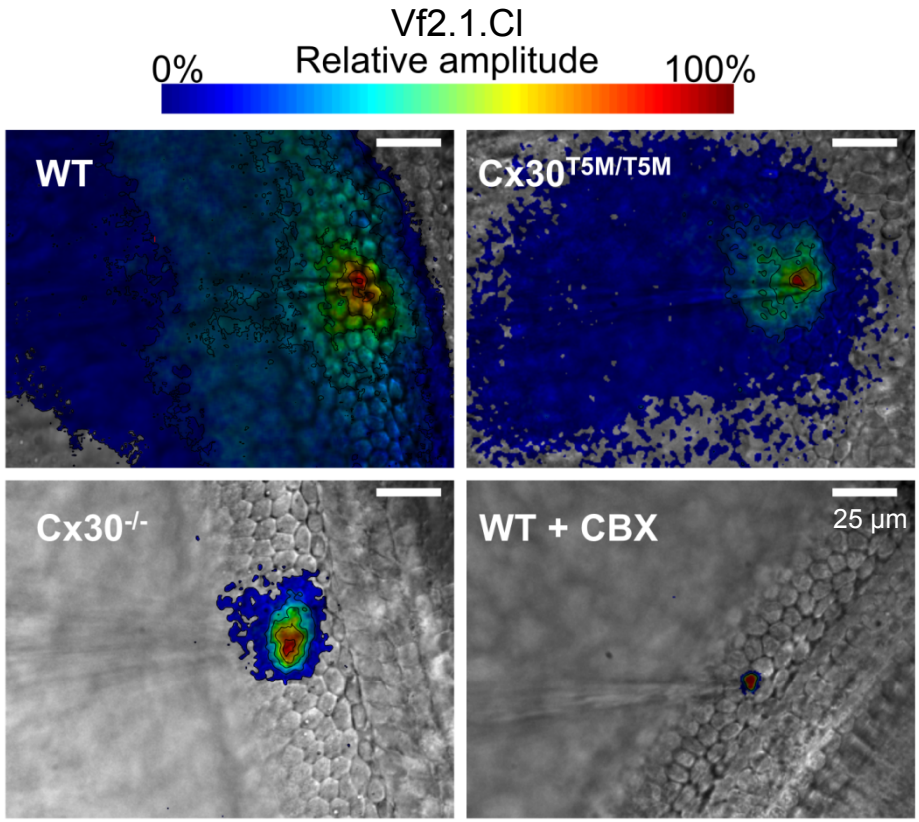

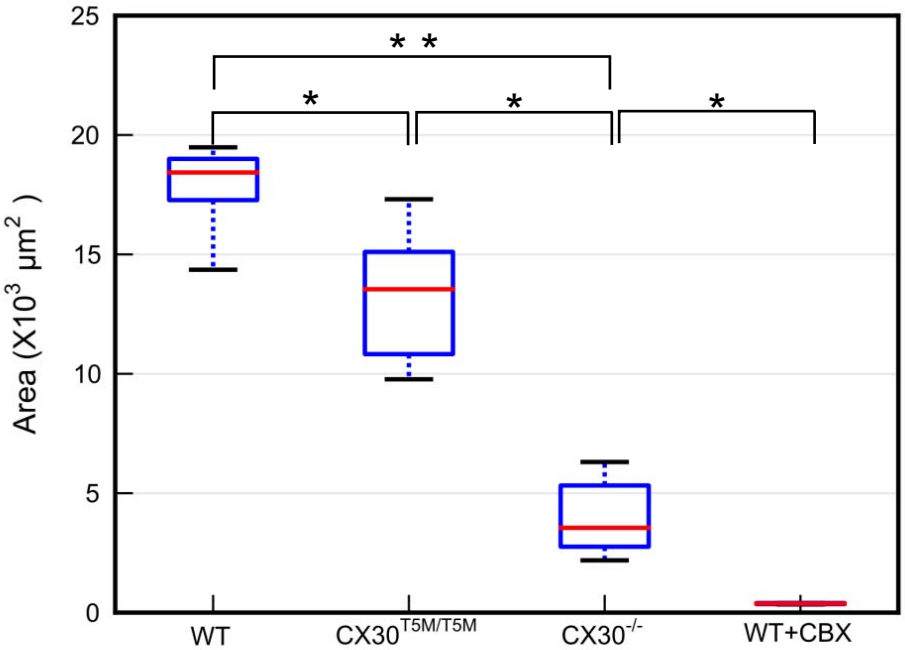

Phase-sensitive detection of Vf2.1.Cl signals allows readout of network connectivity down to at least 10th order cells in less than 10 s.

Ceriani and Mammano *Cell Communication and Signaling* 2013, **11**:78

Data fit by a simple resistive network model that reflects the anatomy

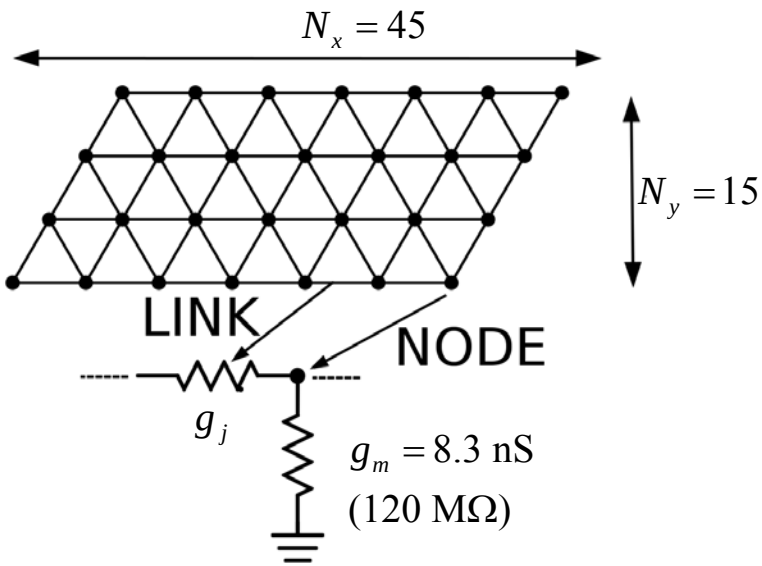

Lagostena | Mammano *Cell Communication and Adhesion* 2001

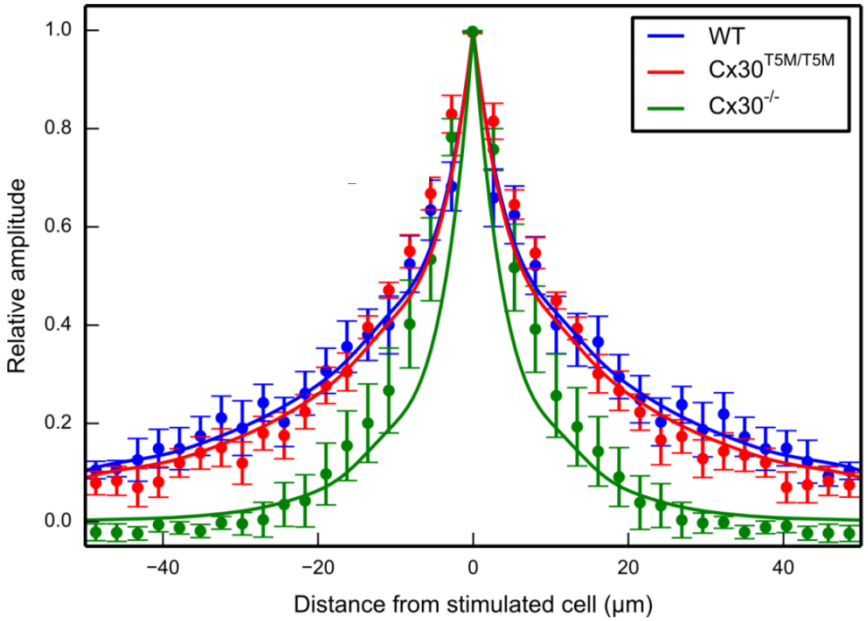

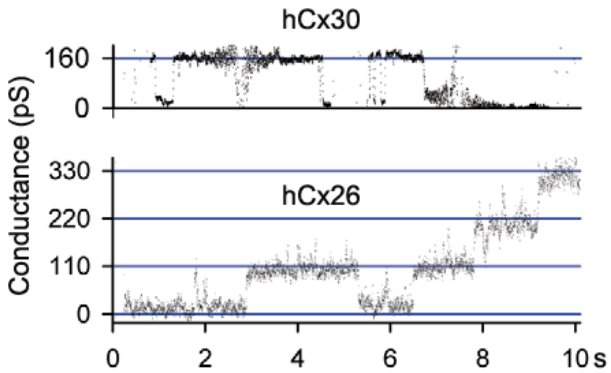

Beltramello | Mammano *Nature Cell Biology* 2005

	Junctional conductance g_j	
WT	206 ns	
Cx30$^{T5M/T5M}$	177 nS	86% of WT
Cx30$^{-/-}$	19 nS	9% of WT

Cochlear supporting cells in WT cultures are coupled by as many as ~1500 channels per cell pair in the high frequency region of the cochlea and ~1085 channels in the low frequency region.

Ceriani and Mammano *Cell Communication and Signaling* 2013, **11**:78

Reduction of junctional conductance correlates with the degree of hearing loss

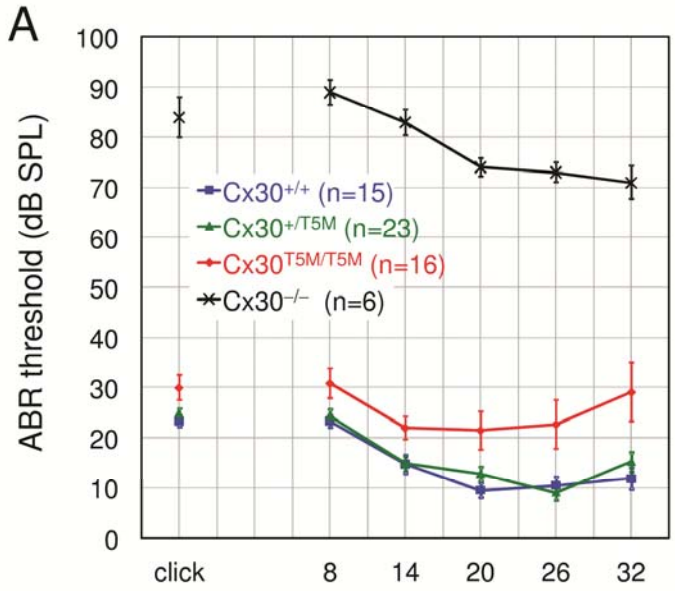

Schütz | Mammano *Human Molecular Genetics* 2010

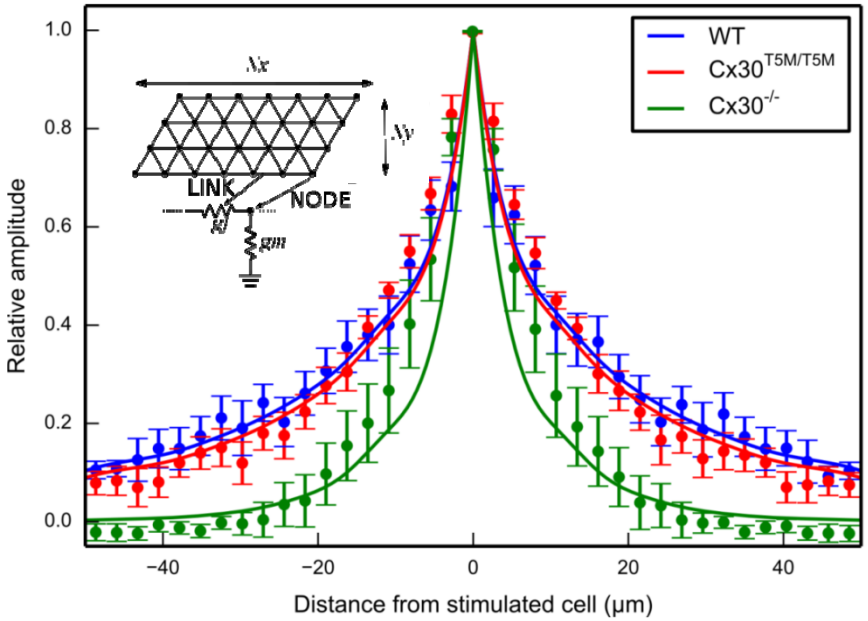

Cx30$^{-/-}$ mouse **Cx30$^{+/+}$ mouse**

Cx26/actin

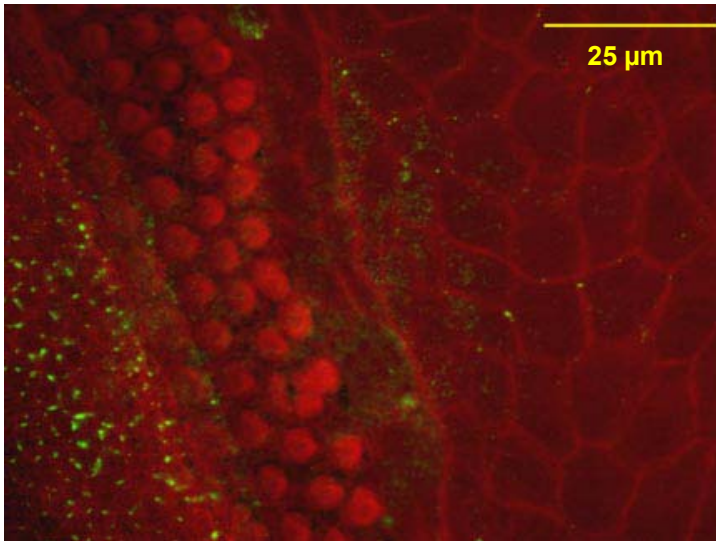

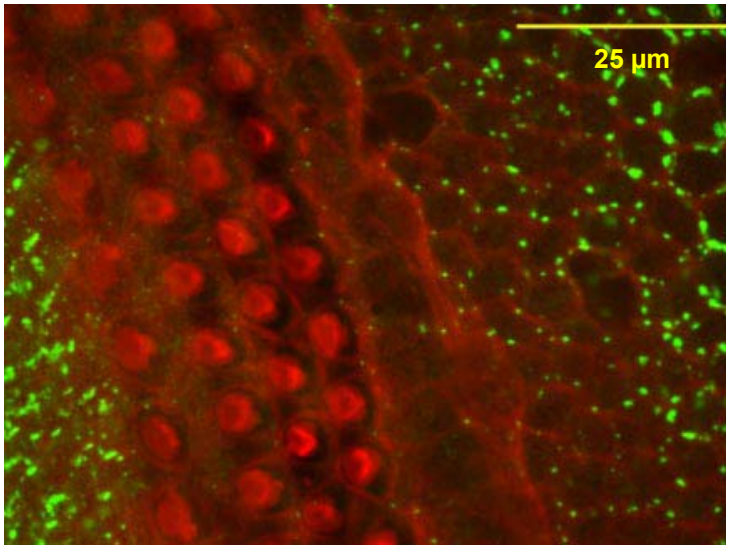

Ortolano | Mammano & Chiorini *Proc Nat Acad Sci USA* 2008

Optical readout of network connectivity in other cell types

HeLa cells transfected with hCx26-CFP

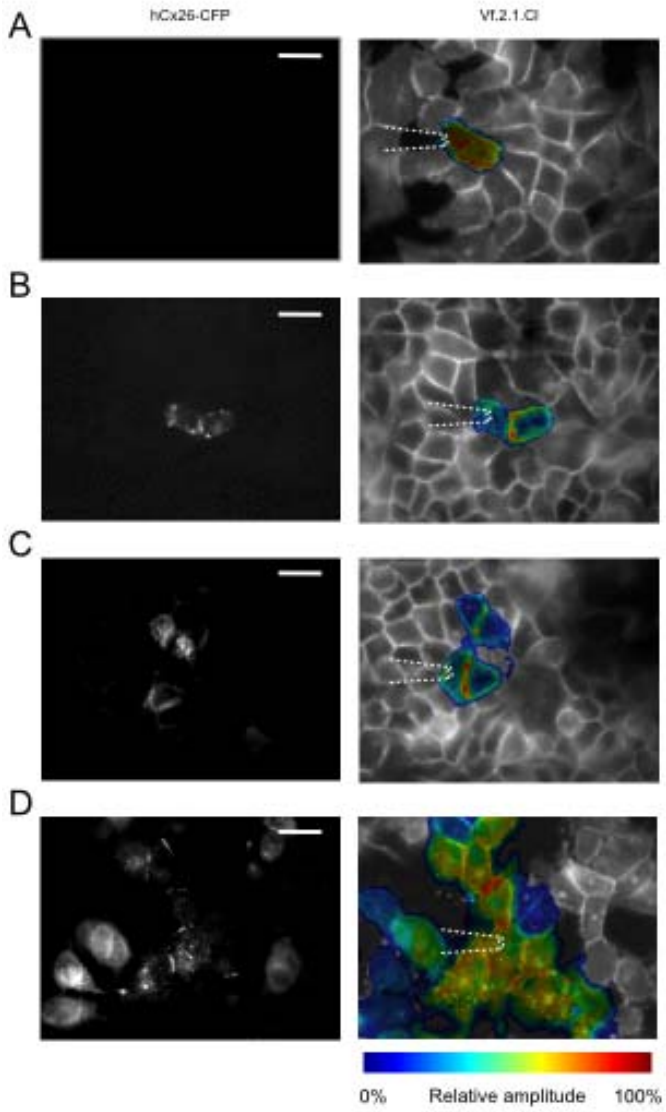

Scale bars: 25 μm

Other tumor cell lines

C26GM

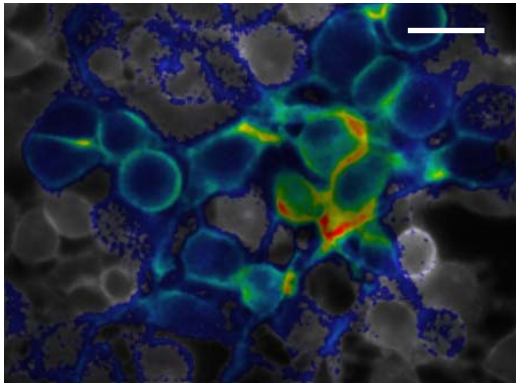

MCA203

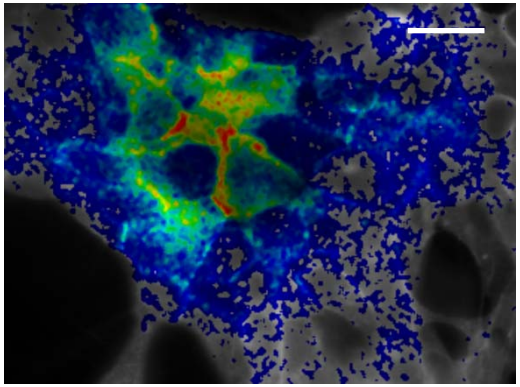

Calì | Mammano *Oncotarget* 2015

Ceriani and Mammano *Cell Communication and Signaling* 2013, **11**:78

Summary

1. The method we developed, based on phase-sensitive detection of Vf.2.1.Cl fluorescence emission, allows greater sensitivity and better time resolution compared to classical tracer-based techniques.

2. Our data indicate that each pair of cochlear non-sensory cells is already well coupled at P5 by ~1500 gap junction channels in the high frequency region and ~ 1085 channels in the low frequency region.

3. Severe hearing loss in $Cx30^{-/-}$ mice correlates with a 91% reduction in the degree of electrical coupling of cochlear non-sensory cells due to (lack of Cx30 and) strong down-regulation of Cx26.

4. Moderate hearing loss in $Cx30^{T5M/T5M}$ mice correlates with a 14% reduction in the degree of electrical coupling of cochlear non-sensory cells.

5. This method is of general interest and can be seamlessly extended to a variety of biological systems (e.g. tumor cells).

Ceriani and Mammano *Cell Communication and Signaling* 2013, **11**:78

Ca^{2+} signaling in the developing cochlea

50 µm

ATP-evoked Ca^{2+} wave

ATP-evoked Ca^{2+} oscillations

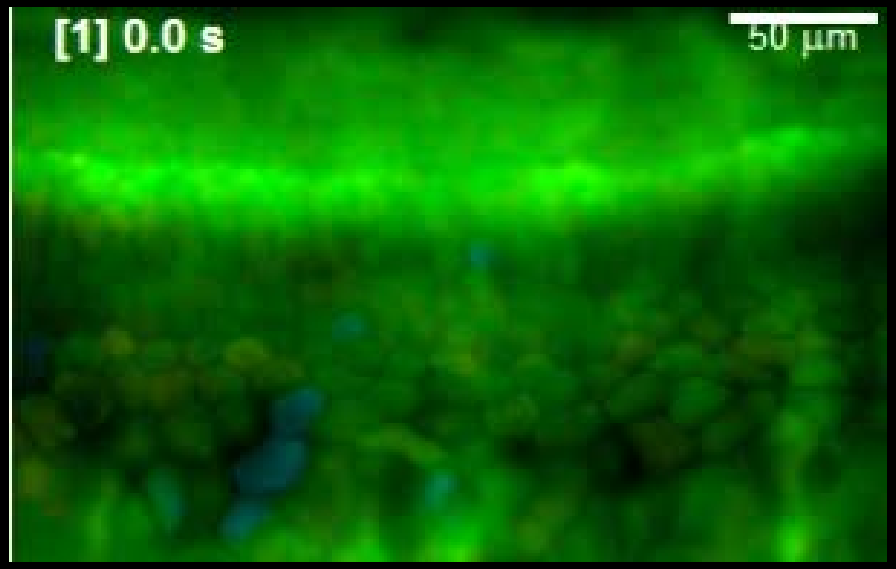

Spontaneous Ca^{2+} transients

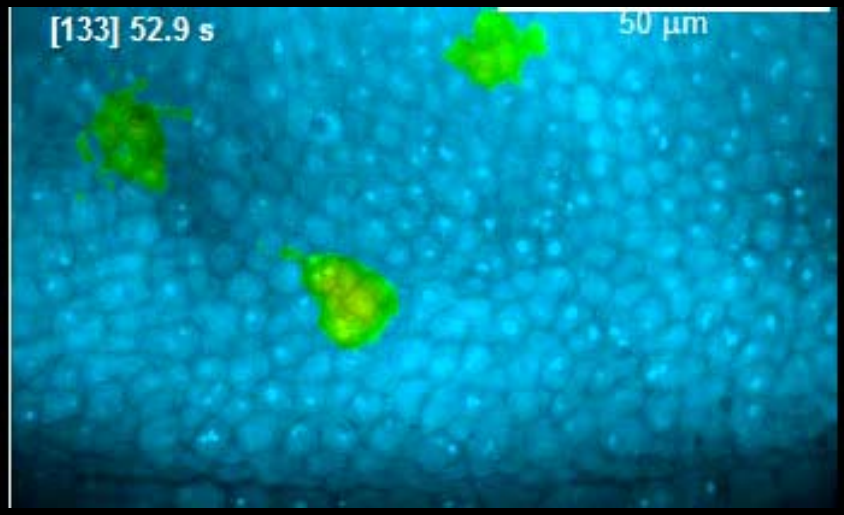

Focal UV photolysis of caged IP_3

Apyrase, which hydrolyses nucleotide triphosphates to monophosphates, reversibly and significantly limits Ca^{2+} wave spread

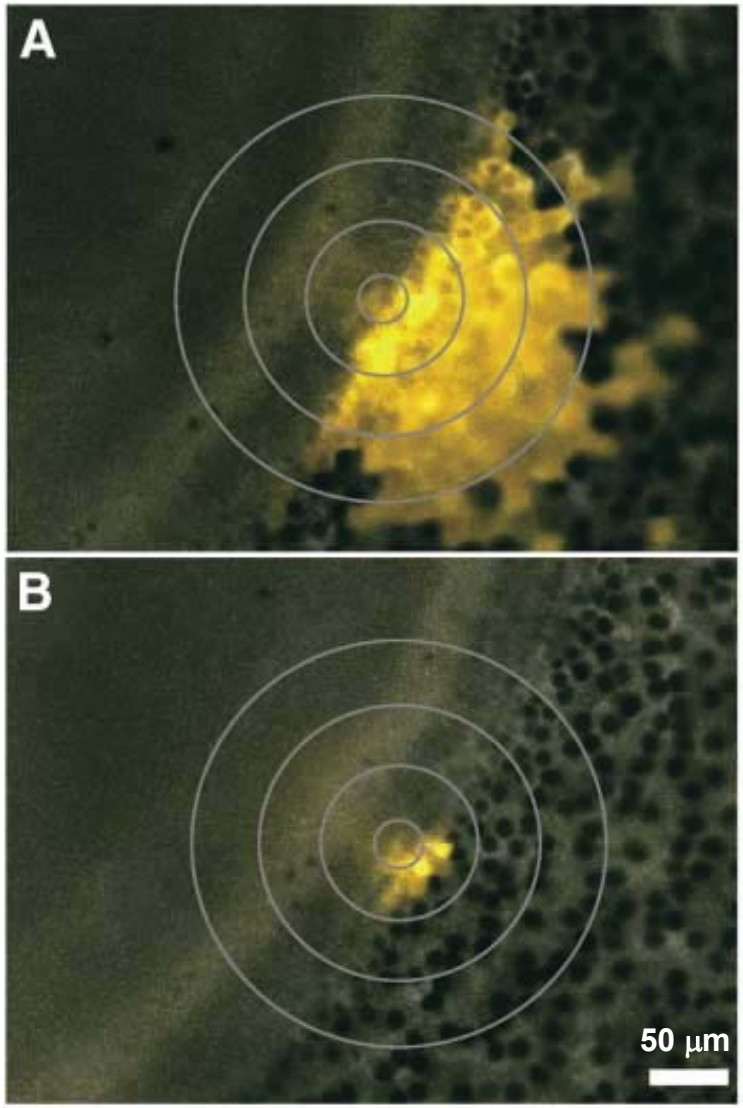

$[Ca^{2+}]_i$ changes measured in annuli centered on the stimulation site; control, gray bars (n = 5); 40 U apyrase, burgundy bars (n = 6); wash, gold bars (n = 6). Significant differences: $p < 0.05$ (*) and $p < 0.01$ (**).

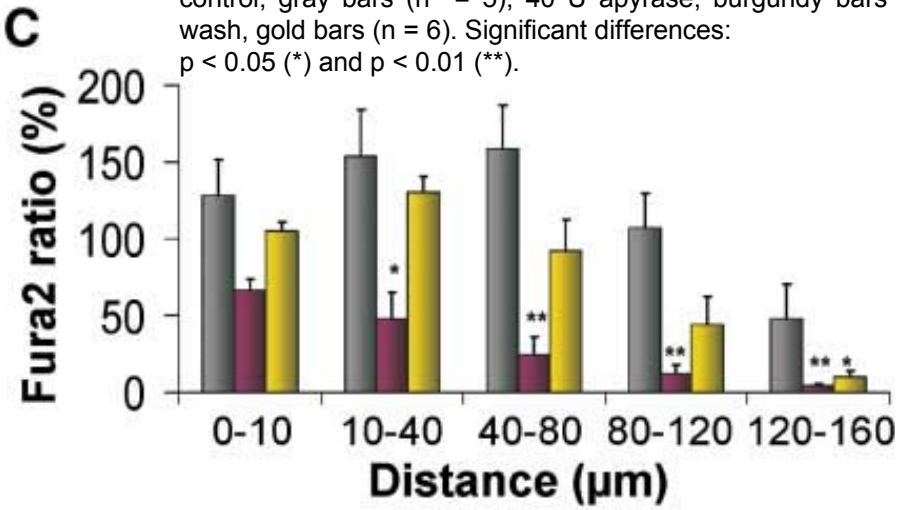

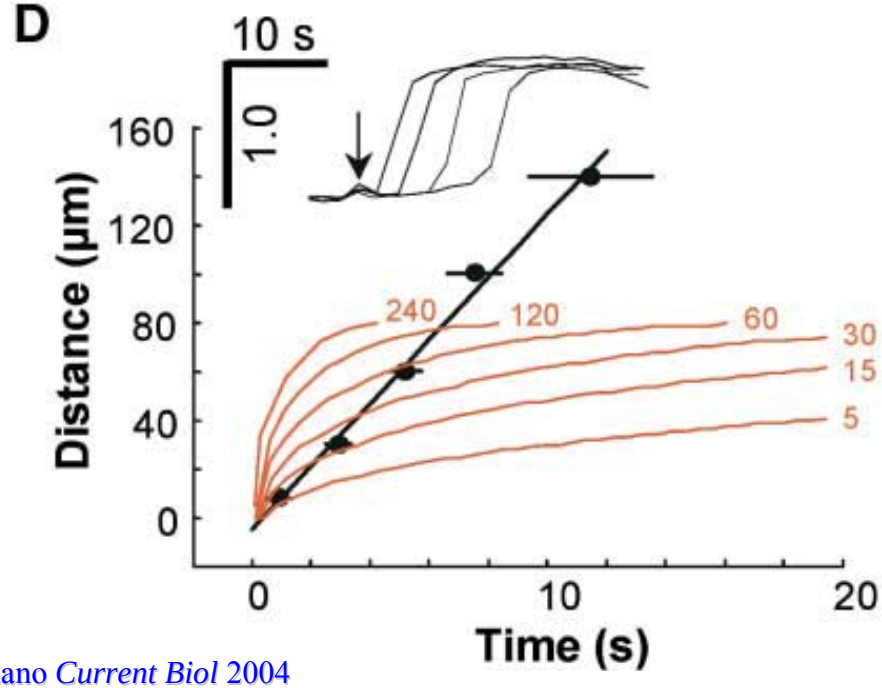

Gale | Mammano *Current Biol* 2004

Spontaneous Ca^{2+} transients in non sensory cells of the greater epithelial ridge are reversibly inhibited by flufenamic acid, a connexin channel inhibitor

Cochlear organotypic culture loaded with Fluo–4 AM

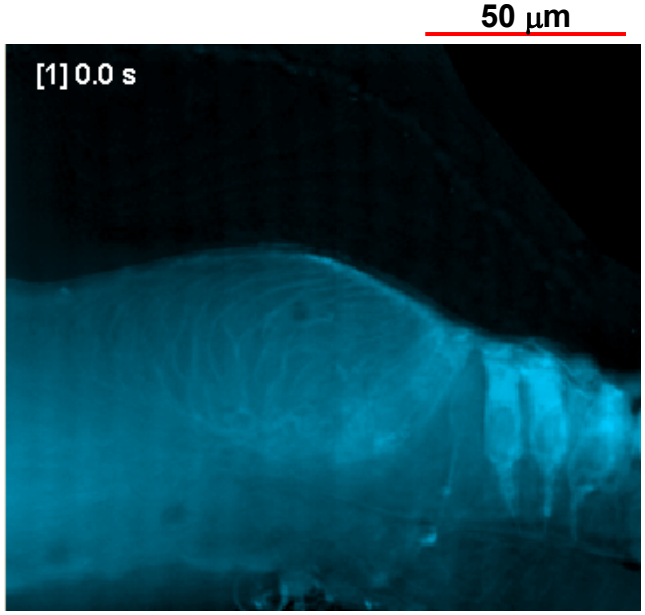

Hemicochlea loaded with Fluo–forte AM

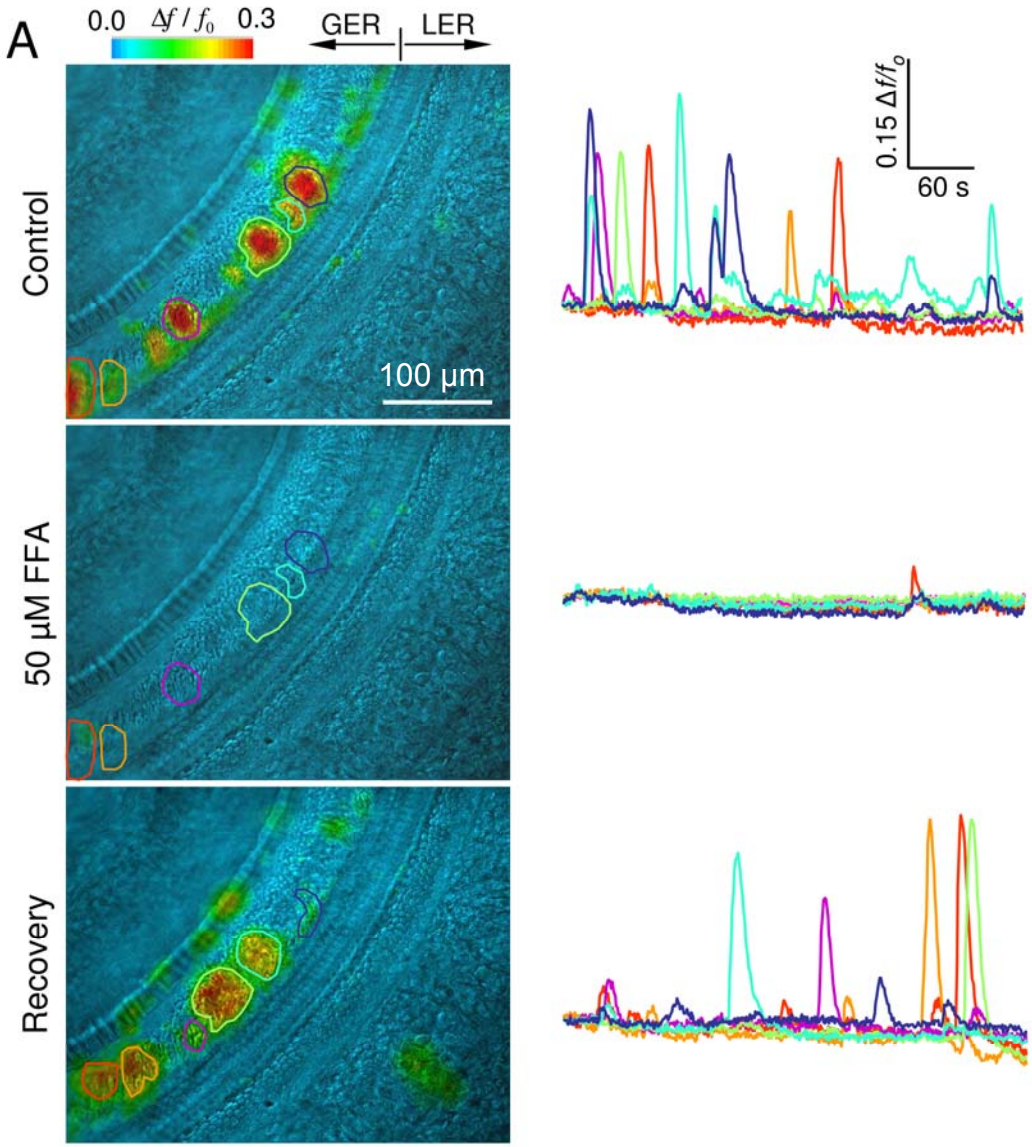

Schütz | Mammano. *Human Molecular Genetics* 2010

CELAbs detect connexin hemichannels at the surface of the sensory epithelium (P6)

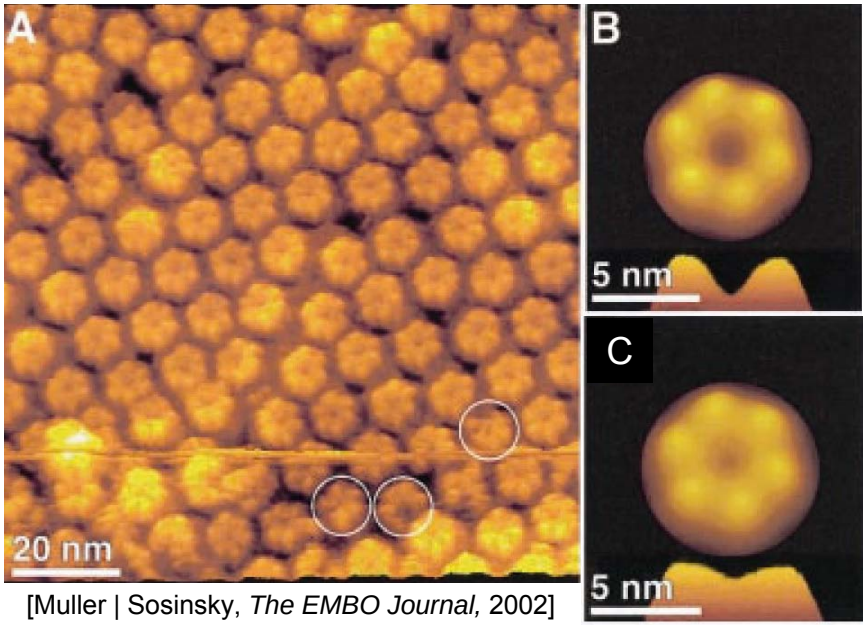

[Muller | Sosinsky, *The EMBO Journal*, 2002]

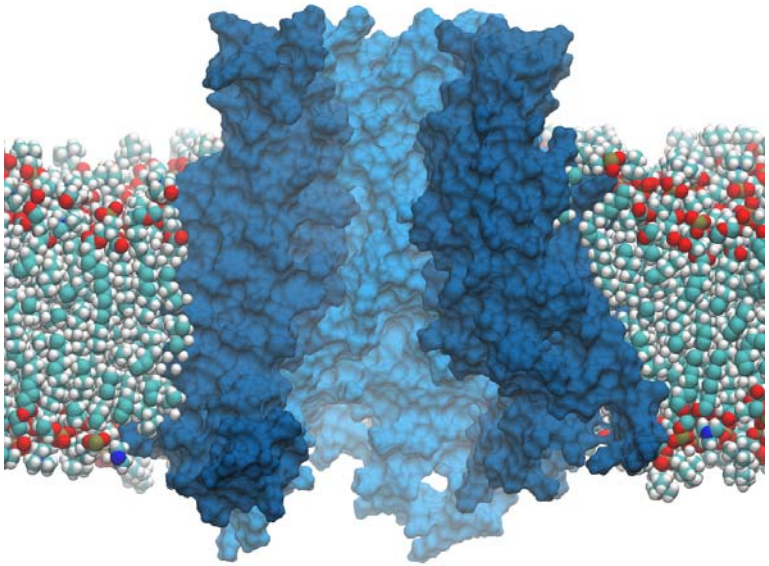

Zonta | Mammano *J Biomolecular Structure & Dynamics* 2012

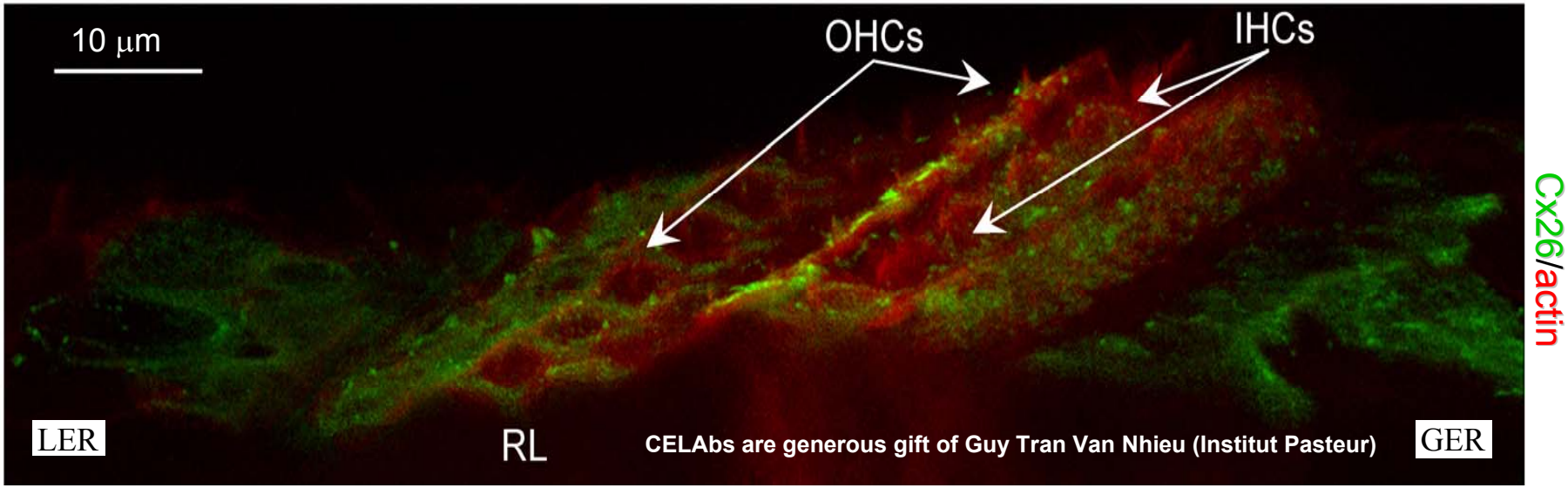

Majumder | Mammano *Purinergic Signaling* 2010

Intracellular delivery of IP_3 in zero $[Ca^{2+}]_o$ triggers Ca^{2+} wave propagation and ATP release at the endolymphatic surface of the sensory epithelium

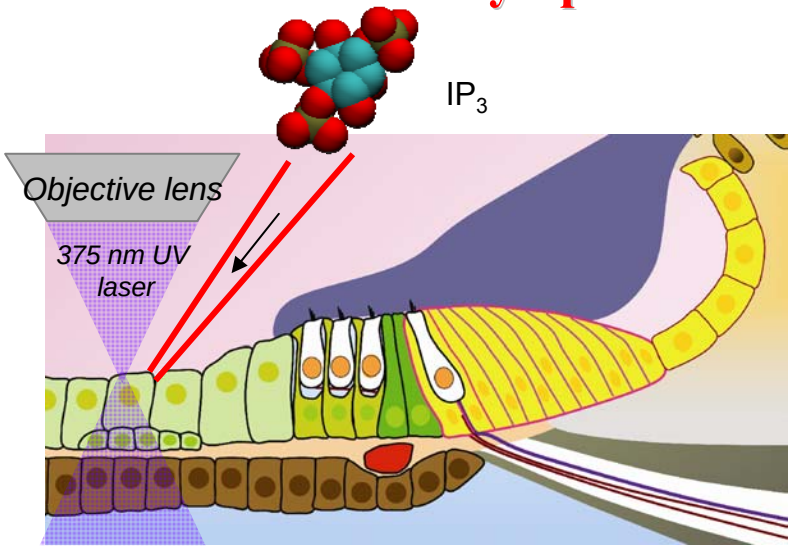

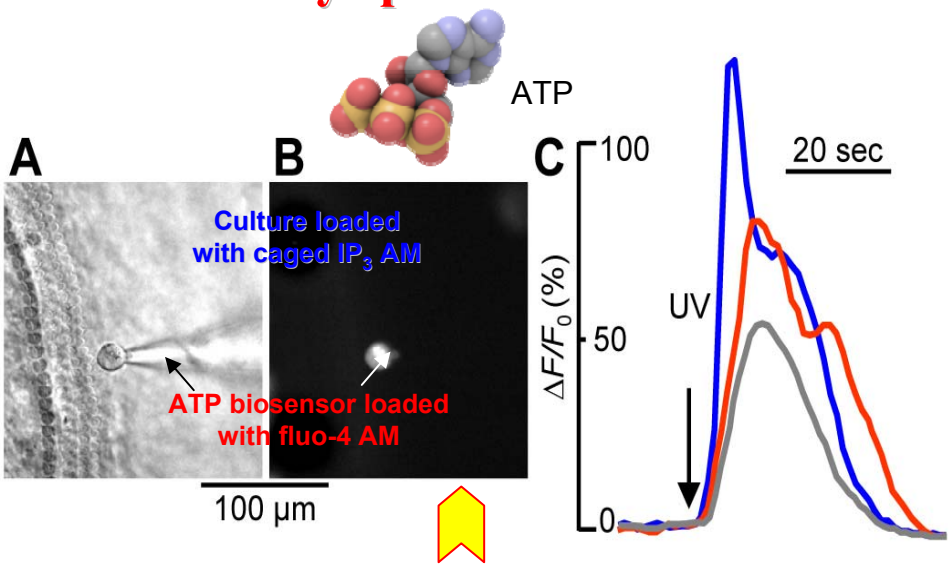

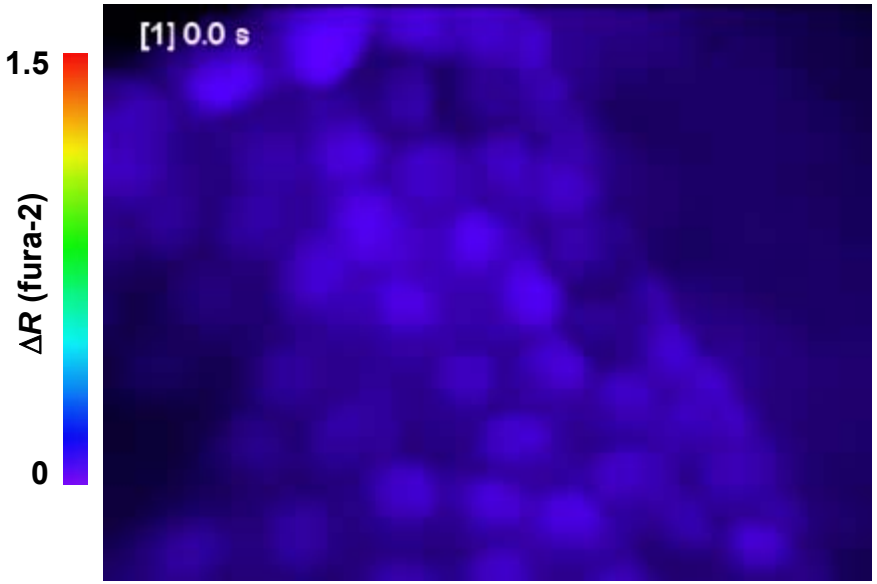

Culture loaded with fura-2, IP_3 100 µM in patch pipette,

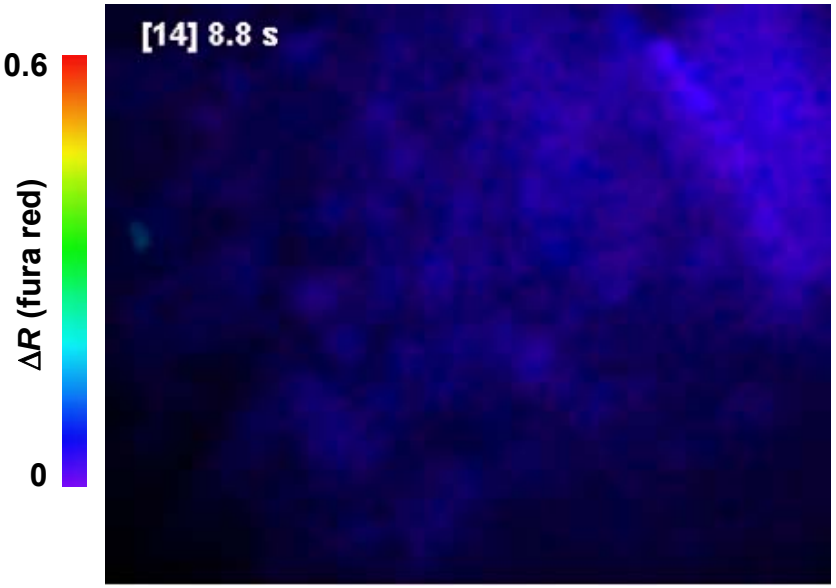

Culture co-loaded with fura red and caged IP_3

Beltramello | Mammano *Nat Cell Biol* 2005

Anselmi | Mammano *Proc Nat Acad Sci USA* 2008

In the presence of suramin, a broad spectrum antagonist of P2 receptors, Ca^{2+} signals fail to spread beyond neareast neighbors

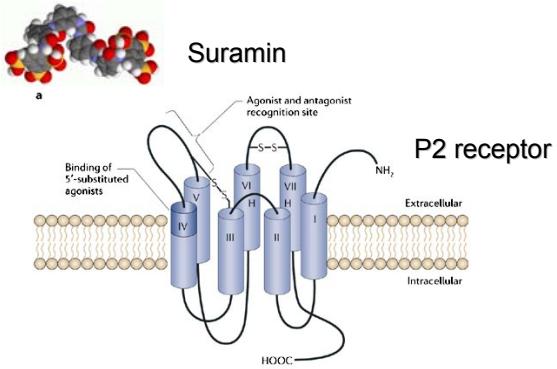

[Fields *et al. Nature Reviews Neuroscience*, 2006]

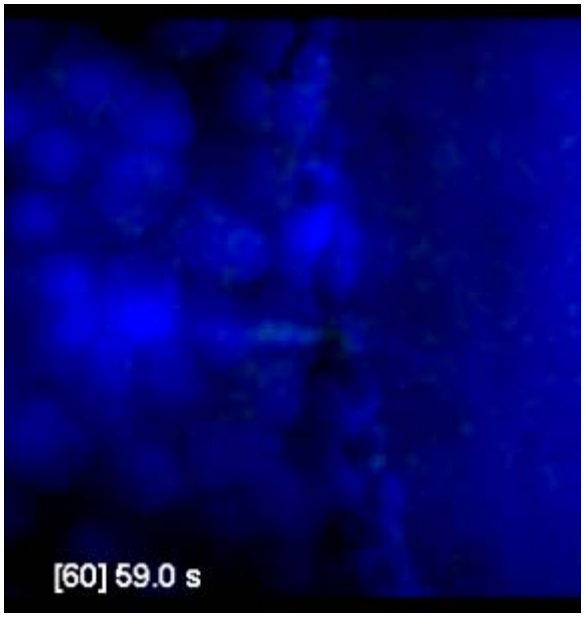

IP_3 500 μM in pipette

Suramin 200 μM extracellular

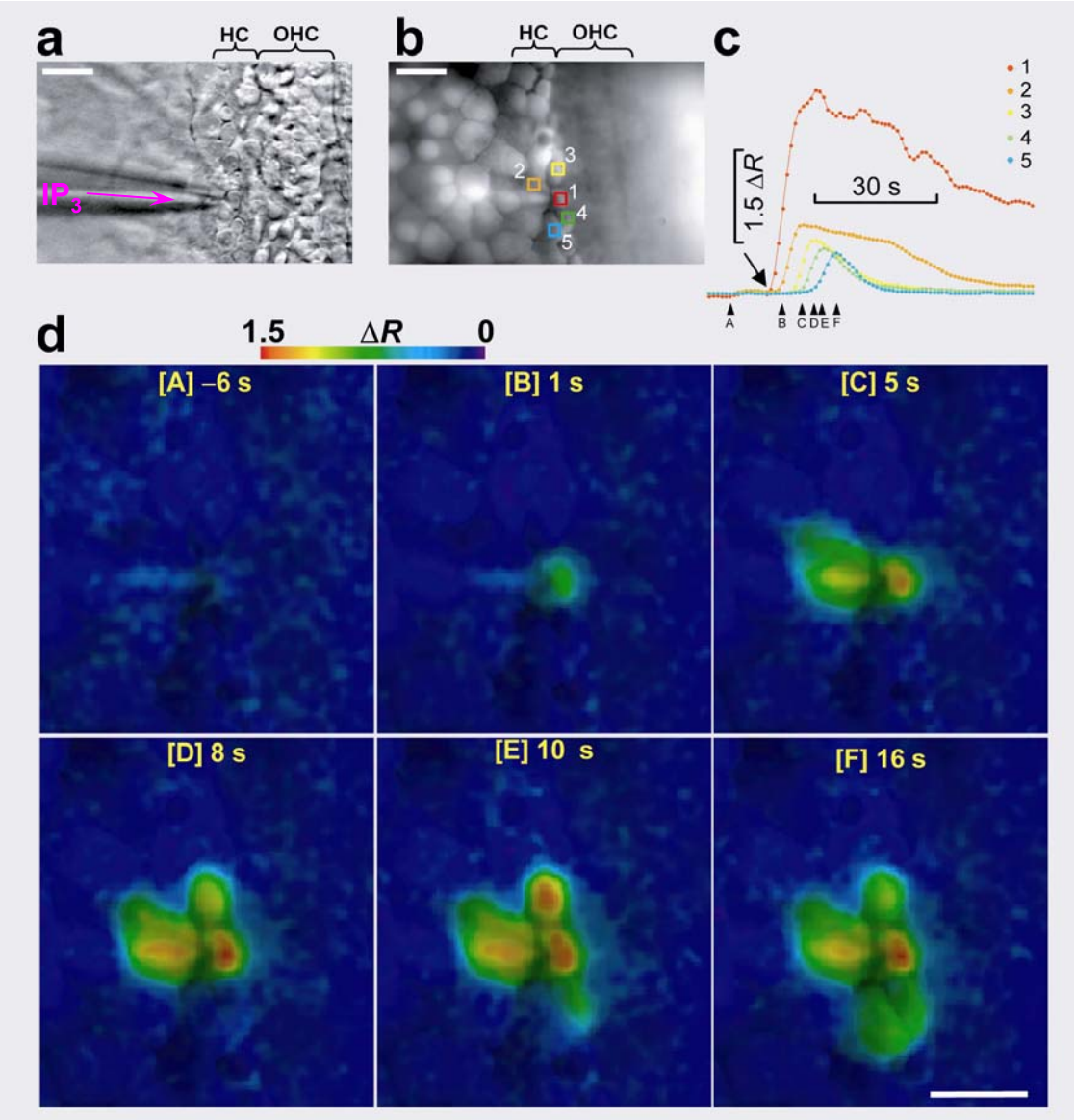

Beltramello | Mammano *Nat Cell Biol* 2005

Connexin channel blockers, but not anion channel blockers, inhibit intercellular Ca^{2+} wave propagation

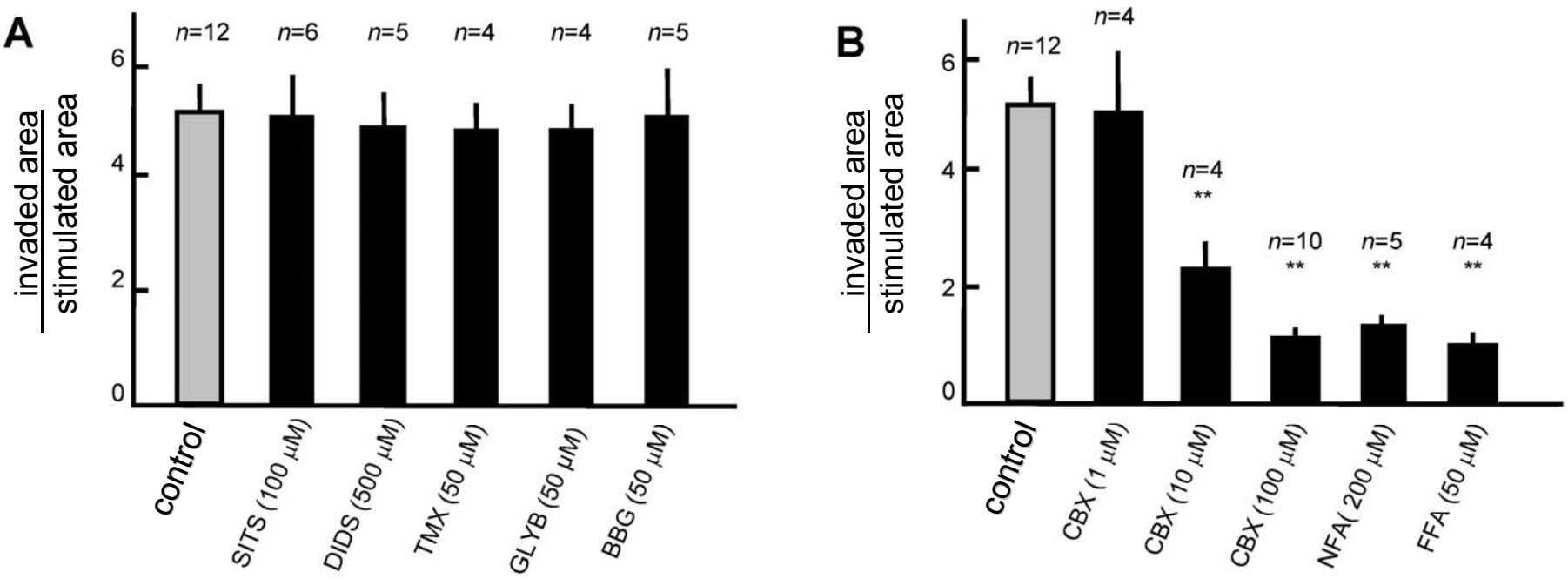

(A) Brilliant Blue G (BBG), 4,4'–di–isothiocyanatostilbene–2,2'–disulfonic acid (DIDS), tamoxifen (TMX), glybenclamide (GLYB), 4–acetamido–4'–isothiocyanostilbene–2',2–disulfonate (SITS),

(B) carbenoxolone (CBX), niflumic acid (NFA), flufenamic acid (FFA).

Data are mean ± S.E. for independently repeated experiments on cultures from *n* ≥ 4 different animals.

Anselmi | Mammano *Proc Nat Acad Sci USA* 2008

Intercellular Ca^{2+} wave propagation is inhibited in connexin deficient cochlear cultures

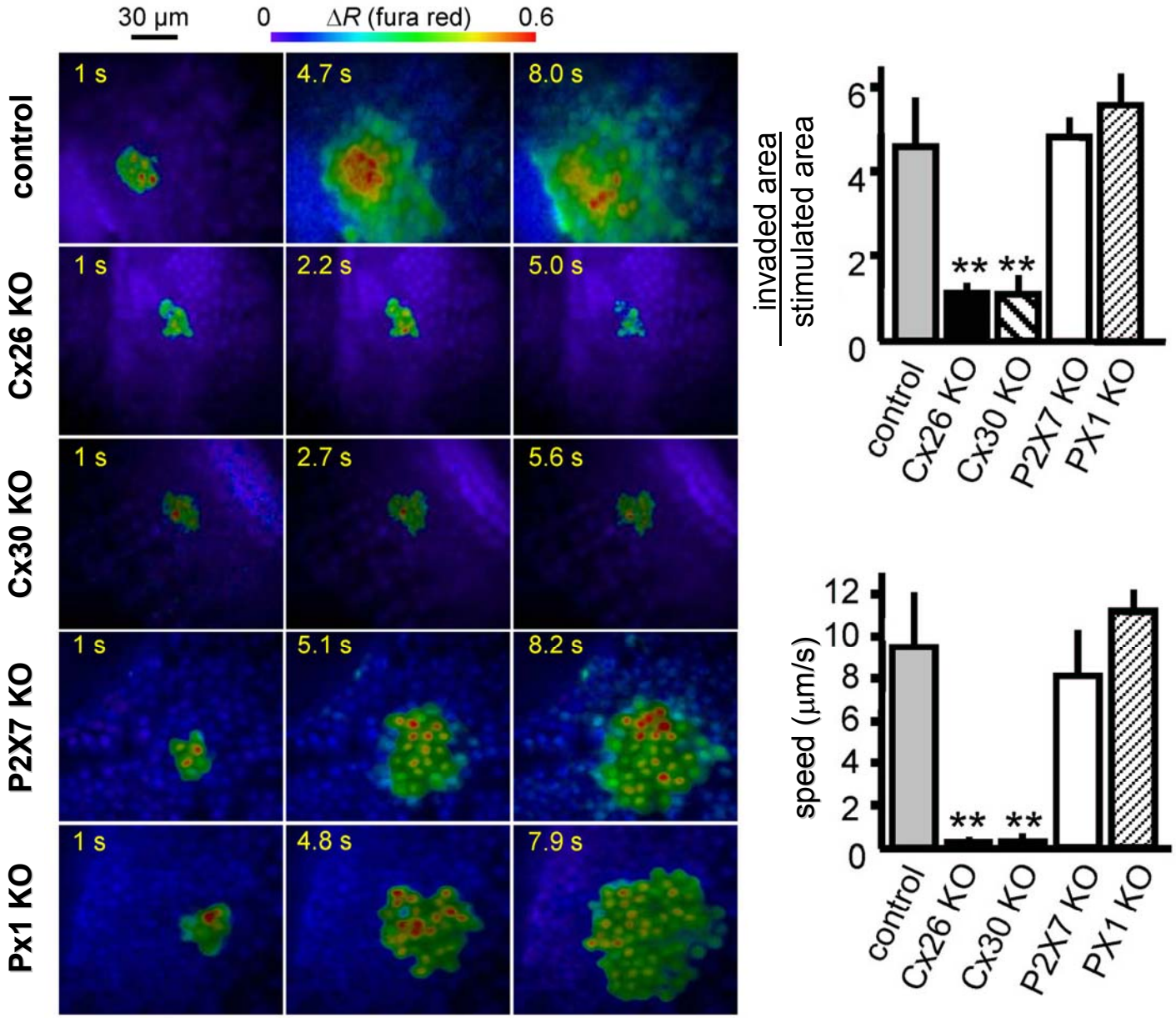

Anselmi | Mammano *Proc Nat Acad Sci USA* 2008

Viral transduction with BAAVCx30GFP restores gap-junction coupling

Cochlear organotypic cultures loaded with calcein-AM

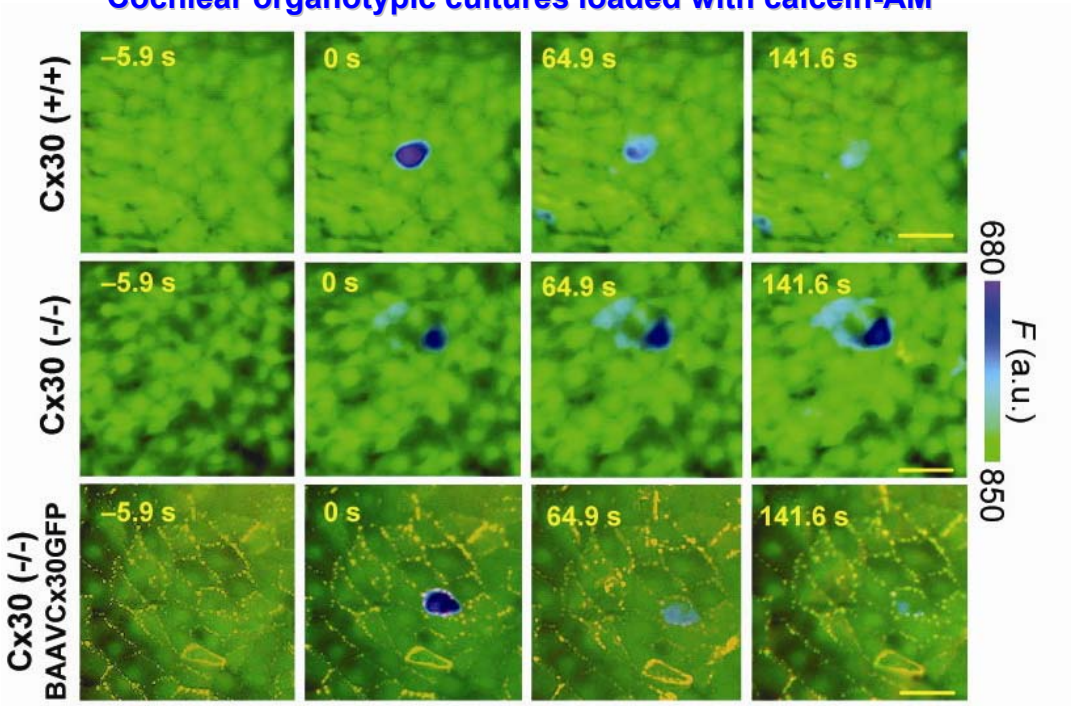

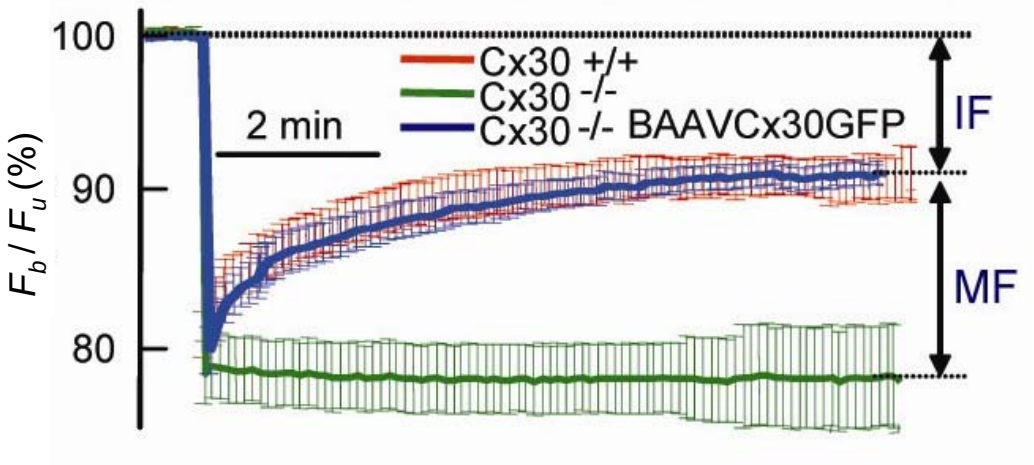

Ortolano | Mamamno & Chiorini *Proc Nat Acad Sci USA* 2008

Viral transduction with BAAVCx30GFP also restores Ca^{2+} wave propagation

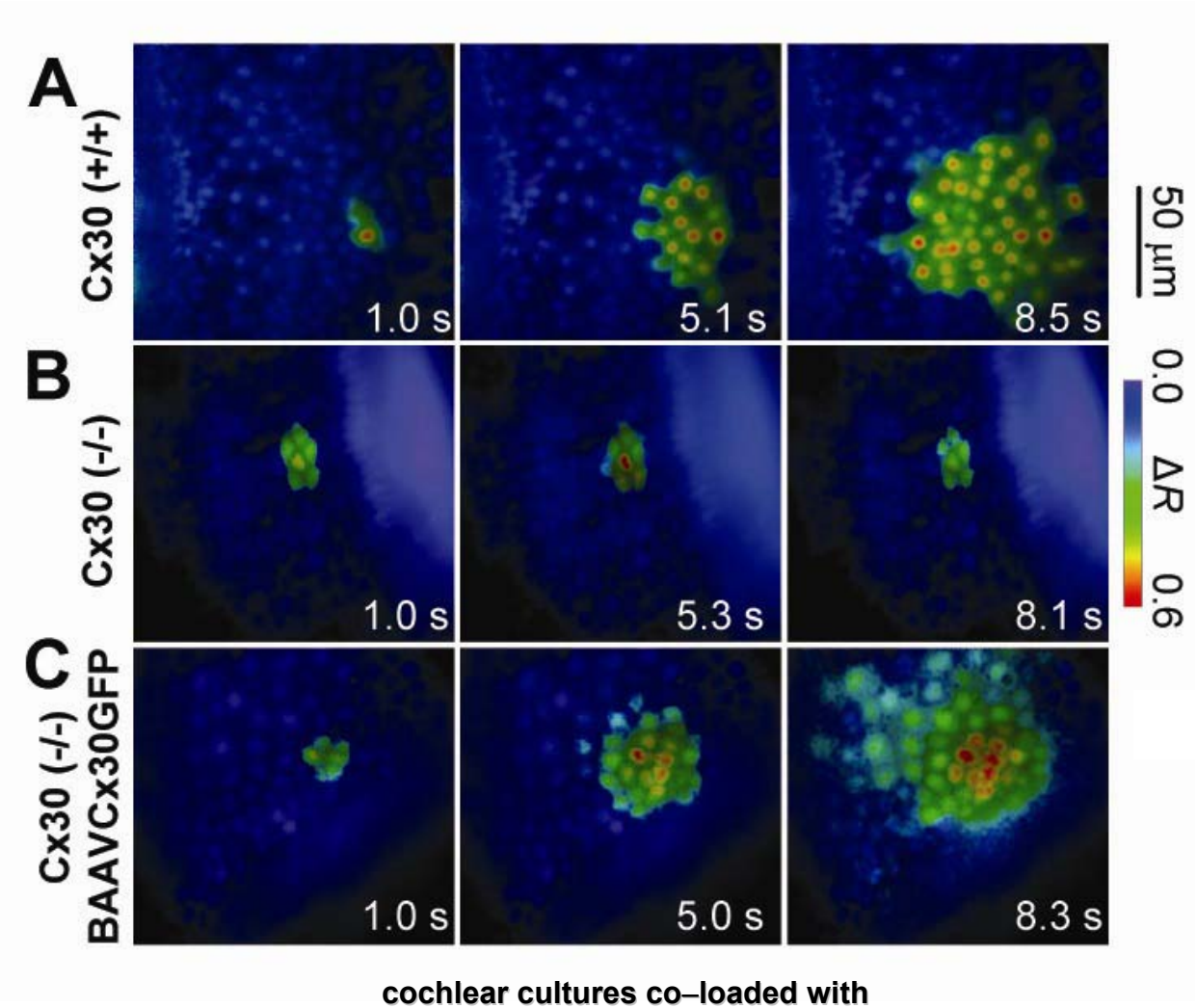

cochlear cultures co–loaded with caged IP_3 AM and fura red AM

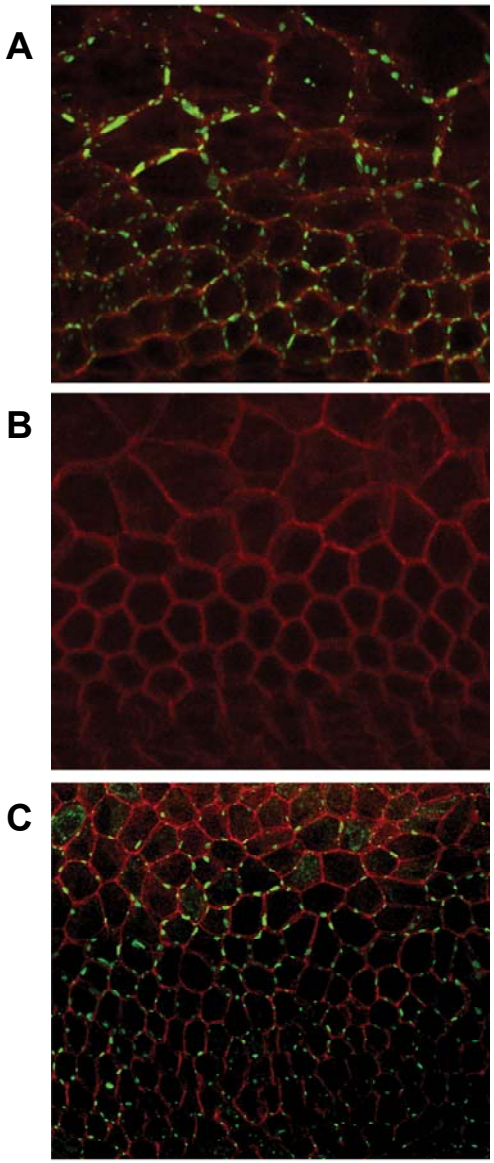

Cx30/actin

ATP-evoked Ca^{2+} signals and spontaneous Ca^{2+} transients share the same IP_3-dependent signal transduction cascade

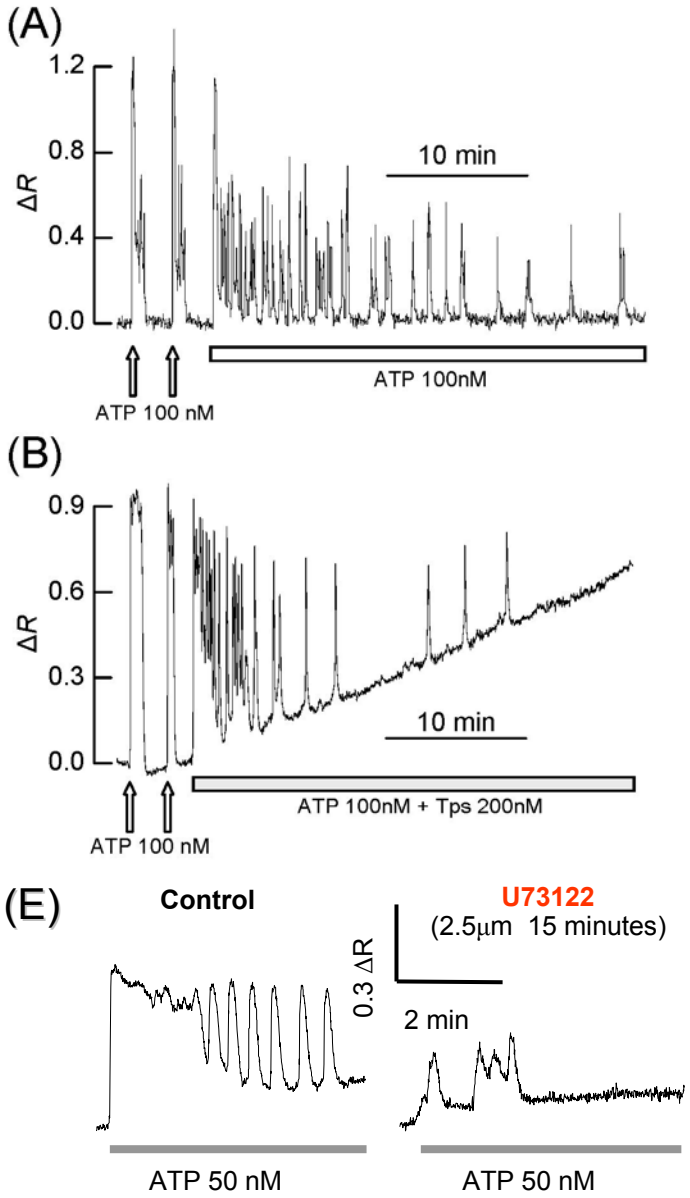

Piazza | Mammano *Cell Calcium* 2007

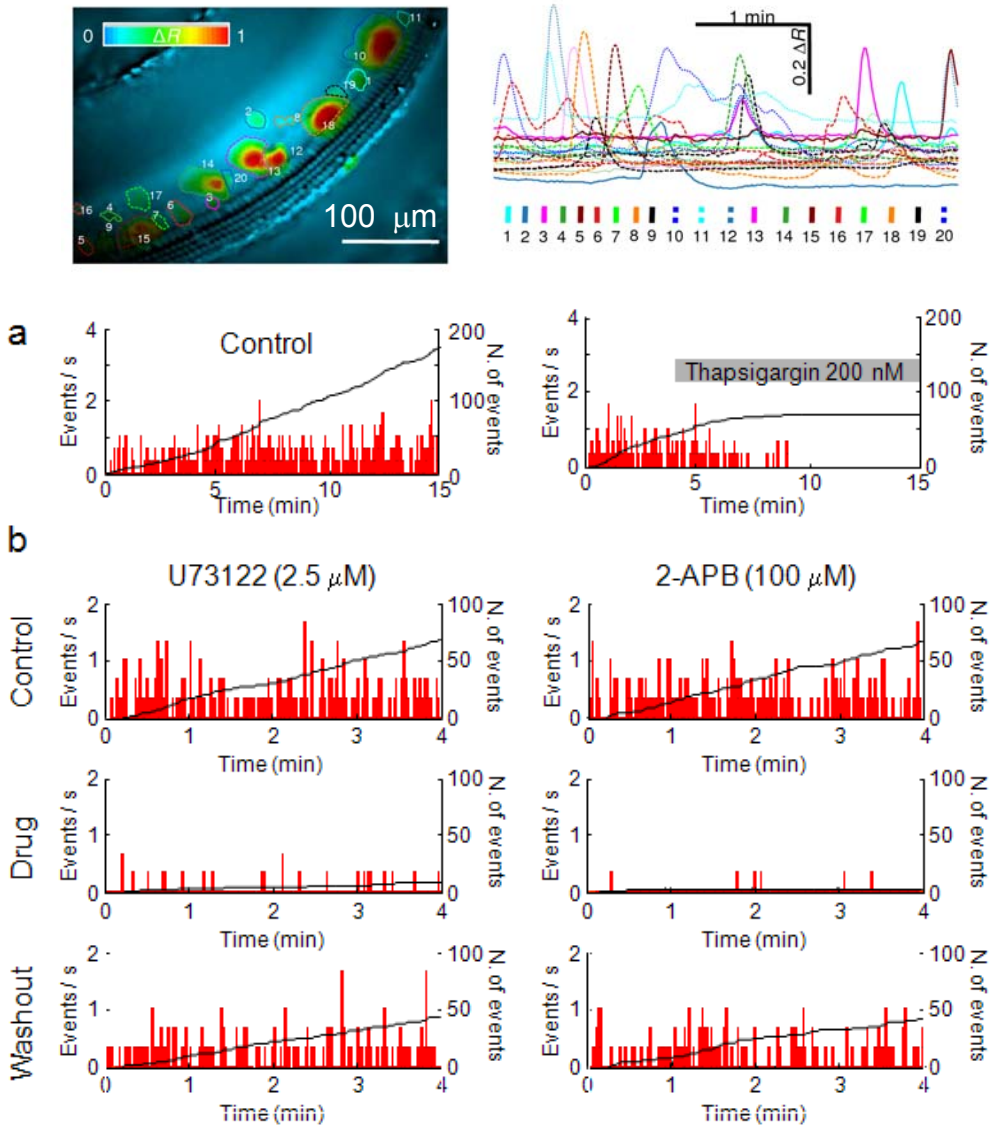

Rodriguez | Mammano *PNAS* 2012

Spontaneous Ca^{2+} signaling activity is significantly reduced in the developing cochlea of $Cx30^{T5M/T5M}$ knock–in mice

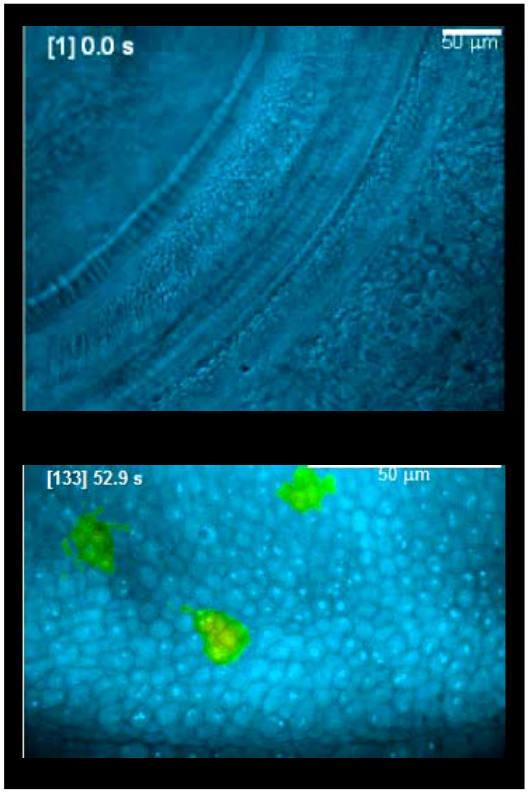

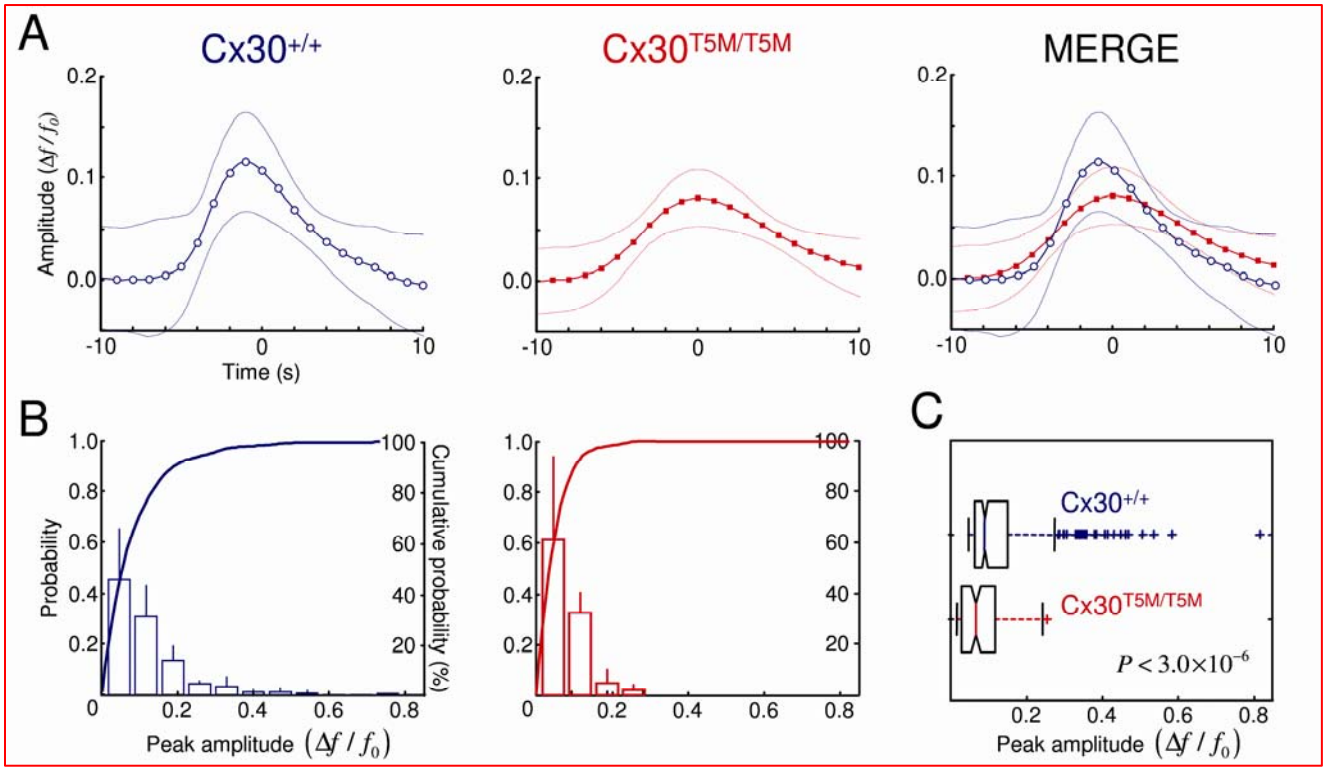

Properties of spontaneous events

	$Cx30^{+/+}$	$Cx30^{T5M/T5M}$	P
Peak amplitude $(\Delta f / f_0)$	0.22 ± 0.14	0.11 ± 0.05	$< 3 \times 10^{-6}$
Events /min	14.0 ± 5.9	3.9 ± 1.3	< 0.015

Data are mean ± s.d. for independent experiments on cultures from n=4 mice of each genotype.

In vivo delivery of flufenamic acid via canalostomy to the inner ear of P4 mice prevents normal hearing acquisition

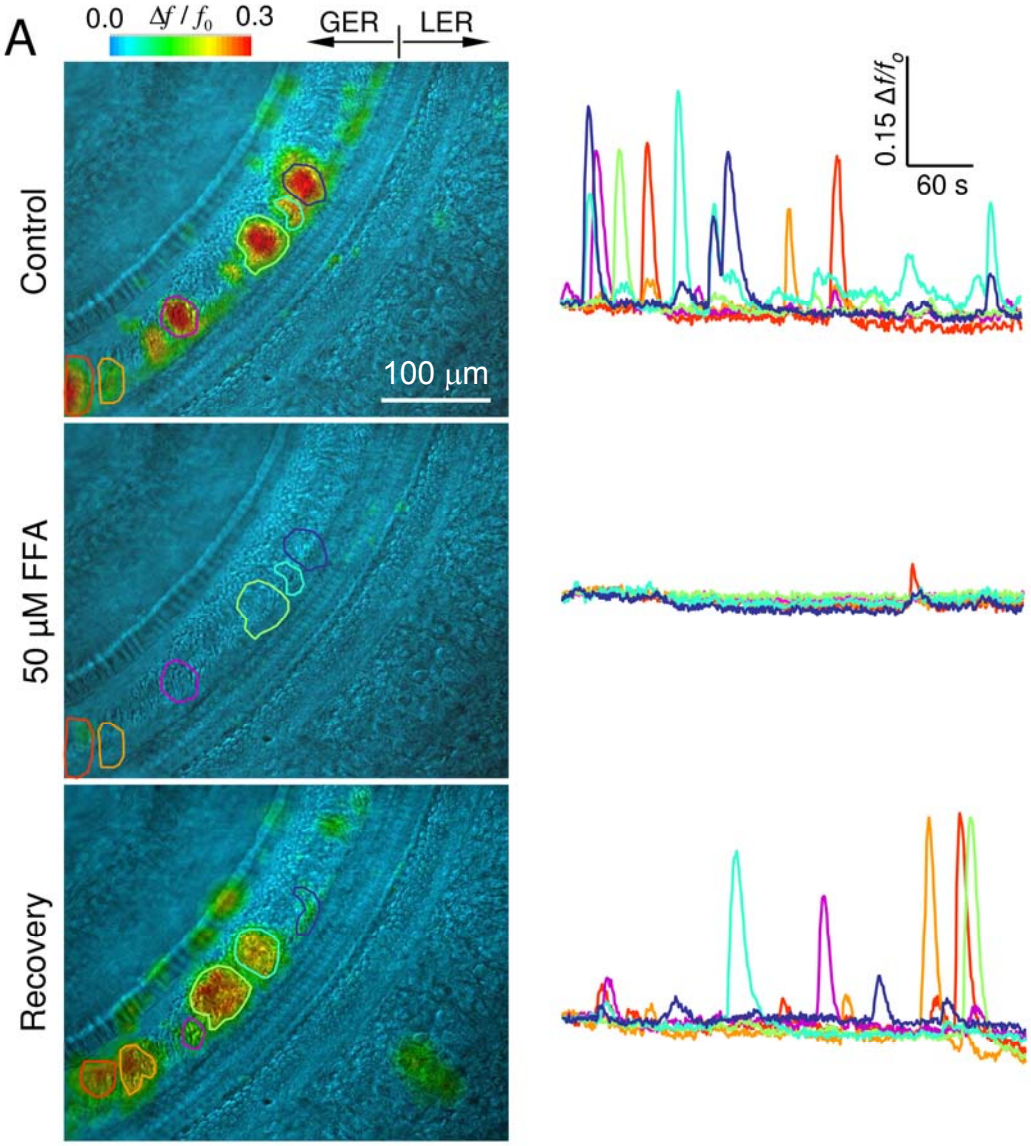

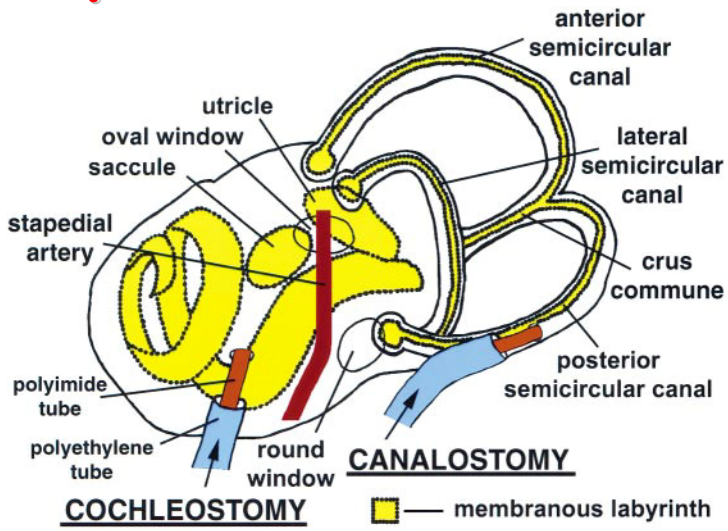

[Kawamoto et al. Mol Ther 2001]

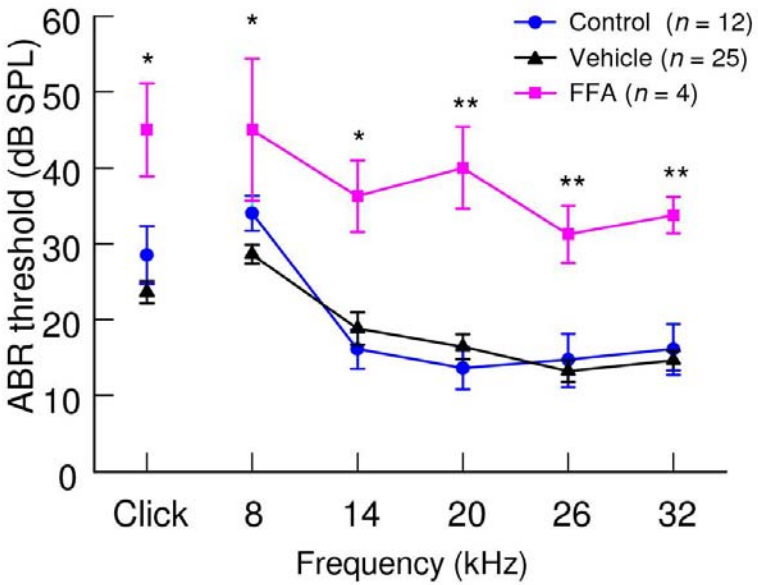

Schütz | Mammano *Human Molecular Genetics* 2010

Rodriguez | Mammano *PNAS* 2012

Mathematical model

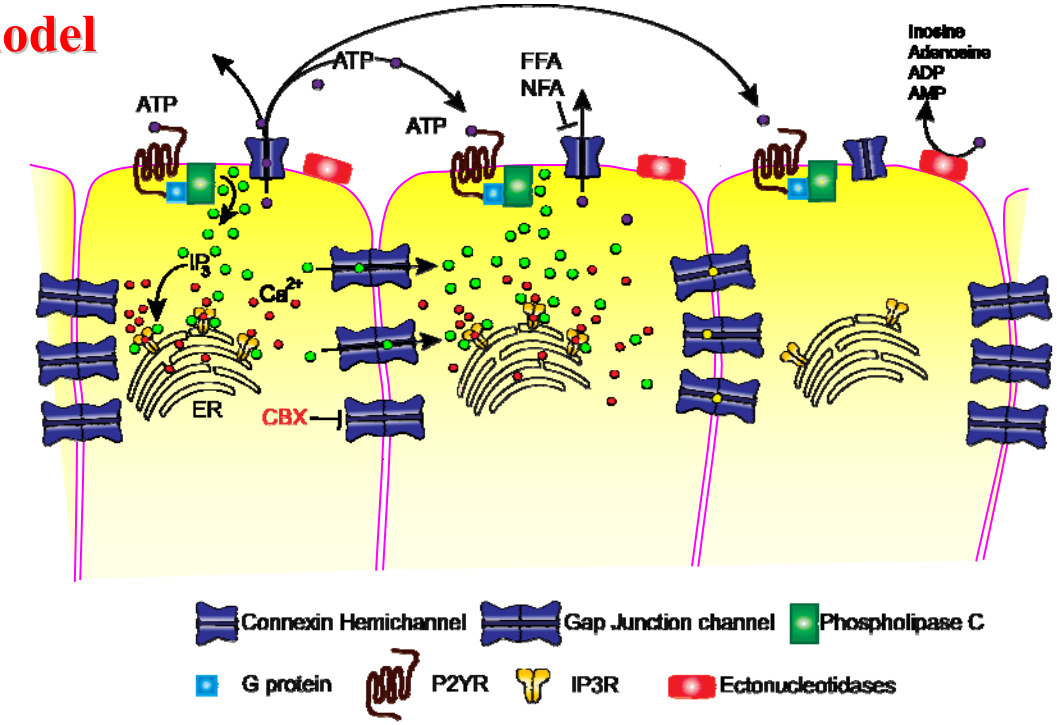

$$\frac{d[Ca^{2+}]_c}{dt} = (k_{IP_3R}h^3 + k_{leak})([Ca^{2+}]_{ER} - [Ca^{2+}]_c) - v_{SERCA}\frac{([Ca^{2+}]_c)^2}{([Ca^{2+}]_c)^2 + K_{SERCA}^2}$$

$$\frac{dh}{dt} = \frac{h_\infty([Ca^{2+}]_c, [IP_3]_c) - h}{\tau([Ca^{2+}]_c, [IP_3]_c)}$$

$$\frac{d[IP_3]_c}{dt} = v_{PLC}\frac{([ATP]_e)^\alpha}{([ATP]_e)^\alpha + (K_{PLC})^\alpha} - k_{deg}^{IP_3}[IP_3]_c + \sum_{n \text{ (nearest neighbours)}} k_j([IP_3]_{c,n} - [IP_3]_c)$$

$$\frac{d[ATP]_e}{dt} = D_{ATP}\nabla^2[ATP]_e + J_{HC}^{ATP}([Ca^{2+}]_c) - k_{deg}^{ATP}[ATP]_e$$

Ceriani, Pozzan, Mammano, ms in preparation

Model validation 1: Ca^{2+} signals elicited by photolitic release of IP_3

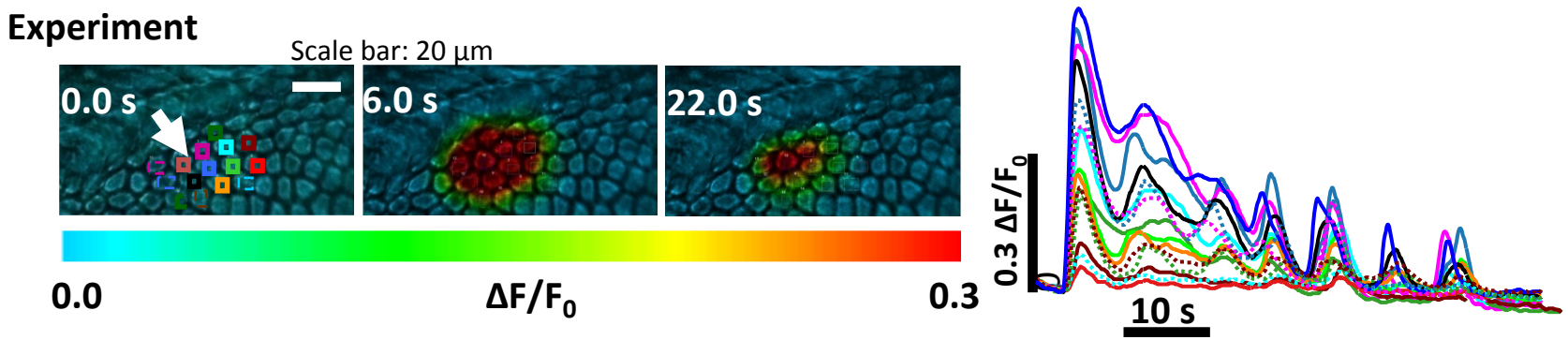

- Apical cultures of mouse cochlea (P5) were loaded with fluo-4 calcium indicator and caged IP_3 (5 µM).
- Flashing a single cell elicited Ca^{2+} oscillations and the propagation of Ca^{2+} signals between adjacent cells.

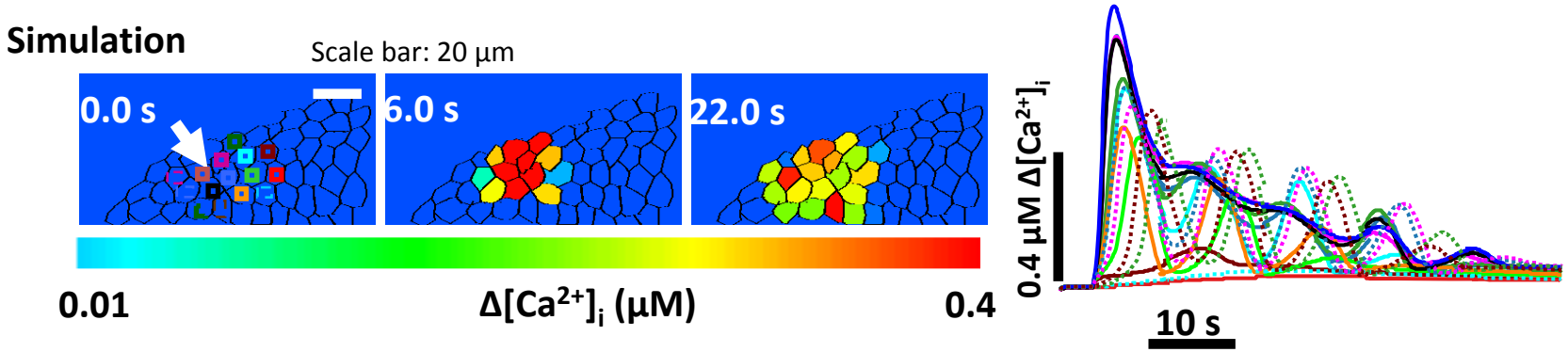

- The experimental data can be reproduced assuming a junctional transfer rate (k_j) of 0.05 s^{-1} for IP_3. Based on the results of Hernandez et al. (2007 Nat Methods) this rate corresponds to ~1080 open channels between each cell pair, in accord with the results of the voltage imaging experiment.

Ceriani, Pozzan, Mammano, ms in preparation

Model validation 2: ATP-evoked Ca^{2+} wave propagation

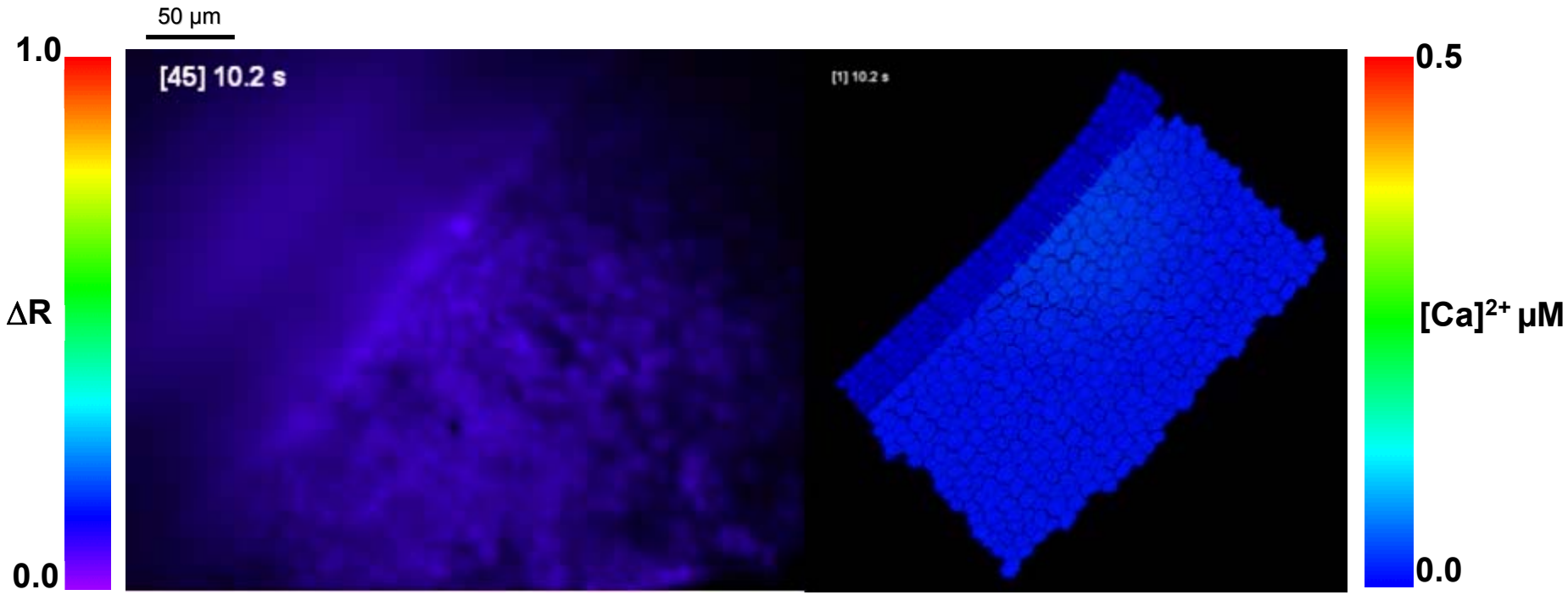

Ceriani, Pozzan, Mammano, ms in preparation

Summary

- The results presented here demonstrate that cochlear non–sensory cells of the lesser and greater epithelial ridge share the same PLC→IP_3R→Ca^{2+}–dependent intracellular signal transduction cascade activated by extracellular ATP.
- Intercellular Ca^{2+} signal propagation requires functional gap junction channels (for IP_3 diffusion) and connexin hemichannel (for ATP release).

- We built a mathematical model to characterize quantitatively Ca^{2+} signals in non-sensory cells of the developing cochlea and their relationship to connexin expression.
- The model comprises:
    a. P2Y receptors and ectonucleotidases at the endolymphatic surface
    b. IP_3-sensitive intracellular Ca^{2+} stores
    c. Gap-junction channels and connexin hemichannels
- At the single-cell level, the model successfully reproduces:
    a. The dose-response relationship between $[ATP]_e$ and peak Ca^{2+} responses
    b. Amplitude, phase and frequency of Ca^{2+} oscillations.
- At the cell-network level, the model reproduces the experimental data provided adjacent cells are coupled by a number of gap-junction channels consistent with the estimate obtained in our voltage imaging experiments.

Take home message

Ca^{2+} signaling in non-sensory cells of the developing cochlea depends on binding of extracellular ATP to G-protein coupled P2Y receptors at the endolymphatic surface of the sensory epithelium.

ATP binding triggers a canonical $PIP_2 \rightarrow PLC \rightarrow IP_3$-dependent signal transduction cascade which promotes Ca^{2+} release from intracellular stores.

Ectonucleotidases responsible for the hydrolysis of ATP at the cell surface terminate signaling.

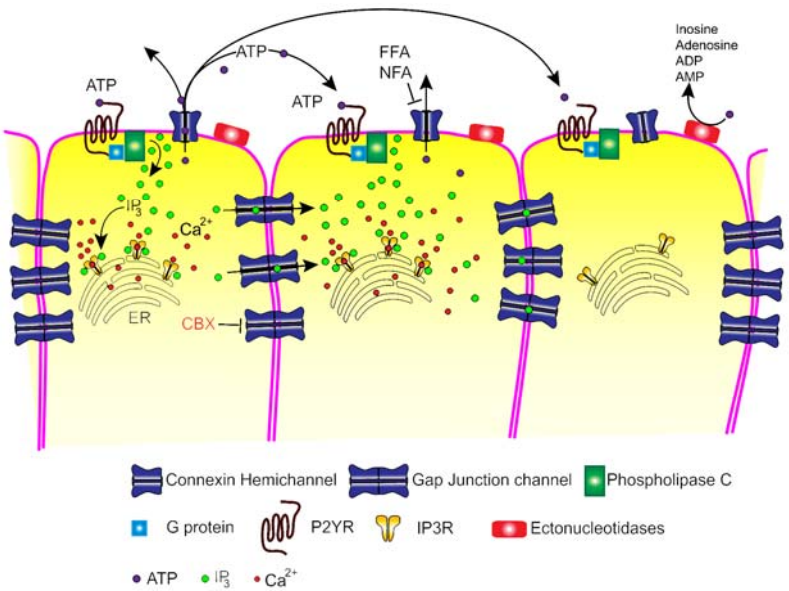

Channels formed by Cx26 and Cx30 enable the cell-to-cell spreading of Ca^{2+} signals by allowing:

(1) ATP release from the cell cytoplasm to endolymph through plasma membrane connexin hemichannels;

(2) IP_3 diffusion from cell to cell through gap junction channels.

Impairment of either intracellular (Ca^{2+}-dependent) or intercellular (connexin-dependent) signaling mechanisms in cochlear non-sensory cells impacts on normal hearing acquisition and leads to profound hearing loss in the adult stage.


Shanghai Institute for Advanced Immunochemical Studies (SIAIS)
免疫化学研究所